

Biotic and abiotic processes in the Laguna de los Pozuelos, Atacama Desert (Argentina)

by

Rhowe Stefanski

B.Sc., University of Wyoming, 2014

A THESIS

submitted in partial fulfillment of the requirements for the degree

MASTER OF SCIENCE

Department of Geology
College of Arts and Sciences

KANSAS STATE UNIVERSITY
Manhattan, Kansas

2020

Approved by:

Major Professor
Dr. Karin Goldberg

Copyright

© Rhowe Stefanski 2020.

Abstract

Laguna de los Pozuelos (LP) is a modern fault-bounded, alkaline lake in northwestern Argentina believed to serve as a potential analog for the genesis of pre-salt reservoirs. The sedimentary succession in a core drilled in Laguna de los Pozuelos was characterized through detailed facies and petrographic analyses, augmented by X-ray diffraction, X-ray fluorescence, isotopic and spectral analyses, to interpret the depositional conditions and relate the different carbonate habits with changes in environmental conditions in the lake. The sedimentary succession is composed of five facies, grouped into three facies associations (sheet flood, lake margin, and lacustrine facies associations). Except for the sheet flood facies association, these contain different types of carbonates, albeit in low abundance (only 12%). Primary carbonates include peloids, stromatolites, thrombolites, and bioclasts, whereas syn-diagenetic carbonates comprise microcrystalline and mosaic calcite and aragonite. These carbonates were precipitated by a mix of biotic and abiotic processes. Integration of the results provides new insights into the environmental and climatic changes that have happened in LP basin in the past 43,000 years. The study core shows that LP has gone through multiple high-frequency lake expansion and contraction cycles, with a peak in deepening and expansion of the lake at around 4.5 m of depth. An overall wetting-upward trend is suggested by evidence that the base of the study core accumulated under a more arid environment, followed by decreasing aridity and salinity in the top half. Water chemistry seems to be characterized by mostly low Mg/Ca ratio, conducive to precipitation of calcite, rather than aragonite. Despite some similarities to the environment envisaged for pre-salt reservoirs, Laguna de los Pozuelos is not a good analog for this system. Differences in water chemistry and sediment source did not generate the conditions necessary to produce the Mg-silicate gels and/or precipitate the expected amount and texture of carbonates found in the pre-salt-type reservoirs.

Table of Contents

List of Figures	v
List of Tables	viii
Acknowledgements	ix
Introduction.....	1
Background.....	4
Methods	10
Facies analysis	11
X-Ray Diffraction	12
X-Ray Fluorescence	13
Isotopic Analysis.....	13
Spectral Analysis	14
Results.....	15
Facies analysis	15
Petrographic Analysis	20
Textures.....	20
Primary Composition	25
Complementary Analyses	32
Discussion.....	39
Depositional Environments.....	39
Stratigraphic Evolution and Paleoclimate.....	41
Controls on Carbonate Precipitation.....	44
Conclusions.....	49
References.....	51
Appendix 1 – Petrographic quantification tables.....	59
Appendix 2 - Photomicrographs from thin sections in LP06-2A	68
Appendix 3 – XRD Diffractograms	76
Appendix 4 – XRF data	95

List of Figures

Figure 1: Adapted from Wright and Barnett (2017). A) Example of the microbial platform – deep lake model that is hypothesized as one of the possible origins for pre-salt reservoirs. B) Shallow lake model also hypothesized for the origin of pre-salt reservoirs.	2
Figure 2: Map of Pre-Quaternary geology of Laguna de los Pozuelos (Camacho & Kulemeyer, 2017).	5
Figure 3: A. example of spherulites as well as Mg-silicates (from Tutolo & Tosca, 2018). B. Shrubs from the pre-salt reservoirs in the Santos Basin, Brazil (from Petersohn & Abelha 2013). C. Laminated carbonate mud from the Barra Velha Formation, Santo Basin (from Terra et al., 2010).	7
Figure 4: Theoretical model of spherulites growing in an Mg-silicate gel that is converted to clay during diagenesis, later dissolved to create porosity (Wright & Barnett, 2017).	8
Figure 5: Photomicrographs from the pre-salt succession in the Campos Basin, showing spherulites precipitated in Mg-silicate matrix, locally dissolved with generated porosity (Wright & Barnett, 2017).	9
Figure 6: Google Earth image of LP, showing the modern extent of the lake and location of the study core (red circle).	10
Figure 7: Sedimentary log of core studied in the Laguna de los Pozuelos, summarizing the results. Facies associations: yellow = sheet flood, brown = lake margin, gray = lacustrine. Compositional quantification: blue = carbonate > 5%, red = total calcite > 5%, green = displacive gypsum present.	19
Figure 8: Representative photomicrographs of the facies associations. A: Massive mud (Cl _m) with intraclasts in the lake margin facies association. B: Intraclastic mud with zebra-like texture (Cl _m) in the lake margin facies association. C: Laminated clay (Cl _l), rich in bioclasts, typical of the lacustrine facies association. D: Coarse granules and pebbles with massive sand (S _m) in the sheet flood facies association. (Int= intraclast, Carb = carbonate, Zebra = clay with zebra-like texture, Char Bio = charophyte bioclast, Ostr = ostracod, Meta. Frag = metamorphic rock fragment, PPL = Plane polarized light, XPL = Crossed polarized light).	22

Figure 9: Photomicrographs of clay textures. A: highly-crystalline, B: Intraclastic, C: Zebra texture. (Ostr = Ostracod, Int = Intraclastic, Carb = Carbonate) 24

Figure 10: Bioconstructions found in LP. A: Stromatolites, B: Thrombolites. (Plane Polarized images on the left and Cross Polarized on the right). 25

Figure 11: Primary constituents found in LP. A: Charophytes in a crystalline mud (XPL), B: Ostracod and ostracod fragments within a clayey-sandy matrix (XPL), C: Undifferentiated bioclasts (PPL), D: Diatoms (PPL), E: Arcella not replaced by round carbonate (PPL), F: Phyllites present in S_m F.A. (XPL) (Char = charophyte, Ostr = ostracod, Bio = Undifferentiated Bioclast, Dia = Diatoms, Arc = Arcella, Phy = Phyllite PPL= Plane Polarized Light, XPL = Cross Polarized Light)..... 27

Figure 12: Representative photomicrographs of diagenetic constituents observed within thin sections. A: Microcrystalline carbonate lamination within a clay matrix (XPL). B: Mosaic carbonate, stained with alizarin, replacing charophyte fragments (XPL). C: “Round” carbonate, stained with alizarin (XPL). D: Gypsum crystals displacing mud (XPL). E: Fe oxide replacing mud in sheet flood facies (XPL). F: Pyrite framboids replacing mud (PPL). (MC = Microcrystalline, M = Mosaic, RC = “Round” carbonate, Gyp = Gypsum , Fe = Iron Oxide, Py = Pyrite.) 29

Figure 13: Representative photomicrographs of diagenetic constituents in thin sections. A: Aragonite crystals growing off of a “Round” carbonate stained with alizarin B: Aragonite crystals growing off of bioclast. C: Rare spherulites developing in a carbonate/clay matrix. (Ar= Aragonite Sph= carbonate spherulites) 31

Figure 14: Scatter plot of Mg/Ca vs Sr/Ca. One data point with abnormally high ratios of Mg/Ca and Sr/Ca is not shown, despite falling along the observed trendline. 33

Figure 15: Scatter plot of Fe/Al vs Cu/Al..... 34

Figure 16: Scatter plot of Fe/Al vs Ni/Al..... 34

Figure 17: Scatter plot of Si/Al vs Zr/Al 35

Figure 18: Carbon and oxygen isotopic values suggestive of decreasing salinity (arrow), from saline to freshwater lake. Ovals represent $\delta^{18}\text{O}$ and $\delta^{13}\text{C}$ the regions of ratios where freshwater and saline lakes are typically found. Not Approximate. (Leng & Marshall, 2004). 36

Figure 19: Variation of the VPCs in core LP06-2A according to depth..... 38

Figure 20: Composite Google Earth image showing water-level changes in Laguna de los Pozuelos. Red circle is the location of the study core..... 42

Figure 21: Oxygen and carbon isotopes plotted along the depth of LP's sedimentary core. 43

Figure 22: Influence of solution Mg:Ca ratio and temperature on CaCO₃ polymorph formed pseudohomogenous precipitates. White squares are aragonite, black squares are calcite, and split squares are situations in which calcite initially precipitates but then aragonite grows on calcite (Morse et al., 1997)..... 46

Figure 23: A: Transversal cut of a Charophyte gyrogonite (taken from 4.6 m 10X XPL). B: Charophyte replaced by mosaic carbonate and overgrown by stromatolitic and thrombolitic bioconstructions (taken from 4.6 m 20X XPL)..... 47

List of Tables

Table 1: Facies identified in LP06-2A from the Laguna de los Pozuelos.	15
Table 2 - – Simplified quantification of the thin sections from the different F.A. in LP06-2A (gray = lacustrine, tan = lake margin, yellow = sheet flood)	21
Table 3: Leading Variable Primary Components (VPCs) and their corresponding mineral/pigment assemblages	37

Acknowledgements

I would like to acknowledge my advisor, Dr. Karin Goldberg for sticking with me and giving me this opportunity to work with her. She truly helped me expand my geologic knowledge and advance my career. I would also like to thank the LacCore at the University of Minnesota for allowing me to use their facilities and core from Laguna de los Pozuelos for my research, and Dr. Michael McGlue for sharing his original stratigraphic spreadsheets for the LP06-2A core. I would like to thank Dr. David Pompeani for teaching me how to perform XRF and for being as interested in Pozuelos as I was. I would finally like to thank Dr. Nivanthi Mihindukulasooriya for performing the spectral analyses upon my samples and processing the data.

Introduction

Carbonate rocks are important reservoirs for oil and gas all across the world, from Kansas to Saudi Arabia. Many of these reservoirs, such as the Mississippian limestone in KS (Mazzullo et al. 2007), were deposited under normal, shallow-marine conditions. Others, such as the pre-salt reservoirs in the marginal Brazilian basin, comprise exotic carbonates and associated phases, such as magnesium phyllosilicates (stevensite, kerolite and talc; Wright 2012; Tosca & Wright 2015), indicating that they formed under very unusual and extreme lacustrine conditions (Wright & Barnett 2015). By investigating sedimentological processes in present day alkaline lakes, we can learn about the genesis of these exotic reservoirs.

The unique characteristics of these reservoirs have few analogues throughout geologic history. Two main models were proposed for the development of pre-salt carbonates. They were initially interpreted as of microbial origin (Carminatti et al., 2008; Nakano et al., 2009), which then resulted in the reservoirs being referred to as 'Pre-Salt Microbialites' (Terra et al. 2010; Rezende & Pope, 2015; Muniz & Bosence, 2015). These 'microbialites' were suggested to have formed in a deep lake, similar to marine platform margins (Figure 1A). These margins would theoretically be biotic factories that would produce large microbial mats of similar size to those found in pre-salt reservoirs (Wright & Barnett, 2017). This model is supported by existing seismic data of pre-salt reservoirs that suggest marine-like platforms.

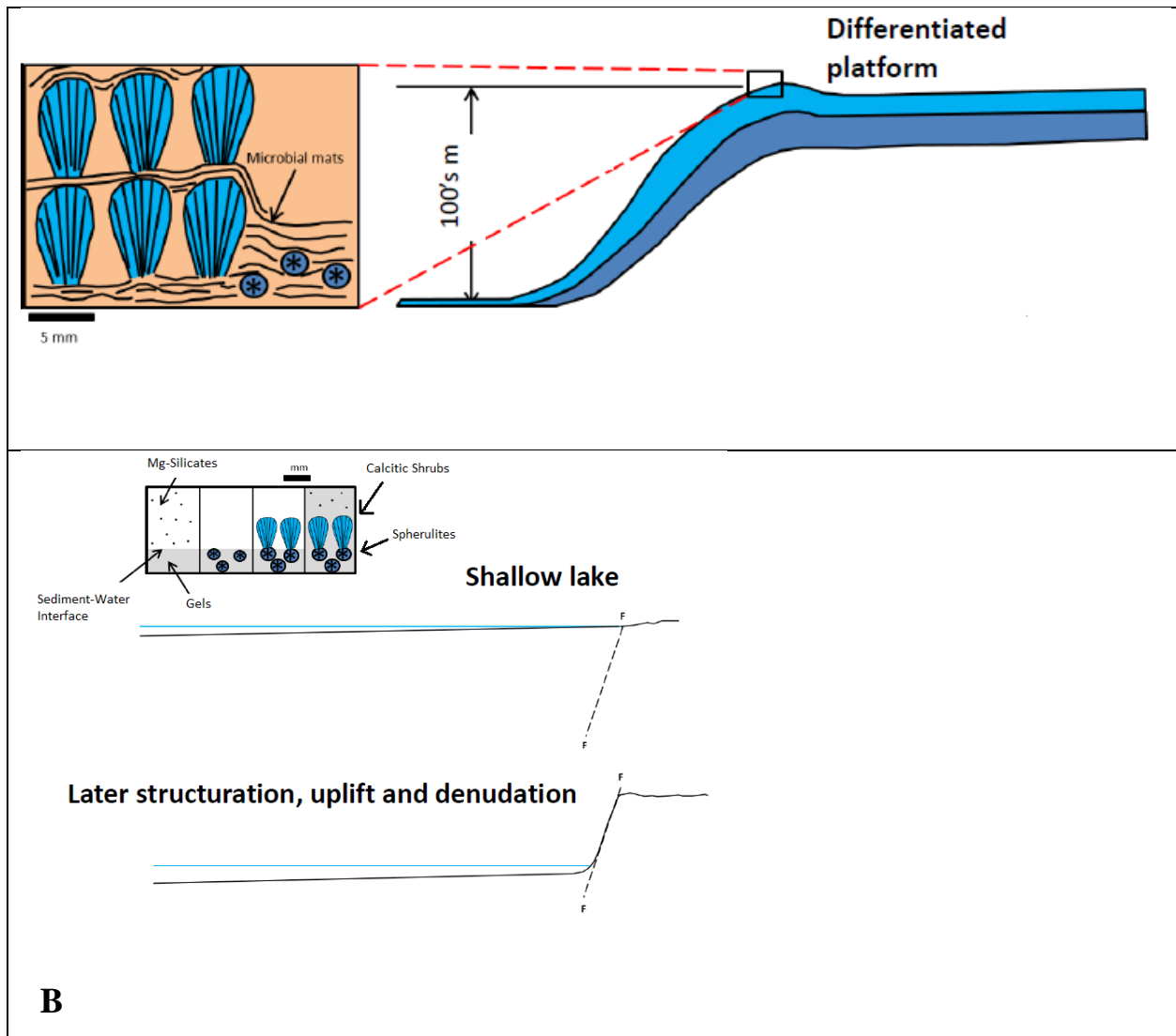


Figure 1: Adapted from Wright and Barnett (2017). A) Example of the microbial platform – deep lake model that is hypothesized as one of the possible origins for pre-salt reservoirs. B) Shallow lake model also hypothesized for the origin of pre-salt reservoirs.

However, other work suggests that the shrub-like and spherulitic textures in these reservoirs (described below) are mostly inorganic (Wright & Barnett, 2015; Herlinger Jr. et al. 2017). The alternative model for the depositional setting of the pre-salt formations is that of extensive, hyper-alkaline, shallow evaporitic lakes (Wright & Barnett, 2015) (Figure 1B). In this model, it is postulated that rivers draining basic volcanic terrains, coupled with thermal to ambient spring inflow and an arid climate, could create a set of conditions (high CO₂ input and carbonate

alkalinity, high dissolved silica, Mg and Ca) ideal for producing the unique deposits in the pre-salt reservoirs (Wright & Barnett, 2015).

Understanding the sedimentological processes in Laguna de los Pozuelos (LP) may provide insights on the genesis of pre-salt reservoirs. Tectonic and sedimentary characteristics of LP are similar to pre-salt, including being fault-bounded in an active tectonic and volcanic system, the ability of hydrothermal fluids to come into the system and produce magnesium, and the association between carbonate and phyllosilicates (stevensite, kerolite, talc). Thus we hypothesize that LP is a suitable modern analog for the pre-salt. The goal of this study is to describe and interpret the lacustrine sediments in a core from LP to determine the depositional environments and physical-chemical characteristics that led to the development of different carbonate textures, e.g., temperature, Mg/Ca ratio, biotic vs. abiotic contributions, etc., evaluating the chemical and microbial processes responsible for the precipitation of different types of carbonate.

Background

Laguna de los Pozuelos (LP) is a high-altitude, fault-bounded, alkaline lake in the Atacama Desert in the northwest corner of Argentina (Figure 2). Tectonostratigraphic relationships indicate that basin formation occurred from 28 to 16 Ma ago (Rubiolo, 1997). The Pozuelos Basin is bounded by westward-verging thrust sheets that carry Ordovician marine siliciclastic and volcanic rocks (McGlue et al., 2012). It is an endorheic, shallow (<2 m), large but seasonably fluctuating lake that can exceed 135 km² during years with above average precipitation (Mirande & Tracanna, 2009).

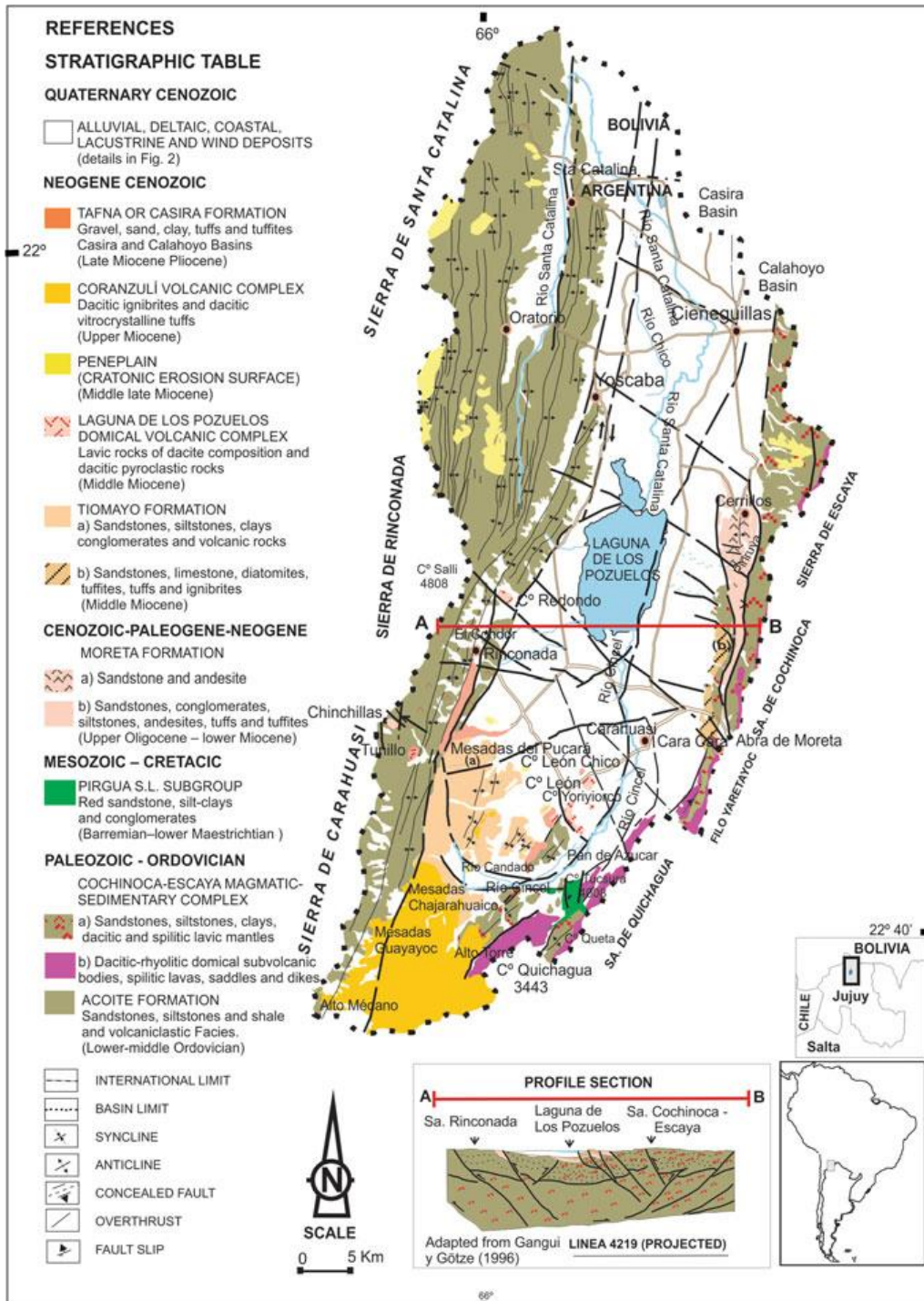


Figure 2: Map of Pre-Quaternary geology of Laguna de los Pozuelos (Camacho & Kulemeyer, 2017).

LP is an underfilled basin that is hydrologically supplied by three river systems: Río Santa Catalina from the north, Río Cincel from the south-east, and the Río Chico from the south-west

(McGlue et al., 2012). LP is also supplied from rainfall and isolated springs to the south of the lake. All fluctuations in lake level are a result of the amount of inflow from these systems compared to the evaporation from the lake surface. Sediments deposited in LP are hybrid in nature and include terrigenous, carbonates, organics, and biogenic silica (McGlue et al., 2012). It is an important habitat for water birds, including all three species of New World flamingos (Mascitti, 2001). The basin is also host to multiple species of shrubs and grasses of both the C₃ and C₄ variants (McGlue et al., 2012).

Previous research on LP has focused on the sedimentation and organic matter accumulation (McGlue et al., 2012). The lake center contains silty clays and diatom oozes, whereas the margins contain silty clays with minor amounts of carbonate (McGlue et al., 2012). Rapid evaporation of lake water, coupled with relatively dilute inflows, appears to constrain widespread crystallization of Mg-rich and Na-rich minerals, preventing larger carbonate deposition (McGlue et al., 2012). Organic matter is preferentially preserved in the lake center, presumably due to the depth in this location not allowing water birds to influence the deposition of organic matter with their feeding habits. Playa marginal facies, marked by lower total organic carbon (TOC) and higher total inorganic carbon (TIC) concentrations, are strongly influenced by evaporation, bioturbation and deflation, and are not conducive to the preservation of organic carbon (McGlue et al., 2012).

Pre-salt reservoirs are sedimentary formations in the South Atlantic developed as a result of depositional processes involving continental rifting, seafloor spreading and sedimentation during the Cretaceous (Beasley et al., 2010; Carminatti et al., 2008; Muniz & Bosence, 2015; Nakano et al., 2009). These carbonate formations were discovered to hold some of the largest petroleum reservoirs found in the last 20 years, totaling in the billions of barrels of oil. Because of the economic potential of these reservoirs, research has been focused on the question of what the

environments were in which these reservoirs formed (Bertani & Carozzi, 1985a,b; Carminatti et al., 2008; Wright, 2012; Chitale et al., 2015; Thompson et al., 2015; Tosca & Wright, 2015; Saller et al., 2016).

Previous research identified three distinct textures within these pre-salt carbonates (Terra et al., 2010; Petersohn & Abelha, 2013; Tutolo & Tosca, 2018):

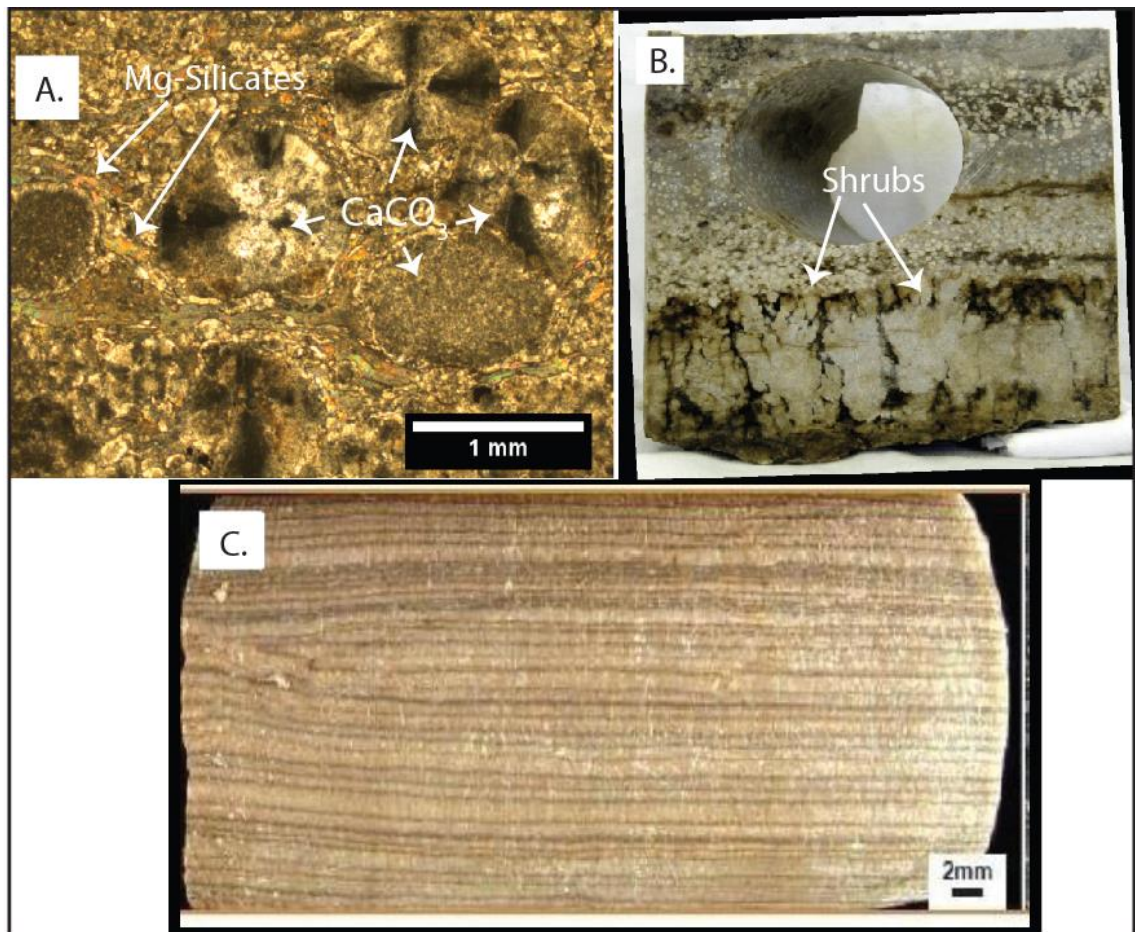


Figure 3: A. example of spherulites as well as Mg-silicates (from Tutolo & Tosca, 2018). B. Shubs from the pre-salt reservoirs in the Santos Basin, Brazil (from Petersohn & Abelha 2013). C. Laminated carbonate mud from the Barra Velha Formation, Santo Basin (from Terra et al., 2010).

(1) spherulitic calcium carbonate within a Mg-silicate matrix (“spherulites”, Figure 3A); (2) calcium carbonate shrubs (“shrubs”, Figure 3B); and (3) mud-grade (“laminites”, Figure 3C). The spherulite facies contains calcite spherules generally under ~3 mm in diameter (published images suggest typical spherule diameters of around several hundred micrometers; Terra et al., 2010; Wright & Barnett, 2015; Saller et al., 2016) embedded in a Mg-silicate matrix (Wright & Barnett, 2015). The shrubs typically contain upward-branching mm to cm-scale carbonate structures that appear to develop on the bottom of the paleo-lake and reach upwards (Wright and Barnett, 2015). Laminites are generally thin, less than 0.3 m thick, composed of limestones with preserved fish fossils (Wright & Barnett, 2015) and are suggestive of a more near-neutral pH during deposition (Alabaster and Lloyd, 2013). The formation of silicate gels, which during diagenesis would convert to crystalline clays, seems to be a key element in the process (Wright and Barnett, 2017) (Figure 4), due to the gels being key growth factories for both the spherulites and shrubs development. These gels, through late clay replacement, would also be the basis for porosity creation within the system as a result of late dissolution of said Mg clay minerals (Figure 5).

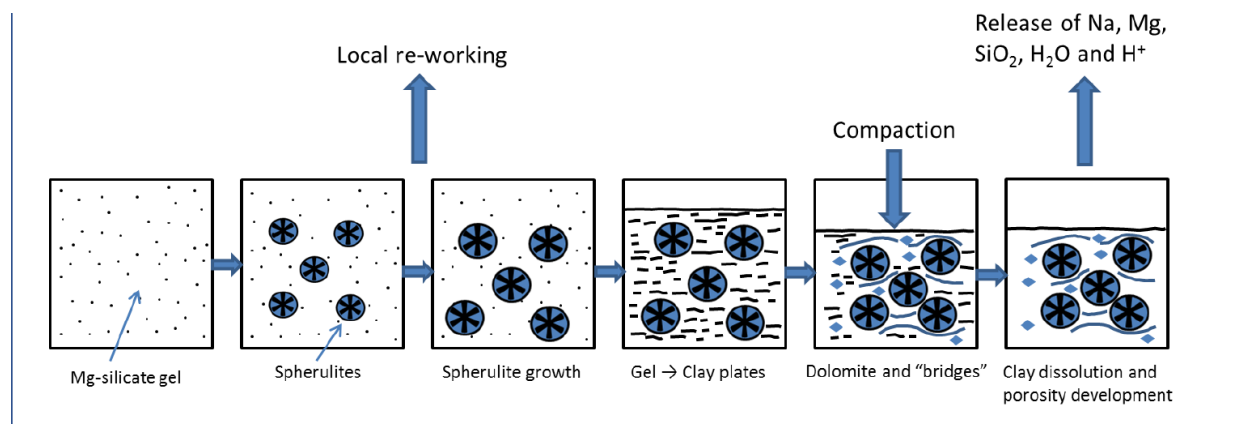


Figure 4: Theoretical model of spherulites growing in an Mg-silicate gel that is converted to clay during diagenesis, later dissolved to create porosity (Wright & Barnett, 2017).

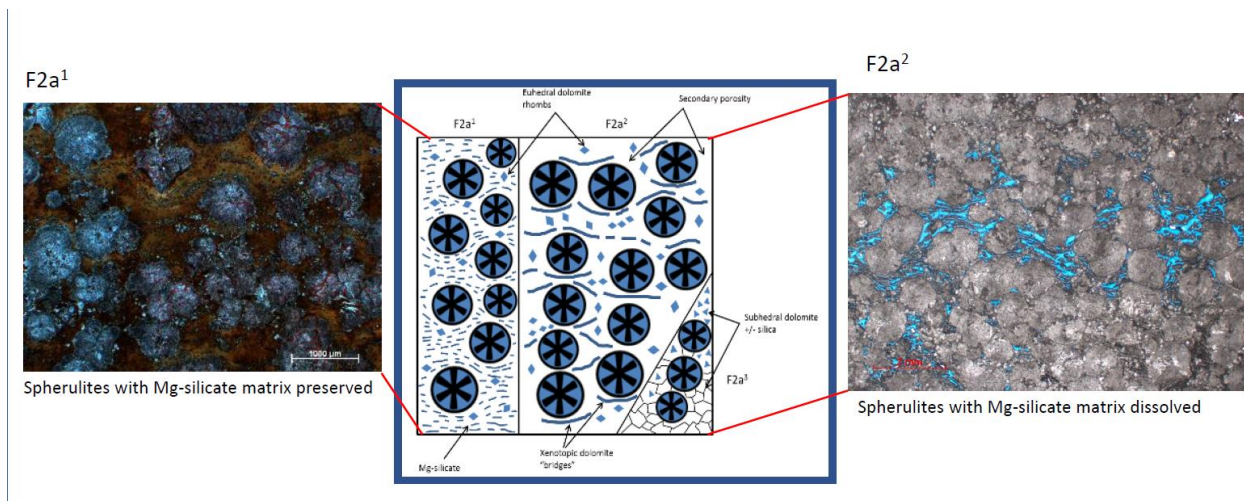


Figure 5: Photomicrographs from the pre-salt succession in the Campos Basin, showing spherulites precipitated in Mg-silicate matrix, locally dissolved with generated porosity (Wright & Barnett, 2017).

The mineralogy and texture of lacustrine carbonates are controlled by a number of chemical and physical parameters, such as Mg/Ca ratio, alkalinity, temperature, degree of saturation, depositional energy, degree of biotic mediation, etc. (Della Porta, 2015). Being able to infer these parameters is paramount to proposing a reliable interpretation of the genesis of these deposits, hence this research's goal of understanding the development of carbonate texture in LP.

Methods

Detailed facies analysis was carried out both micro- and macroscopically using core samples (AAFBLP-LP06-2A) taken from a marginal area at the northwest corner of LP (Figure 6). The core, approximately 12 meters thick and 4 cm wide, is housed in the National Lacustrine Core Facility (LacCore) at the University of Minnesota in Minneapolis.



Figure 6: Google Earth image of LP, showing the modern extent of the lake and location of the study core (red circle).

Sediment sampling followed macroscopic description of the core and selection of areas of interest for in-depth analysis. Selected intervals of key facies were also compared to sampled core

intervals from previous research done by McGlue et al. (2012) on Laguna de los Pozuelos. The sampling procedure involved using thin aluminum cubes placed face down in the core in an area of interest. These cubes were roughly 2-3 cm in width, depending on the features observed within the core. The cubes would be pressed down into the clay and fishing line was then run down the sides and underneath the cube to disconnect the sample from the rest of the core. If the sample was a sand, however, due to the friable nature of the sediment, it was scooped out of the core with tools while being careful to not contaminate the sample with sediment from outside the sample area. These samples were frozen with liquid nitrogen to preserve them for the creation of thin sections with blue staining, which was done by the University of Minnesota. This sampling technique produced 16 thin sections that have been used for the petrographic analysis. Samples were taken from within these sampled areas for use in other petrographic analyses, including XRF and XRD.

Facies analysis

Facies analysis involved a detailed sedimentologic description (1:20 scale) and the construction of a lithological log with grain size on the X axis and bed thickness on the Y axis. Bed by bed descriptions of lithology, composition, texture, sedimentary structures, degree of bioturbation, and organic matter were used to determine which sections to sample for additional analysis. Facies identified in this study were grouped into facies associations, which were determined by similarities within the sediment based on macroscopic and microscopic observations, the sediment classified within each facies, and the understanding of basic sedimentology.

A sedimentological log was created from the sedimentary descriptions and facies analysis of the entire core. It was determined through conversations with the original core driller, Dr. McGlue, that, during drilling, slumping of some intervals occurred within the core hole. This

resulted in missing sections as well as repeat sections within the cores. To remedy the situation, the initial data from Dr. McGlue's research were gathered and his estimated composite depths were used to identify intervals of repeated sections. These were then excluded from the sedimentological log, reducing the total thickness of the log from 12 meters to approximately 5.6 meters in the corrected log. The positions of data points gathered from the duplicate sections were corrected and repositioned to fit the actual depth.

Petrographic analysis focused on identifying compositional, textural and structural characteristics of the studied succession that are similar to the pre-salt reservoirs (Figure 3). A staining solution of alizarin red plus potassium ferricyanide was used to differentiate the carbonates in the thin sections, according to the methodology proposed by Dickson (1965). The petrography involved performing quantitative analysis of each thin section in an attempt to determine the abundance of different minerals and carbonates. Quantification of primary and diagenetic constituents was obtained by counting 300 points per thin section, using the Gazzi-Dickinson quantification method (cf. Zuffa, 1985). Data were stored and processed in Petroledge® software (De Ros et al. 2007). These data were then exported to Microsoft Excel® spreadsheets for processing and interpretation of the data set.

X-Ray Diffraction

X-ray diffraction (XRD) was used to interpret mineral composition, specifically clay types within LP. XRD was performed in bulk and clay fractions. In the clay fraction, ethylene-glycol was used to check for the presence of swelling clay, such as smectite. XRD data were processed and analyzed at the Huffington Department of Earth Sciences, Southern Methodist University.

X-Ray Fluorescence

X-ray fluorescence (XRF) was used to determine the elemental composition (Mg, Al, Si, P, S, K, Ca, Ti, V, Cr, Mn, Fe, Co, Ni, Cu, Zn, As, Se, Rb, Sr, Zr, Ag, Cd, Sn, Sb, Ba, Hg, Tl, and Pb). Elemental concentrations were acquired through the use of a Bruker Tracer 5i wavelength-dispersive X-ray fluorescence (XRF) analyzer. Major and trace elements were measured consecutively, with sampling spanning 180 seconds for major elements and 120 seconds for minor elements. Ten measurements of the soil standard (Bruker CS-M2) were conducted before and after analyzing unknowns to ensure accuracy within acceptable limits.

XRF provides semi-quantitative measurements of elemental concentrations, which were used to calculate ratios (e.g., Mg/Ca, Sr/Ca, Fe/Al) that served as proxies for key chemical parameters. Those were used to generate chemostratigraphic logs and cross plots to compare and contrast the data. Sr/Ca was used as a proxy for salinity and Mg/Ca was used to evaluate temperature and salinity (Horne et al., 2012). Fe/Al was used as a proxy for the redox state (Clarkson et al., 2014), Cu/Al and Ni/Al for primary productivity (Becker & Kirchgasser, 2007), and Si/Al and Zr/Al to determine the silica origin within the system (Calvert & Pedersen, 2007).

Isotopic Analysis

Carbon and oxygen isotopic analyses of eight samples taken from the sediment core were used for interpretation of water chemistry, temperature, lake type and climate history. In lacustrine environments, changes in $\delta^{18}\text{O}$ values are associated with changes in temperature or precipitation/evaporation ratio; whereas those of carbon are used to highlight climatically induced changes in carbon, nutrient cycling, and productivity within the lake (Leng & Marshall, 2004). Bulk-rock stable isotopic analyses in samples with different carbonate constituents and textures were done at Huffington Department of Earth Sciences, Southern Methodist University. The bulk

samples were powdered and reacted with 100% phosphoric acid at 25°C. The evolved CO₂ was analyzed for carbon and oxygen isotopes on a mass spectrometer. Based upon replicate standards of NBS-19 and an internal laboratory Carrara marble standard (n=15) analyzed during the interval of analysis, $\delta^{18}\text{O}$ values had a reproducibility of $\pm 0.14\%$, $\delta^{13}\text{C}$ values have a reproducibility of $\pm 0.07\%$. The notation used for stable isotopes is Vienna Pee Dee Belemnite (VPDB). Values are reported as $\delta^{18}\text{O}$ and $\delta^{13}\text{C}$ ‰.

Spectral Analysis

Spectral analysis was performed to determine the principal components of sediment composition. Measurements of diffuse spectral reflectance were collected using a spectrophotometer, and the components were identified by comparing the principal component (PC) loading spectra for each of the PCs with center-weighted reflectance derivative spectra for previously published pigments, known mineral standards in the USGS spectroscopic library, or minerals measured in Ortiz' lab at Kent State University (Gantt, 1975; Robertson et al., 1999; Graham and Wilcox, 2000; Schagerl and Donabaum, 2003; Schagerl et al., 2003; Toepel et al., 2005; Clark et al., 2007; Yurco et al., 2010; Ortiz et al., 2009; Ortiz, 2011). The data were quantified to understand the relative importance of each pigment or mineral in the PC by fitting a weighted-average of the empirically selected standards to each principal-component loading pattern. The quality of the fit was determined by linear correlation. This process is identical to the approach previously applied to marine cores (Ortiz et al., 2009; Ortiz, 2011; Bouchard et al., 2013) and similar to spectral matching methods used in X-ray Diffractometry (Eberl, 2003, 2004). This analysis was performed at Northwest Missouri State's Department of Natural Sciences (Mihindukulasooriya, 2011).

Results




Facies analysis

The detailed sedimentological description (1:20 scale) allowed the recognition of five facies in the studied core (Table 1). The facies identified were labeled in relation to their grain size (Cl = clay, S = sand) or composition (O = organic rich), as well as their structure (subscript: m = massive, l = laminated).

The most common facies are Cl_m, Cl_l, and S_m, and rarely S_l (only at 5.54 m) and O (only in lenses within Cl_l facies).

Table 1: Facies identified in LP06-2A from the Laguna de los Pozuelos.

Facies Code	Description	Interpretation	Facies Photos
S _l	Medium sand, laminated, with scattered granules and pebbles; greenish	Deposition of plane beds by currents in upper flow regime (Miall, 1977; Best and Bridge, 1992), and/or washed-out dunes and hummock dunes (transition between subcritical and supercritical flows) (Harms et al., 1982; Bridge and Best, 1988).	
S _m	Very fine to fine, muddy, sand, massive to normal-graded, locally with Fe oxide staining and sparse burrows; tannish-green	Rapid deposition from heavy sediment-laden flows during waning floods (Todd, 1989; Maizels, 1993), and/or later modification by biological disturbance.	

<p>Cl_m</p>	<p>Silty clay to clay, massive or with incipient lamination; locally mottled and/or with root traces, some Fe oxide staining; sparse to moderate organic content (plant debris); gray color with variable hues of brownish, tan, reddish or greenish</p>	<p>Suspension settling dominantly from standing water or weak unidirectional flows; later modified by pedogenetic processes; lack of lamination due to (i) flocculation of clay suspension or (ii) loss of lamination associated with intensive bioturbation; post-depositional graying under reducing conditions (Miall 1977; Foix et al., 2013; Turner, 1980; Jo and Chan, 2000); post-depositional reddening under oxidizing conditions (Miall, 1977; 1990; Foix et al., 2013).</p>	
<p>Cl_l</p>	<p>Laminated clay, variable amounts of Fe oxide staining, moderate to high organic content (plant debris); gray color with variable hues or reddish, brownish, and reddish brownish</p>	<p>Suspension settling, dominantly from standing water (Rogers and Astin, 1991; Mangano et al., 1994), with episodic deposition of plant debris. Suspension settling on overbank areas; later modified by pedogenetic processes; post-depositional graying under reducing conditions (Miall 1977; Foix et al., 2013; Turner, 1980; Jo and Chough, 2001); post-depositional reddening under oxidizing conditions (Miall, 1977; 1990; Foix et al., 2013).</p>	
<p>O</p>	<p>Clay, massive, carbonaceous, very rich in organic debris (plant debris); brown</p>	<p>Paleosol horizons formed by pedogenetic processes in swampy areas</p>	

The five facies identified in the study core were grouped into three facies associations (F.A.): 1) sheet flood, 2) lake margin, and 3) lacustrine.

The sheet flood F.A. includes S_m and S_l , deposited in a high-energy fluvial environment. This is evidenced by the coarse grain size, including granules and pebbles. S_l is greenish, laminated medium-grained sand with scattered granules and pebbles. S_m is a very fine to fine, muddy sand, massive to normal-graded. It is tannish-green in color, locally with Fe oxide staining and sparse burrows. The presence of hyperconcentrated (S_m) and transitional-to-upper (S_l) flow deposits, and the lack of well-developed floodplain deposits, suggests ephemeral currents, typical of a seasonal regime. Intense rainfall would lead to the development of fast-moving currents with high sediment loads, deposited around and at the lake margins. The local occurrence of normal grading in these sediments agrees with waning flows. The absence of scour surfaces and erosional bases suggest tabular, sheet floods from all the surrounding regions rather than incised channels.

The lake margin F.A. comprises mostly Cl_m (subordinately O), deposited under low energy conditions along the shores, where water level is highly fluctuating. During high lake levels, slight agitation by waves and/or current forms clay peloids. Cl_m is a silty clay to clay, massive or with occasional incipient lamination. It is typically gray with variable hues of brownish tan, reddish or greenish colors, with some Fe oxide staining. The common bioturbation in Cl_m suggests shallow, oxygenated waters, and the local presence of root traces indicate episodic colonization by plants. Association with O facies suggests the accumulation of organic matter in boggy areas.

The lacustrine F.A. is characterized by Cl_l and O. The dominance of laminated deposits indicates a low-energy environment where gravitational settling is the main process, without any reworking by flows and/or organisms. Cl_l is a laminated clay, typically gray with variable hues of

reddish, brownish, and reddish brownish colors due to Fe oxide staining. O is brown, massive clay, very rich in carbonaceous (plant) debris. The common occurrence of Charophyte algae and ostracods within these two facies points to a highly alkaline body of water. The concentration of oriented plant debris along laminations, or in centimetric layers, suggests the episodic supply of plant debris, brought in by currents and settling from suspension into deeper portions of the lake. Moderate to high organic content suggests a poorly-oxygenated subaqueous environment. Cl_m could also be partially associated with this F.A., specifically where massive clay is devoid of root traces.

Figure 7 shows the distribution of the F.A. in the study core, as well as the interpretation of lake level and isotopic and chemical indices (discussed below).

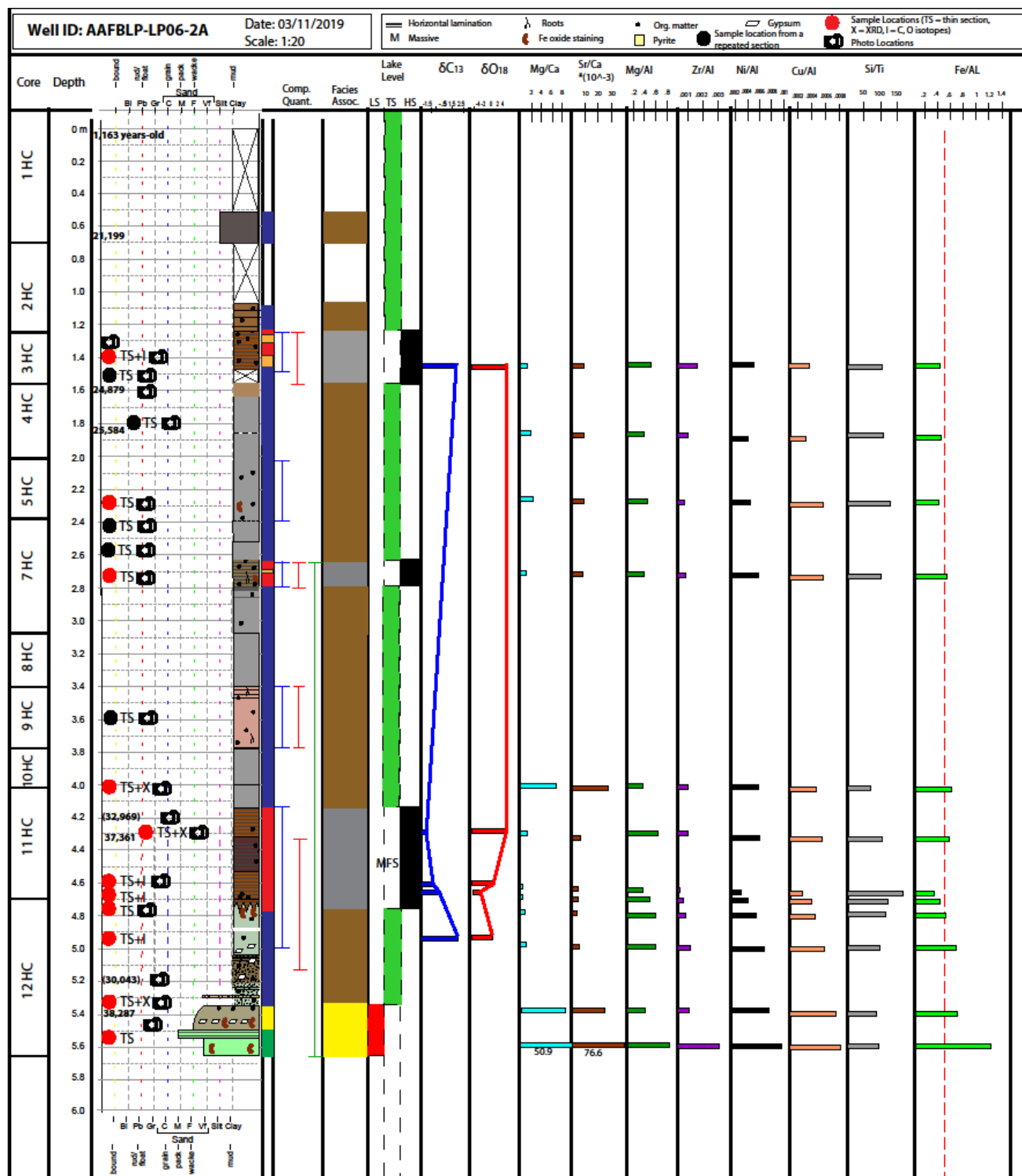


Figure 7: Sedimentary log of core studied in the Laguna de los Pozuelos, summarizing the results. Facies associations: yellow = sheet flood, brown = lake margin, gray = lacustrine.

Compositional quantification: blue = carbonate > 5%, red = total calcite > 5%, green = displacive gypsum present.

Petrographic Analysis

Detailed petrographic analyses were carried out on 16 thin sections of LP06-2A well, representative of the different facies associations (seven thin sections from the lacustrine F.A., seven from the lake margin F.A., and two from the sheet flood F.A.). The results of the petrographic analysis are described below, with relevant average and maximum values displayed in Table 2, and representative photomicrographs in Figures 8-13. The complete quantification and photomicrographs for each thin section can be found in Appendices 1 and 2.

Textures

Most of the studied core comprises massive or laminated clay (Cl_l and Cl_m facies) that occurs either in situ (as syndepositional matrix) or reworked (as clay peloids and/or intraclasts) (Figure 8A-C). Both in situ and reworked clays may display three different textures: homogeneously laminated, zebra-like or highly crystalline.

Textures in the study core vary depending on the F.A. The sheet flood facies association is dominated by sand grains rich in rock fragments (average 22%; maximum 41%) (Figure 8D). In situ clay is subordinate (average 11%; maximum 20%), and carbonates were not found within this F.A.

Table 2 - – Simplified quantification of the thin sections from the different F.A. in LP06-2A (gray = lacustrine, tan = lake margin, yellow = sheet flood)

ID	LP2A 2.7 i LP2A 3.2 i LP2A 6.65 LP2A 10.4 LP2A 10.7 LP2A 10.8 LP2A 11.1 m								LP2A 3.85 LP2A 4.9 i LP2A 5.1 i LP2A 5.6 i LP2A 8.35 LP2A 10.1 LP2A 11.3 m								LP2A 11.7 LP2A 11.9 m						
Depth (m)	2.70	3.20	6.65	10.40	10.75	10.80	11.10				3.85	4.90	5.10	5.60	8.35	10.10	11.30			11.70	11.90		
Adjusted depth (m)	1.40	1.55	2.70	4.30	4.60	4.68	4.75				1.80	2.30	2.42	2.57	3.60	4.00	4.92			5.31	5.54		
Well	LP06-2A	LP06-2A	LP06-2A	LP06-2A	LP06-2A	LP06-2A	LP06-2A				LP06-2A	LP06-2A	LP06-2A	LP06-2A	LP06-2A	LP06-2A	LP06-2A			LP06-2A	LP06-2A		
Facies code	CIL	CIL	CIL	CIL	CIL	CIL	CIL	Average	Maximum	CIM	CIM	CIM	CIM	CIM	CIM	CIM	CIM	Average	Maximum	SM	SL	Average	Maximum
Constituents	%	%	%	%	%	%	%			%	%	%	%	%	%	%	%			%	%		
In situ clay	48.00	59.33	56.66	58.66	35.67	30.00	42.00	47.19	59.33	67.66	66.67	60.67	71.66	51.66	62.67	52.67	61.95	71.66	20.00	2.00	11.00	20.00	
Reworked clay	15.67	9.33	7.00	4.67	2.00	1.33	1.33	5.90	15.67	17.33	12.00	16.00	7.67	13.33	18.34	21.00	15.10	21.00	3.33	0.00	1.66	3.33	
Bioconstruction	0.00	0.00	0.00	0.00	13.66	0.00	0.00	1.95	13.66	0.00	0.00	0.00	0.00	1.00	0.00	0.00	0.14	1.00	0.00	0.00	0.00	0.00	
Carbonate peloid - As intrabasinal constituent	3.33	1.33	3.00	1.33	8.33	3.00	4.00	3.47	8.33	1.33	2.67	3.33	2.33	2.33	4.00	0.33	3.00	2.43	4.00	0.00	0.00		
Carbonate bioclasts (total)	3.00	1.33	4.66	6.33	12.66	25.33	21.33	10.62	25.33	1.33	2.67	2.33	2.00	2.00	0.33	0.33	1.57	2.67	0.00	0.00	0.00	0.00	
Non-carbonate bioclasts	0.33	1.67	3.67	5.34	2.00	0.67	1.34	2.15	5.34	0.00	3.33	0.66	1.67	1.33	2.66	1.00	1.52	3.33	0.00	0.00	0.00	0.00	
Total bioclasts	3.33	3.00	8.33	11.67	14.66	26.00	22.34	12.76	26.00	1.33	6.00	2.99	3.67	3.33	2.99	1.33	4.95	7.33	0.00	0.00	0.00	0.00	
Carbonaceous organic matter - As intrabasinal constituent	4.33	2.00	9.67	3.33	0.67	0	0.33	2.90	9.67	2.33	1.67	1.33	1.33	2.67	1.33	0.33	1.57	2.67	1.00	0	0.50	1.00	
Extrabasinal grains	10.33	6.33	3.00	1.67	1.33	0.67	1.00	3.48	10.33	5.33	5.00	4.67	3.00	6.33	6.33	0.67	4.48	6.33	4.33	49	26.67	49.00	
Detrital quartz	4.33	2.67	0.67	0.67	0.67	0	1.00	1.48	4.33	2.67	2.00	1.00	0.00	2.00	2.67	0.33	1.52	2.67	1.67	1.33	1.50	1.67	
Detrital feldspar	1.33	0.67	0.33	0.00	0.00	0	0.00	0.33	1.33	0.33	0.33	0.33	0.00	0.67	0.33	0.00	0.29	0.67	0.33	0.67	0.50	0.67	
Rock fragments	2.67	1.33	1.34	0.67	0.00	0.00	0.00	0.86	2.67	1.33	1.00	1.33	1.67	1.33	2.33	0.00	1.28	2.33	2.33	41.34	21.84	41.34	
Total aragonite	0.00	0.33	0.00	0.00	1.00	2.00	3.67	1.00	3.67	0.00	0.00	0.00	0.00	0.00	2.00	0.00	0.29	2.00	0.00	0.00	0.00	0.00	
Round Calcite	6.33	5.33	1.00	0.67	1.67	2.00	0.33	2.48	6.33	0.33	0.67	3.67	1.33	5.33	0.33	1.33	1.86	5.33	0.00	0.00	0.00	0.00	
Other calcite	0.00	0.00	0.00	0.00	2.66	9.66	4.67	2.43	9.66	0.00	0.00	0.00	0.00	0.00	0.00	0.00	0.00	0.00	0.00	0.00	0.00	0.00	
Microcrystalline calcite	2.67	1.33	4.00	1.00	4.33	4.00	3.33	2.95	4.33	1.00	1.33	1.00	0.33	1.33	0.00	10.67	2.24	10.67	0.00	0.00	0.00	0.00	
Total calcite	9.00	6.66	5.00	1.67	8.66	15.66	8.33	5.38	13.66	1.33	2.00	4.67	1.66	6.66	0.33	12.00	4.09	12.00	0.00	0.00	0.00	0.00	
Total Fe oxide	0.00	0.00	0.00	0.00	0.00	0.00	0.00	0.00	0.00	0.00	0.00	0.00	0.00	0.00	0.00	0.00	0.00	0.00	64.33	26.00	45.17	64.33	
Lenticular gypsum	0.00	0.00	0.67	12.00	5.34	6.33	3.00	3.91	12.00	0.00	0.00	0.00	0.00	1.32	2.00	3.34	0.95	3.34	0.00	0.00	0.00	0.00	
Other gypsum	0.00	0.00	0.00	0.00	0.00	0.00	0.00	0.00	0.00	0.00	0.00	0.00	0.00	0.00	0.33	0.67	0.14	0.67	3.32	0.00	1.66	3.32	
Total gypsum	0.00	0.00	0.67	12.00	5.34	6.33	3.00	3.91	12.00	0.00	0.00	0.00	0.00	1.32	2.33	4.01	1.09	4.01	3.32	0.00	1.66	3.32	
Total pyrite	3.33	5.00	4.34	4.33	5.00	3.33	5.33	4.38	5.33	2.33	2.66	1.67	6.00	2.00	2.67	1.00	2.62	6.00	2.00	0.00	1.00	2.00	

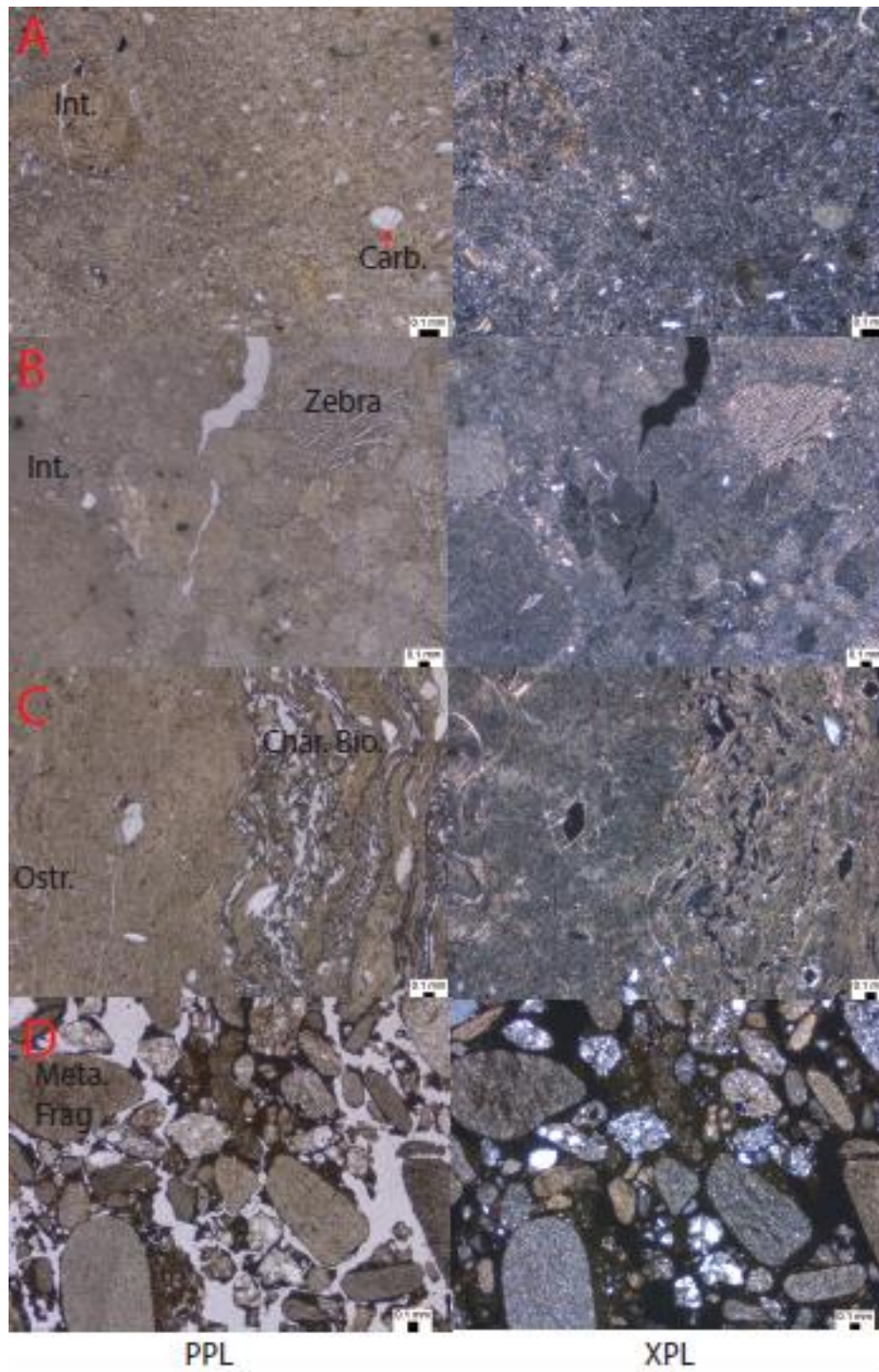


Figure 8: Representative photomicrographs of the facies associations. A: Massive mud (Cl_m) with intraclasts in the lake margin facies association. B: Intraclastic mud with zebra-like texture (Cl_m) in the lake margin facies association. C: Laminated clay (Cl), rich in bioclasts, typical of the lacustrine facies association. D: Coarse granules and pebbles with massive sand (S_m) in the sheet flood facies association. (Int= intraclast, Carb = carbonate, Zebra = clay with zebra-like texture, Char Bio = charophyte bioclast, Ostr = ostracod, Meta. Frag = metamorphic rock fragment, PPL = Plane polarized light, XPL = Crossed polarized light).

The lake margin and lacustrine F.A. are predominately composed of clay, with the most in situ clay found within the lake margin F.A. (average 62%; maximum 72%), and slightly less in the lacustrine F.A. (average 47%; maximum 59%). Cl_m has the highest abundance of reworked clays (average 15%; maximum 21%), mostly peloids, compared to the Cl_l (average 6%; maximum 16%). The sheet flood F.A. shows very little reworked clay content (average 1%; maximum 3%).

The dominant clay facies in both lake margin and lacustrine F.A.s displayed different textures microscopically, occurring as highly-crystalline, intraclastic and/or zebra-like clay. Highly-crystalline clay was identified as clay composed of well-formed, homogenous platelets, intraclastic as displaying areas with different texture and/or orientation, and zebra-like as composed of large, lenticular clay platelets that resemble a zebra pattern (Figures 9 and 10). Highly-crystalline clay is the most common texture in the study core.

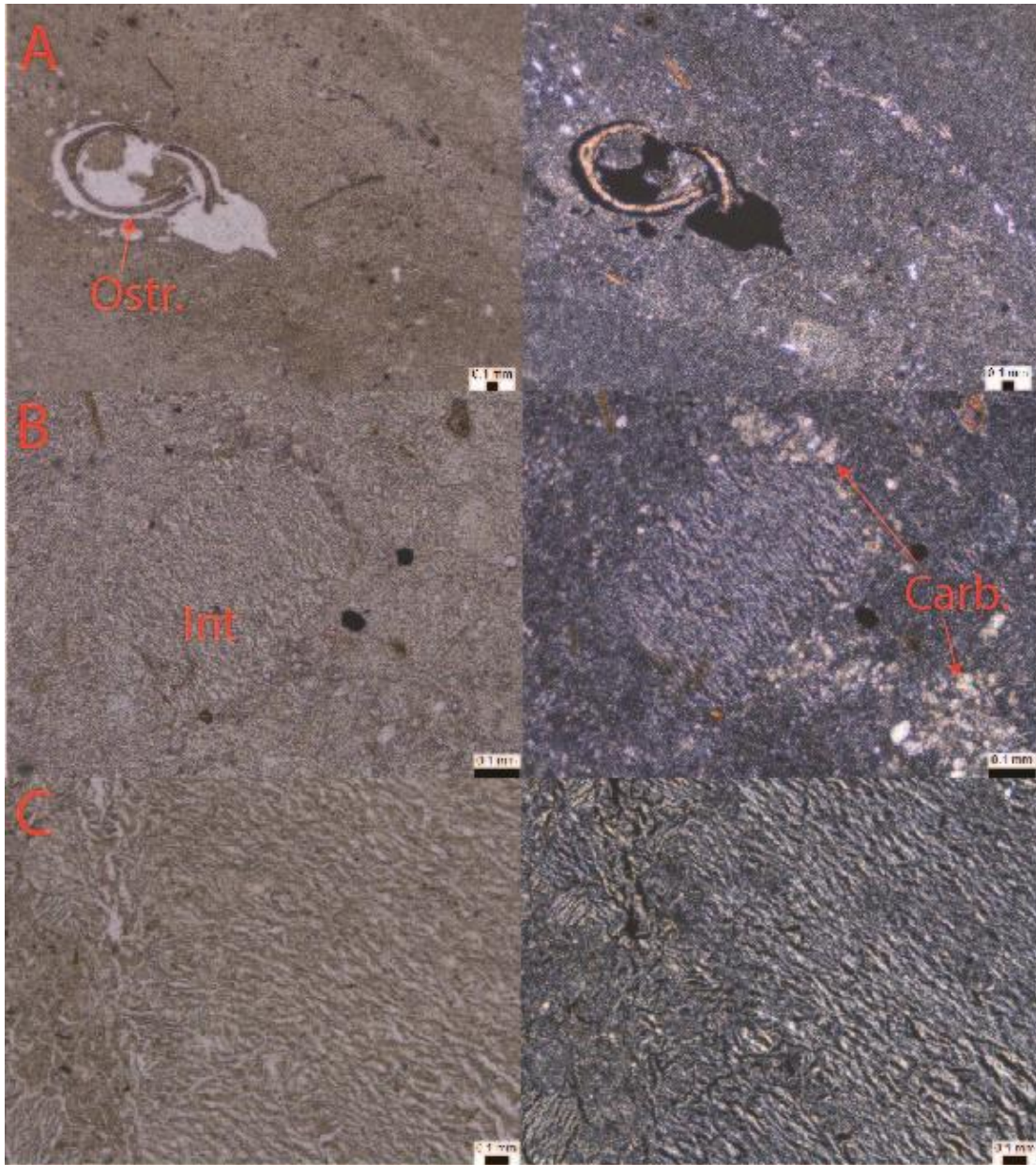


Figure 9: Photomicrographs of clay textures. A: highly-crystalline, B: Intraclastic, C: Zebra texture. (Ostr = Ostracod, Int = Intraclastic, Carb = Carbonate)

Primary Composition

The most abundant primary constituent in LP is clay minerals, mostly occurring in the lake margin and lacustrine F.A.s (total clay average 77% and 53%; maximum 85% and 69%, respectively), in comparison to the sheet flood F.A. (total clay average 12%; maximum 23%). Carbonate primary constituents are found only in the lake margin and more abundantly in the lacustrine F.A.s, while being conspicuously absent in the sheet flood. Bioconstructions (average 2%; maximum 14% in lacustrine F.A., and average < 1% in lake margin F.A.) include microbial buildups, stromatolites and thrombolites (Figure 10A-B).

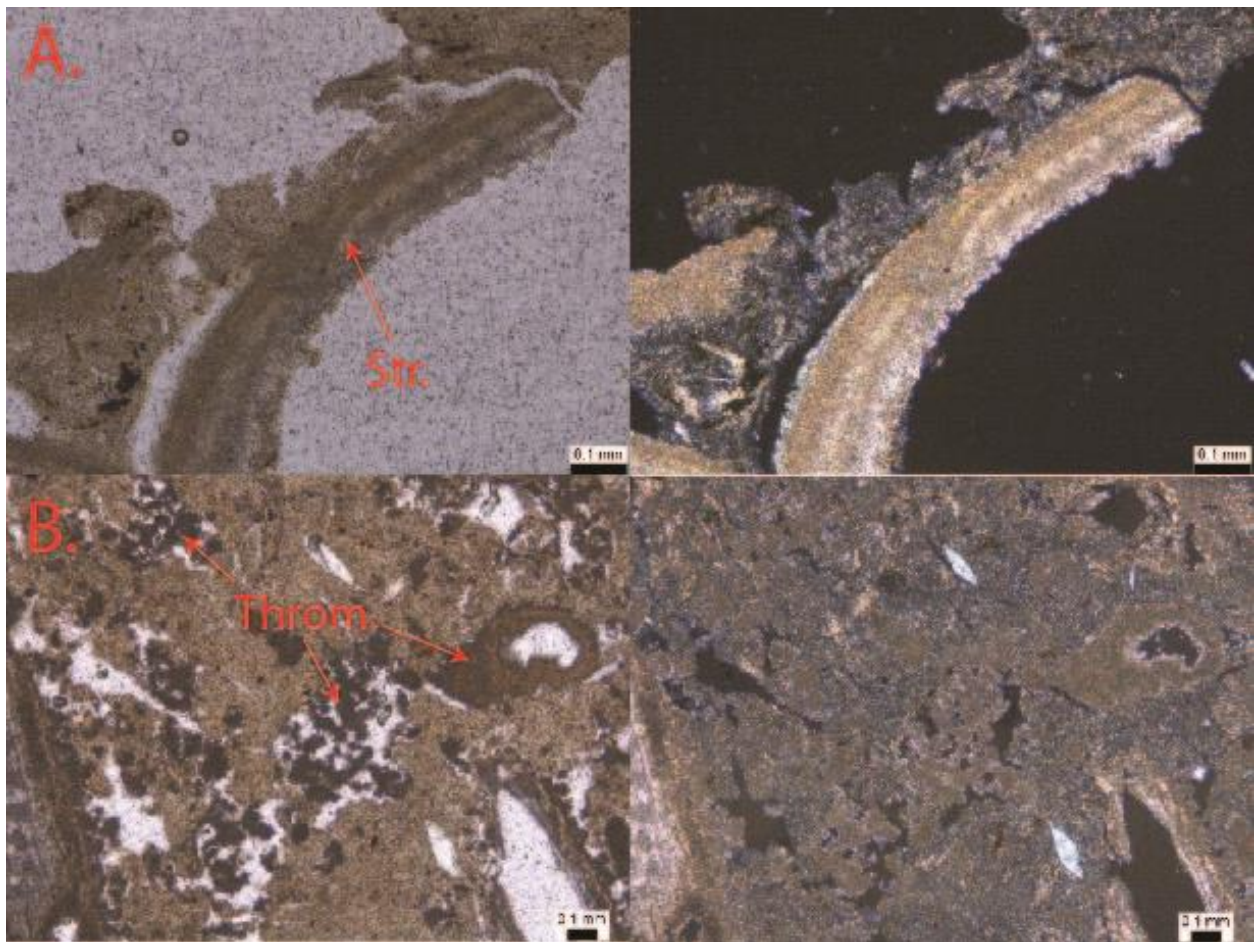


Figure 10: Bioconstructions found in LP. A: Stromatolites, B: Thrombolites. (Plane Polarized images on the left and Cross Polarized on the right).

Other carbonate particles include ooids, peloids and intraclasts (average 4%; maximum 8% in lacustrine F.A., and average 2%; maximum 4%; in lake margin F.A.); and carbonate bioclasts, including charophytes, ostracods and undifferentiated carbonate bioclasts (average 13%; maximum 27% in lacustrine F.A., and average 2%; maximum 3%; in lake margin F.A.) (Figure 11A-C). Non-carbonate bioclasts, including diatoms, organic-walled organisms (Arcella, filled by round carbonates) and phosphatic bioclasts (Figure 11D-E), are present in both the lake margin (average 2%; maximum 3%) and the lacustrine (average 2%; maximum 5%) F.A.

Carbonaceous organic matter is a minor constituent of the lacustrine (Average 3%; Maximum 10%) and lake margin (Average 2%; Maximum 3%) F.A., but it is absent in the sheet flood F.A.

Extrabasinal grains are mostly found in the sheet flood F.A., although they can also occur in the lake margin and lacustrine F.A. (Average 1%; Maximum 2-3%) Rock fragments are the dominant primary constituent in the sheet flood F.A. (Average 22%; Maximum 41%), with phyllites accounting for the majority of it (Average 12%; Maximum 23%) (Figure 11F). Other extrabasinal grains, such as quartz, feldspar, plagioclase, biotite, and other lithics are all minor constituents, averaging less than 1%.

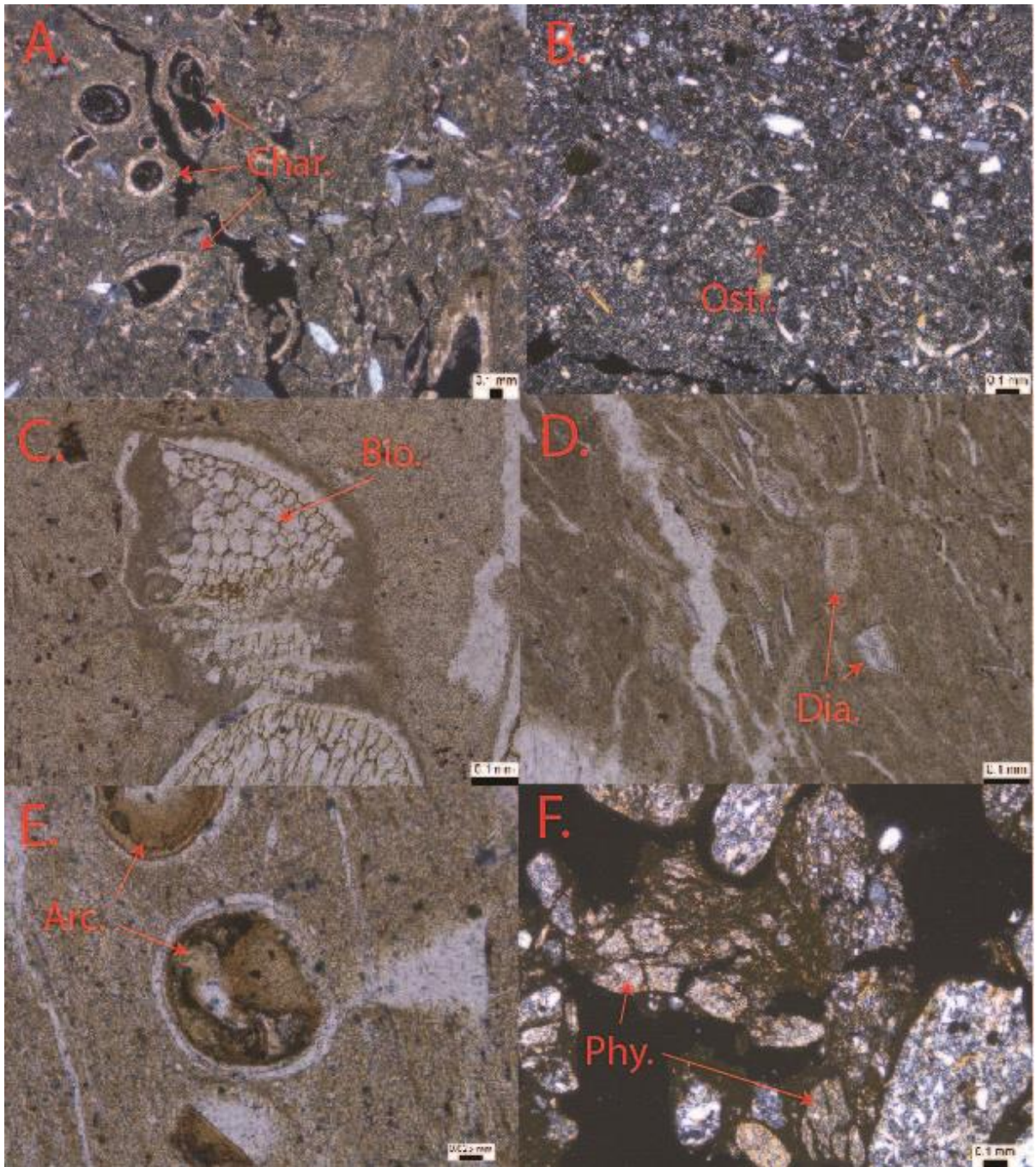


Figure 11: Primary constituents found in LP. A: Charophytes in a crystalline mud (XPL), B: Ostracod and ostracod fragments within a clayey-sandy matrix (XPL), C: Undifferentiated bioclasts (PPL), D: Diatoms (PPL), E: Arcella not replaced by round carbonate (PPL), F: Phyllites present in S_m F.A. (XPL) (Char = charophyte, Ostr = ostracod, Bio = Undifferentiated Bioclast, Dia = Diatoms, Arc = Arcella, Phy = Phyllite PPL= Plane Polarized Light, XPL = Cross Polarized Light)

Diagenetic constituents

The diagenetic components, from most to least abundant, include calcite (microcrystalline, mosaic, prismatic, anhedral, round), gypsum (lenticular, prismatic, rosette), Fe oxide, pyrite, aragonite, siderite, and jarosite. Overall, diagenetic constituents are more prevalent in the lacustrine facies association, followed by the lake margin facies association.

Calcite is present in every sample from both the lake margin and the lacustrine F.A.'s (total calcite average: 5%; maximum 14%). Calcite is typically microcrystalline (average 3%; maximum 4% in the lacustrine F.A., and average 2%; maximum 11% in the lake margin F.A.). The maximum value in the lake margin F.A. corresponds to the presence of millimetric microcrystalline laminations in one of the samples at 4.92 m (Figure 12A). Microcrystalline calcite replaces the siliciclastic mud matrix and/or fills shelter pores. Despite the fact that microcrystalline calcite was quantified as a diagenetic constituent, it is possible that part of it (or locally most of it, like in the calcite laminations mentioned above) is actually a primary constituent, hence forming hybrid sediments. Mosaic, prismatic, and anhedral calcite (Figure 12B) were only found in the lacustrine F.A. ("total other calcite" average 2%; maximum 10%), replacing or covering bioclasts. Round carbonates (Figure 12C) are intraparticle pore-fills of organic-walled algae (*Arcella?*) found in both lacustrine (average 2%; maximum 6%) and lake margin (average 2%; maximum 5%) F.A.

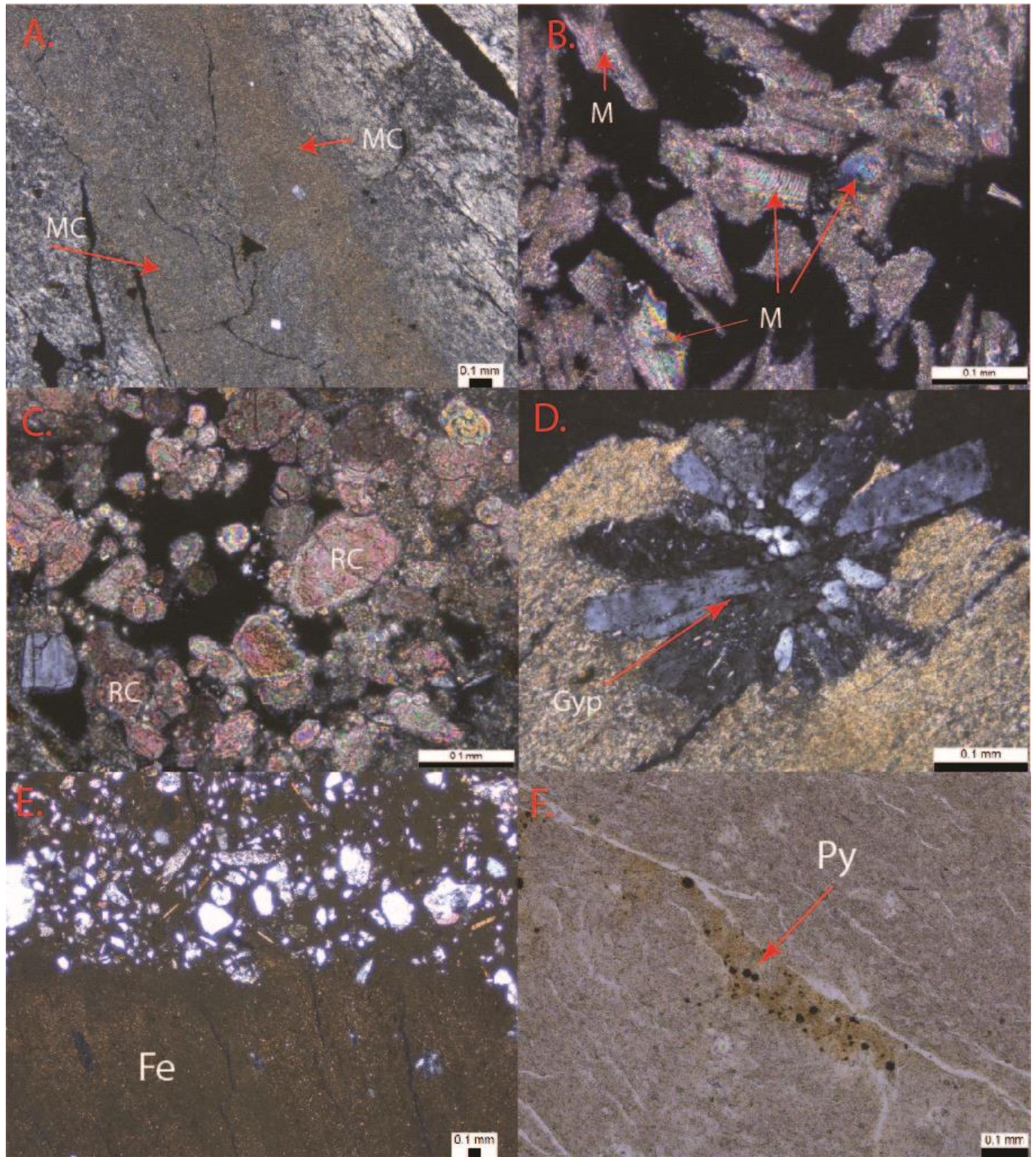


Figure 12: Representative photomicrographs of diagenetic constituents observed within thin sections. A: Microcrystalline carbonate lamination within a clay matrix (XPL). B: Mosaic carbonate, stained with alizarin, replacing charophyte fragments (XPL). C: “Round” carbonate, stained with alizarin (XPL). D: Gypsum crystals displacing mud (XPL). E: Fe oxide replacing mud in sheet flood facies (XPL). F: Pyrite framboids replacing mud (PPL). (MC = Microcrystalline, M = Mosaic, RC = “Round” carbonate, Gyp = Gypsum , Fe = Iron Oxide, Py = Pyrite.)

Gypsum occurrence is not dependent on facies associations at all, but is instead related to depth. This constituent occurs only below the depth of 2.65 m, and it is relatively abundant (average 2%; maximum 12%) in the lower half of the core down to 5.6 m, with the exception of the sample at 5.54 m, which is devoid of gypsum. It mostly displaces (and subordinately replaces) the siliciclastic mud matrix (Figure 12D). Gypsum habits do not correlate with depth or any specific facies.

Microcrystalline Fe oxide only occurs in the sheet flood F.A. It is abundant in this F.A. (average 45%; maximum 64%), cementing and replacing siliciclastic mud matrix (Figure 12E), occurring in minor amount in the other F.A.

Framboidal pyrite occurs in every studied thin sections, replacing siliciclastic mud matrix (Figure 12F) and filling shelter pores. Pyrite abundance is comparable in the lake margin (average 4%; maximum 5%) and lacustrine (average 3%; maximum 6%) facies associations.

Minor amounts of aragonite occurs in the lacustrine (average 1%; maximum 4%), and rarely in the lake margin (average <1%, maximum 2%) facies associations. No aragonite was found in the sheet flood F.A. Aragonite occurs as acicular crystals that form a rim around primary constituents (Figure 13A and 13B). Another diagenetic carbonate (spherulites) (Figure 13C) was observed in one thin section, but in such minor amounts that it was not enough to be quantifiable.

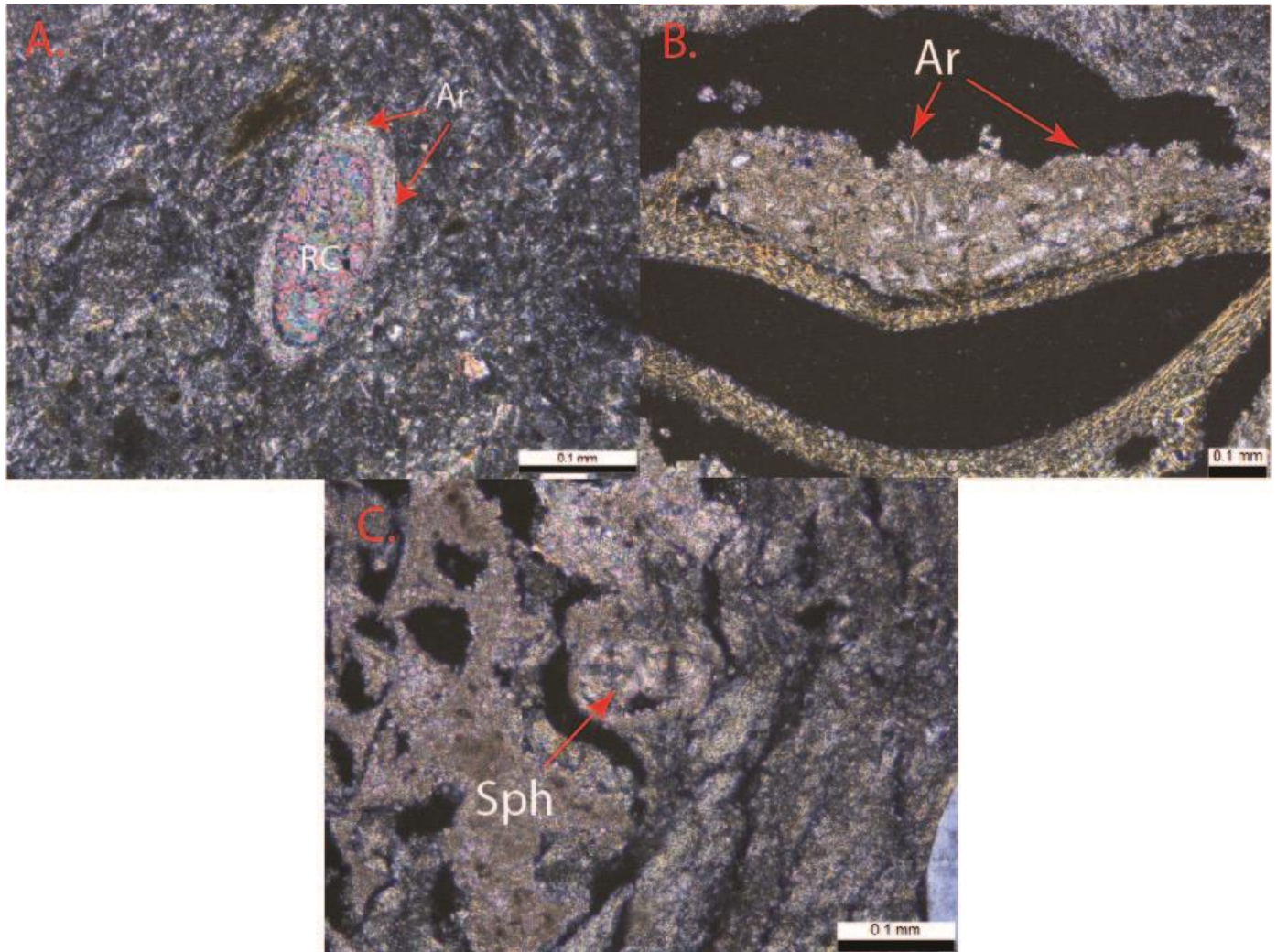


Figure 13: Representative photomicrographs of diagenetic constituents in thin sections. A: Aragonite crystals growing off of a “Round” carbonate stained with alizarin B: Aragonite crystals growing off of bioclast. C: Rare spherulites developing in a carbonate/clay matrix. (Ar= Aragonite Sph= carbonate spherulites)

Porosity (as fracture, growth framework, intergranular, intragranular, shelter, shrinkage, and vug pores) was quantified as part of the modal point-counting. However, porosity was not evaluated, since the core comprises unconsolidated sediments and handling of these soft sediments during thin section preparation possibly created artifacts that could be interpreted as primary pores.

Complementary Analyses

1. X-ray diffraction

XRD diffractograms for the analyzed samples can be found in Appendix 3. XRD analysis shows that the clay fraction is rich in micas, illite, phlogopite, halloysite, as well as gismondine, a zeolite typically found in basaltic lavas. Gismondine naturally forms in areas where volcanic rocks react with alkaline groundwater, leading to the chemical weathering that produces said mineral. Illite was observed with a strong peak at the correct angstrom for identification as well as the list of best match minerals provided by SMU. There are no swelling clay minerals (as evidenced by a lack of change in the peak position in glycolated analyses). XRD analysis shows that clay mineralogy does not vary in any section of the study core, and that Mg-clays are not present in LP, as initially hypothesized. Instead it contains Al-clays, like halloysite.

2. X-ray fluorescence

Elemental concentrations (Mg, Ca, Fe, Si, Ti, Al, Zr, Sr, Cu and Ni) obtained from XRF analysis (Appendix 4) were used to calculate the indices shown in Figure 7. Variations in these indices along the core (Figure 7) suggest the existence of three distinct intervals. The highest values are found from the base of the core to roughly 5.2 m for all of the indices, except for Si/Ti, which has moderate values. From 5.2 to 4.4 m, the core displays another interval with the low values for all indices, once again except for Si/Ti, which has high values during this interval. From 4.4 to the top, all indices display moderate values.

The positive linear correlation in the crossplot between Mg/Ca and Sr/Ca (Figure 14) with both Pearson and Spearman coefficients (r^2 and ρ) suggests a salinity control in these indices (De Deckker & Forester, 1988).

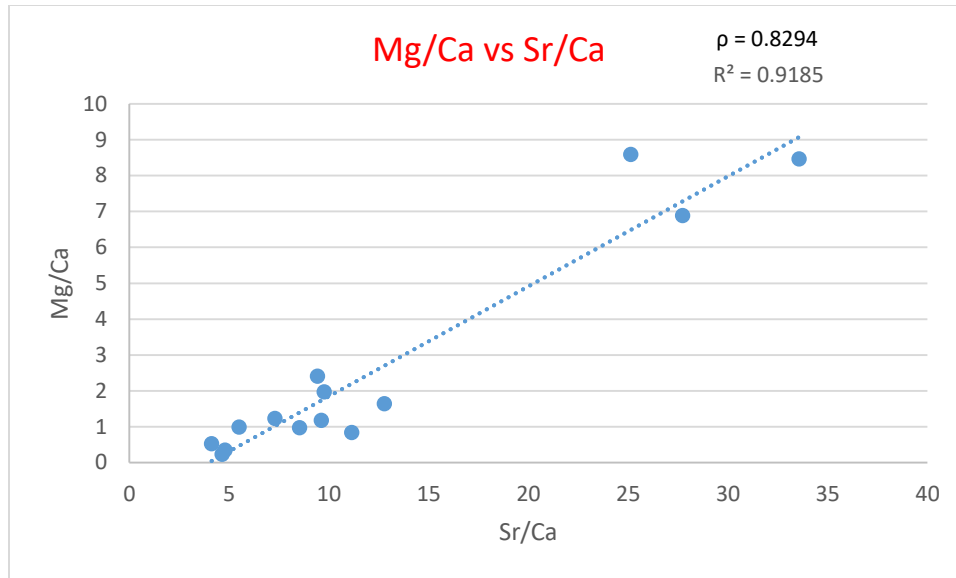


Figure 14: Scatter plot of Mg/Ca vs Sr/Ca. One data point with abnormally high ratios of Mg/Ca and Sr/Ca is not shown, despite falling along the observed trendline.

The positive correlation between Fe/Al with both Cu/Al and Ni/Al suggests that the primary productivity in the lake may be controlling the degree of oxygenation in LP due to the increase in Cu and Ni with Fe (Figures 15 and 16). Enrichments in reactive iron occur under euxinic conditions, as a result of iron being scavenged from the euxinic water column during syngenetic pyrite formation and deposited in the underlying sediments (Lyons & Severmann, 2006). Cu and Ni behave as micronutrients and are delivered to the sediments in close association with organic matter, and therefore are used as proxies for the organic carbon sinking flux (Tribovillard et al., 2006).

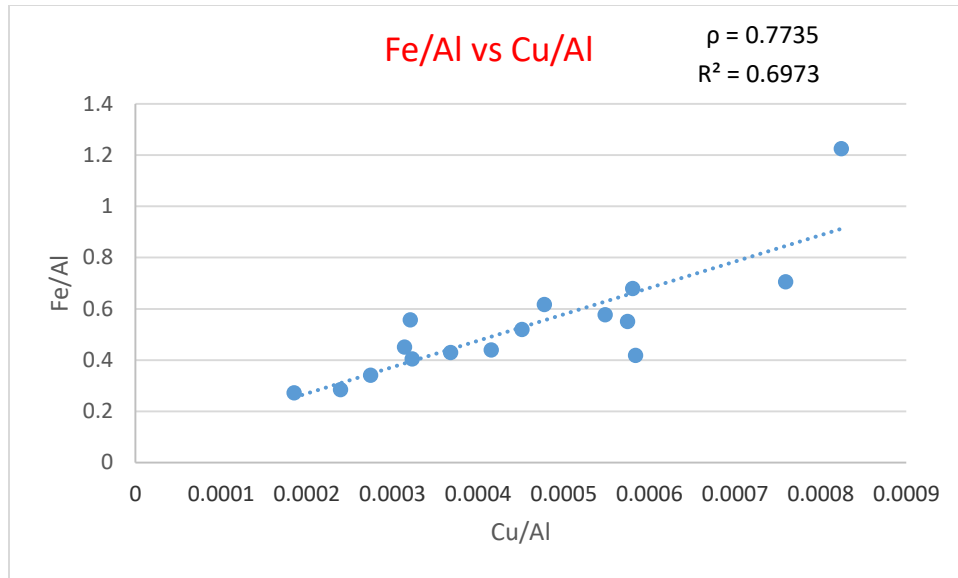


Figure 15: Scatter plot of Fe/Al vs Cu/Al

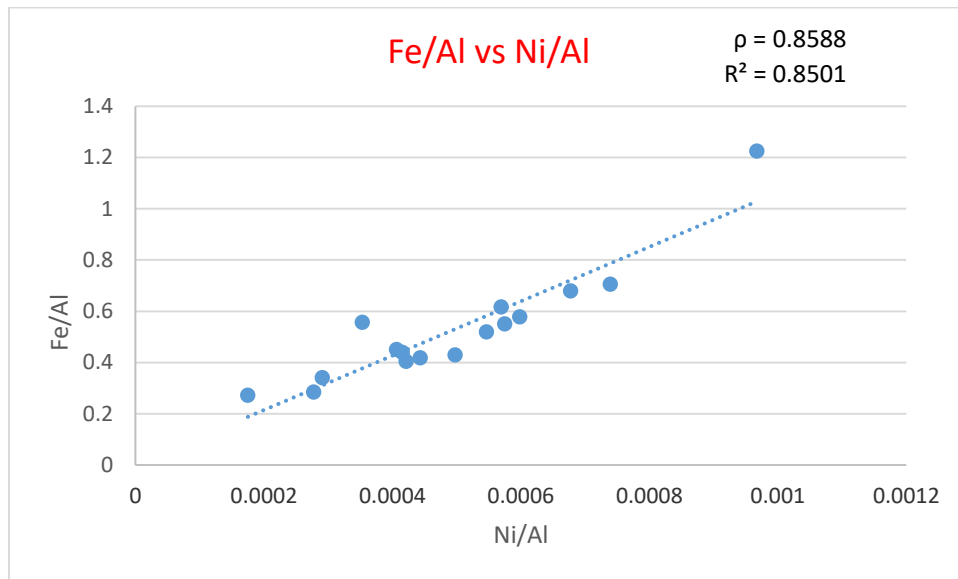


Figure 16: Scatter plot of Fe/Al vs Ni/Al

The positive correlation between Si/Al vs Zr/Al (Figure 17) suggests that the silica in the samples analyzed is mostly a result of detrital input, rather than biogenic contribution. Zr is present in zircon, igneous in origin but also common in the heavy mineral assemblage in

sediments (Taylor & McLennan, 1985), while Si is present both in silicate minerals and siliceous organisms.

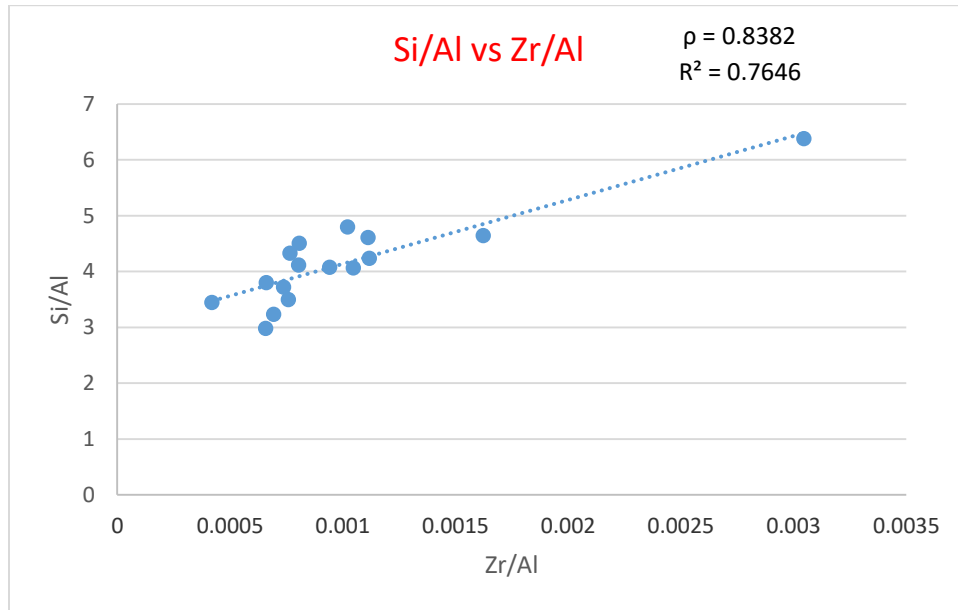


Figure 17: Scatter plot of Si/Al vs Zr/Al

3. Isotopic analysis

Values for $\delta^{18}\text{O}$ range from -3.1 (at a depth of 4.65 m) to +4.6 ‰ (at a depth of 4.3 m), and for $\delta^{13}\text{C}$ from -1.8 (at 1.55 m) to +2.3 ‰ (at 4.92 m) (Figure 18). Most of the samples lie along a trend consistent with a lacustrine environment with variable salinity (Leng & Marshall, 2004), from positive to negative, covariant $\delta^{18}\text{O}$ and $\delta^{13}\text{C}$. Covariance between oxygen and carbon isotopic signatures suggest that LP is a closed basin (McGlue et al., 2013). Values that fall off of this trend may be due to pedogenic alteration or increased bioturbation (Cerling, 1991).

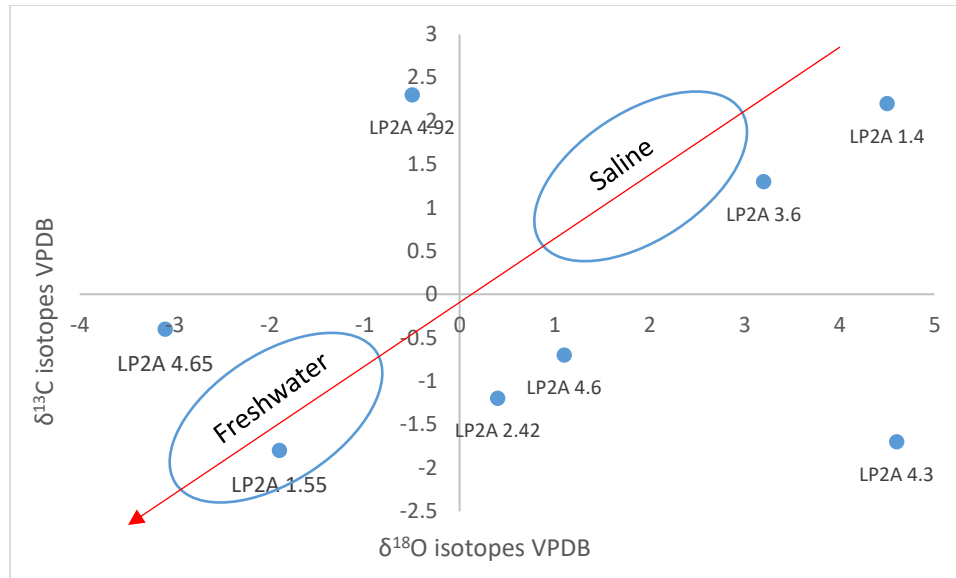


Figure 18: Carbon and oxygen isotopic values suggestive of decreasing salinity (arrow), from saline to freshwater lake. Ovals represent $\delta^{18}\text{O}$ and $\delta^{13}\text{C}$ the regions of ratios where freshwater and saline lakes are typically found. Not Approximate. (Leng & Marshall, 2004).

$\delta^{18}\text{O}$ values of precipitation among Puna Basins, similar in elevation and latitude to LP, show light $\delta^{18}\text{O}$ values (ranging from -7 to -20‰; Jordan et al., 2019), much lower than LP, highlighting that evaporation is an important factor in LP and evidence of high salinity (Gierlowski-Kordesch, 2010).

4. Spectral Analysis

Reflectance data were transformed into coefficients using multiple linear regression (Table 3). Negative coefficients mean negative relationships between the leading variable primary component (VPC) and the given pigment/sediment. For instance, gypsum has a coefficient of -0.82 which means higher VPC 3 scores would represent less gypsum and vice versa.

Table 3: Leading Variable Primary Components (VPCs) and their corresponding mineral/pigment assemblages

VPC	% of Variance explained	Pigment/mineral mixture	coefficients	Correlation R
1	46.326	Calcite+ (Chlorite+Smectite)	Calcite -0.26 (Chlorite+Smectite) -0.83	0.94
2	36.045	Neoxanthin+hematite+illite(not smectite)	neoxanthin 0.32 hematite 0.48 illite 0.86	0.91
3	9.408	gypsum	gypsum -0.82	0.84
4	4.321	Phycocyanin+chlorophyll C+neoxanthin (diatoms, cyanobacteria, etc.)	phycocyanin 0.4 chlorophyll-c drdl -1.05 neoxanthin drdl 0.54	0.98

The results of linear regression from the spectral analysis highlights four primary components that explain 96% of the reflectance data. The main primary component (explaining 46% of the reflectance data) is a mixture of calcite and, subordinately, chlorite plus smectite (Figure 19). The second component is a mixture of neoxanthin, hematite and illite. The third primary component is gypsum, and the fourth a mixture of phycocyanin, chlorophyll c and neoxanthin. This fourth component is representative of the cyanobacteria present in the core.

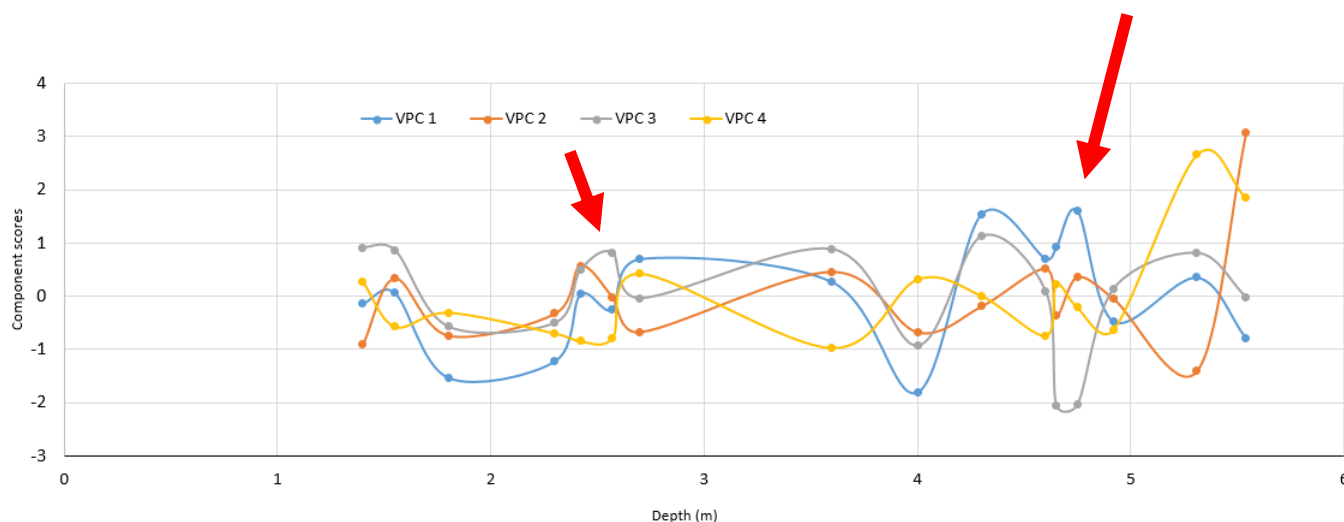


Figure 19: Variation of the VPCs in core LP06-2A according to depth

The results of spectral analysis indicate a strong cyclicity in these components, with strong covariation between VPC 1 (calcite, subordinately chlorite + smectite) and VPC 3 (gypsum), except for two points at 4.75 meters and 2.57 (arrows) meters, which inverse correlations may be due to their location in the transition of lake margin and lacustrine zones. There also is an inverse correlation between VPC 2 (hematite + illite) and 4 (pigments representing plants, cyanobacteria and algae). This covariation may be modulated by climate, as discussed below.

VPC 4 could potentially be used as a primary productivity index, since it derives from autotrophs like diatoms, brown algae, dinoflagellates and cyanobacteria. In this case, spikes in this component would correlate with planktonic blooms.

Discussion

Depositional Environments

The facies associations identified in Laguna de los Pozuelos are key to understanding the development of the lake and associated depositional environments. The sheet flood F.A., interpreted as having formed by flood events resulting from high precipitation episodes and snowpack melts during the spring and summer months, occurs only at the base of the study core, from 5.31 m to 5.65 m (Figure 7). Sheet flood events are typical of semi-arid and arid settings, much like what altered the LP region 43 kyr ago (McGlue et al., 2012). The sheet flood F.A. is followed by a lake margin F.A. from 4.75 m to 5.31 m. This is evidence of an increase in the base level, probably the consequence of a wetter period, with a higher lake level indicated by the larger percentage of clays than sands as compared to the sheet flood F.A. This is followed by an interval of lacustrine F.A. from 4.15 m to 4.75 m, marking a period of persistently deeper lake in the basin from 37 to 43 kyr ago (McGlue et al. 2013). This interval corresponds to the maximum flooding in the studied LP core, and it marks a change in the chemical indices between intervals 2 and 3 (Figure 7). From that point upwards in the core, the sedimentological record shows a cyclicity in LP, with alternating lake margin and lacustrine F.A. to the top of the core (Figure 7). This high frequency cyclicity, also apparent in the results of spectral analysis (discussed below), starts with an initial wetting and increase in water levels (from the base to 4.15 m deep), followed by partial dry-out, with periodic expansion and contraction of the lake margins. During periods of lake contraction, vegetation colonizes formerly lacustrine areas along the lake margin. This is evident by observations of root traces within lake margin thin sections. The location of the study core, in a marginal area of the current lake, favors the detection of variations in the position of lake margins.

The interpretation of increased aridity at the base of LP is based on the presence of gypsum, and chemical and isotopic indicators (discussed below). However, this interpretation conflicts with past research (McGlue et al. 2012; 2013), which interprets the depositional environments in LP as changing from profundal, to palustrine, to a saline lake, from base to top of the core. Former interpretations were also based on F.A.'s and age dating, but lacked the complementary data, such as XRF chemical indices and $\delta^{18}\text{O}$.

The alternation between lake margin and lacustrine environments is also shown by the different clay constituents and textures. Clay peloids are found in both the lake margin and lacustrine F.A. and are potentially a result of low-energy wave action, rolling the mud into these peloidal shapes. Peloids are also potentially formed by fecal pellets (Macintyre, 1985) and can be either abiotic or biotic in origin (Bosak et al, 2004). In LP, it appears that the peloids are mostly abiotic, i.e. non-fecal pellets, showing minimal to non-existent carbonate growth or biotic textures (Perri et al., 2013) within the clay peloid.

Clay intraclasts are interpreted as resulting from slight reworking of mud by weak currents and/or waves, mostly associated with periods of lake contraction.

The zebra-like texture is found in the core from depths of 2.42 m to 3.6 m. It is mostly present in the lake margin, and subordinately in the lacustrine F.A. Since this texture does not appear to correlate with a specific F.A. or facies, it is possible that the zebra-like texture is controlled by environmental and/or climatic factors. For example, this could be a result of desiccation and evaporation within the sediments, leading the clay to expand and create "empty pockets" that have the appearance of zebra stripes. The scarcity of swelling clays (smectites), however, does not favor this hypothesis. Another possibility is that this texture develops through

freeze-thaw of the clay, as Laguna de los Pozuelos is located at high altitude and the temperature gradient within the basin is conducive to freeze-thaw cycles.

Stratigraphic Evolution and Paleoclimate

Sedimentological, isotopic and spectral data indicate that Laguna de los Pozuelos underwent cyclical changes during basin evolution. As discussed above, the facies associations suggest a high-frequency cyclicity of a few thousand years superimposed on a cycle of a higher-order (> 10,000 years), as the entire lower half of the core displays displacive gypsum crystals (indicative of lower precipitation-to-evaporation rates) that are absent in the top half (suggesting higher precipitation-to-evaporation). From the behavior of chemical indices and sedimentary facies, three intervals can be identified. From base to top, interval 1 ends at 5.2 m deep, interval 2 has an upper boundary at around 4.4 m, and the third interval includes the rest of the samples, up to the top (1.4 m).

Likewise, cyclicity displayed in the reflectance data may be climatically-controlled and representative of lake contraction and expansion.

During the past 43 kyr, (McGlue et al., 2013), variations in water levels seem to be part of the dynamics in LP during the past decades (Figure 20), probably in response to changing climatic conditions within the region. These variations also resulted in the development of pyrite throughout the core as a result of anaerobic conditions during periods of consistent lake levels. Isotopic signatures and the presence of gypsum in the deeper sections of the core suggest a change from saline to freshwater conditions, resulting in an underfilled basin, with accommodation exceeding the rate of sedimentation in the lake (McGlue et al., 2013). The $\delta^{18}\text{O}$ signatures are compatible with what is expected for a closed basin lake (Leng & Marshall, 2004).

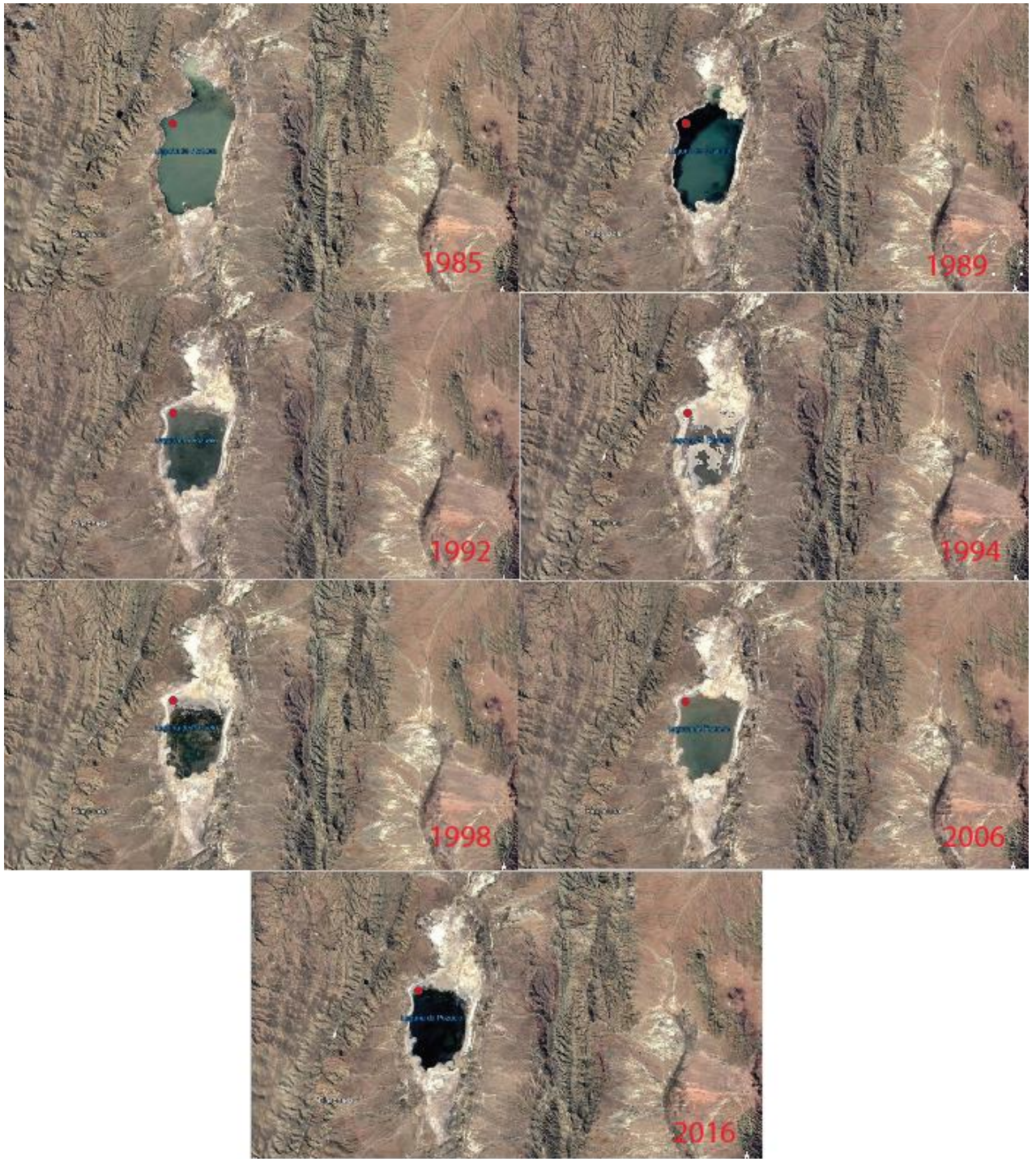


Figure 20: Composite Google Earth image showing water-level changes in Laguna de los Pozuelos. Red circle is the location of the study core.

The decline in $\delta^{18}\text{O}$ during interval 2 suggests wetter conditions in LP during this time. This theory is backed by existing research showing that the region was wetter than present day (McGlue et al., 2013). The $\delta^{18}\text{O}$ and $\delta^{13}\text{C}$ isotopes are observed interacting on a similar cyclicity and intervals as seen within the reflectance data and chemical indices (figure 21). This again highlights that LP may be climatically controlled and cycling between freshwater and saline lake chemistry throughout the last 43 kyr.

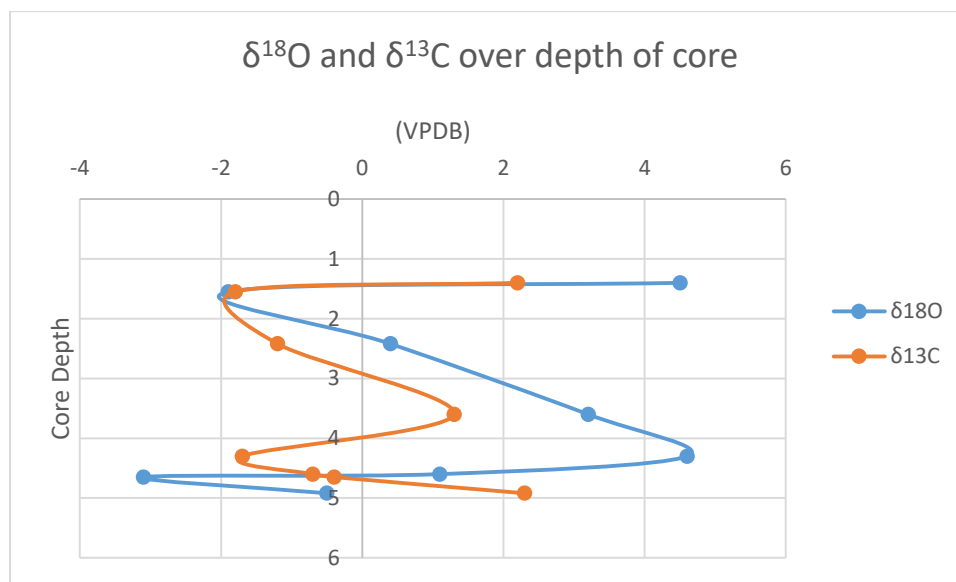


Figure 21: Oxygen and carbon isotopes plotted along the depth of LP’s sedimentary core.

Clay minerals in LP are illite and halloysite, both non-swelling aluminosilicates, in addition to phlogopite, a Mg-rich mica. Illite can form in high altitudes (Velde and Meunier, 2008), much like where Laguna de los Pozuelos is located, as well as during diagenesis from smectite in dry environments (Eberl, 1993). However, illite development from smectite requires deep burial, and/or high K^+ activity. Since smectite is likely not present in LP (or at least, not abundant, since spectral analysis indicates smectite and chlorite), and it is unlikely that these sediments were deeply buried (considering that they are still unconsolidated), illite in LP was probably not formed

by diagenetic transformation of smectite. Illite also preferentially develops in dry salt-rich, evaporitic environments (Singer, 1984), much like what Laguna de los Pozuelos appears to have been for the last 43 kyr. It is also potentially detrital in origin, being transported in from the surrounding regions. But the quantity and past environment suggests it developed within LP.

The absence of Mg-clays and other smectites in LP suggests that it does not have the required chemistry to produce clays analogous to those found in the pre-salt reservoirs, where Mg-silicates are needed to produce the gels that prompt the precipitations of carbonate spherulites and shrubs prevalent in those rocks. The Mg percentages of the weathered and erosional sediments transported into the lake are too low to generate said carbonates. The scarcity of carbonates in LP also suggest that this alkaline lake is not a good analog for the formation of pre-salt reservoirs.

Controls on Carbonate Precipitation

The key factors that influence carbonate deposition include Mg/Ca ratio, temperature, carbonate saturation, and microbial activity (Dupraz et al, 2004; Mercedes-Martin et al, 2016; Morse et al, 1997). The Mg/Ca ratio is an important factor in determining the carbonate mineralogy (Rushdi et al, 1992) (e.g. aragonite and/or calcite). Any variation in the Mg/Ca ratio will affect the proportion of mineral assemblages, with precipitation of calcite or aragonite. An Mg/Ca ratio of 1:1 or lower will produce calcite (Morse et al, 1997) (figure 22). At higher ratios, it will produce Mg-rich calcite and then aragonite, or just aragonite, depending on the temperature (Figure 22). This points to the fact that temperature is another important factor in carbonate precipitation, equally if not more influential than Mg/Ca ratio in determining carbonate mineralogy within a system (Kießling, 2015). A higher temperature system will typically produce more aragonite than a low temperature system, which is more favorable for calcite precipitation.

Saturation is important to determine whether there is enough carbonate in solution to precipitate out, as well as to control the habits (crystal shape and size). Lastly, microbial activity also tends to affect the development of the carbonates. Biotic mediation will control carbonate micro- and macrostructure, forming stromatolites, spherulites, thrombolites etc. (Dupraz et al 2004).

The carbonate system in LP appears to favor the precipitation of calcite over aragonite, with a Mg/Ca ratio (calculated from all XRF data) close to 5.5:1, which would favor aragonite precipitation. However, if the ratio is calculated disregarding the one spurious data point in the Mg/Ca data (51:1) that is clearly an outlier, the new Mg/Ca ratio is 2.5:1. This new ratio is consistent with the current average temperature of this region of around ten degrees Celsius (Legates & Willmott, 1990a,b), as well as the paleoclimate, with this region just coming out of the last glacial period approximately 11,700 years ago. Petrographic analysis shows the common occurrence of calcite, with very little aragonite, which is found to grow off of the calcitic carbonate. The temperature of the region throughout its paleohistory ties well into the Mg/Ca ratio, which helps inhibit the development of the aragonite, with primary components being 56% calcite, chlorite and smectite.

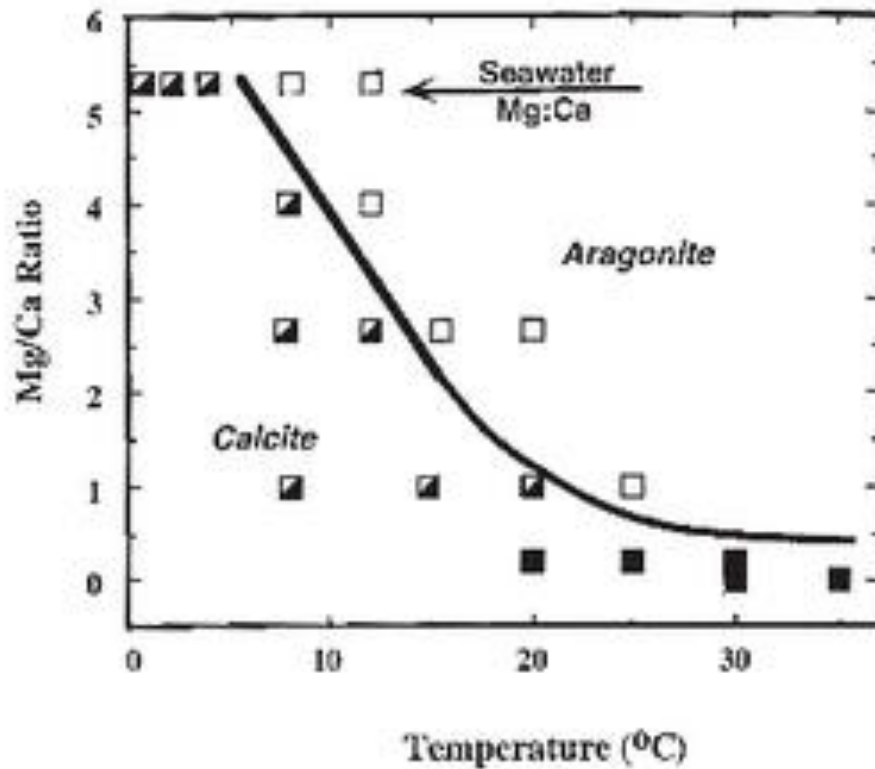


Figure 22: Influence of solution Mg:Ca ratio and temperature on CaCO_3 polymorph formed pseudohomogenous precipitates. White squares are aragonite, black squares are calcite, and split squares are situations in which calcite initially precipitates but then aragonite grows on calcite (Morse et al., 1997).

The total carbonate content in LP is less than 12% of the hybrid sediments. Carbonate precipitation seems to be a result of both organic and inorganic processes. Carbonate particles are mostly in the form of bioclasts (charophytes and ostracods), locally bioconstructions (stromatolites, thrombolites, rare shrubs) indicative of microbial precipitation. The typical bioclastic carbonates are charophyte gyrogonites (Figure 23A).

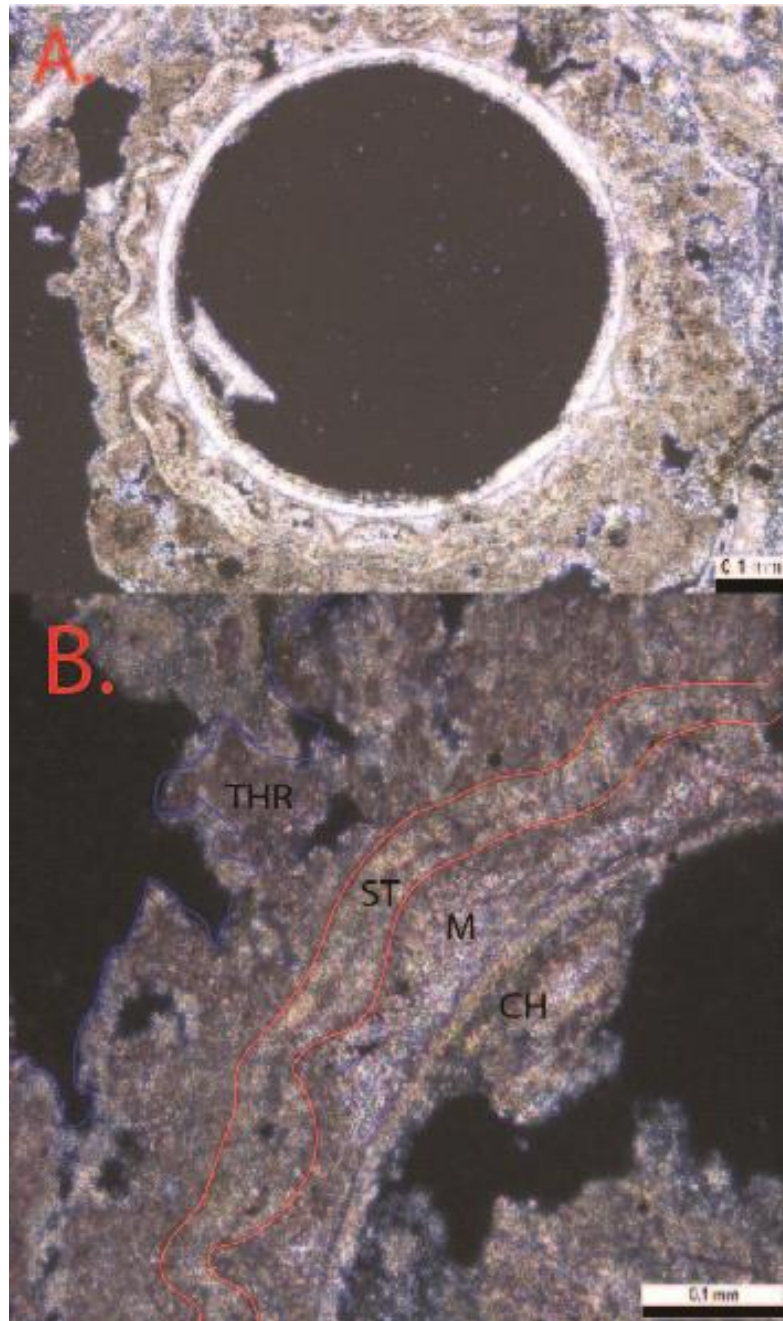


Figure 23: A: Transversal cut of a Charophyte gyrogonite (taken from 4.6 m 10X XPL). B: Charophyte replaced by mosaic carbonate and overgrown by stromatolitic and thrombolitic bioconstructions (taken from 4.6 m 20X XPL).

These bioclasts occasionally develop a mosaic texture from replacement of the shell by diagenetic calcite. Carbonate stromatolites and thrombolites are biotic in nature and precipitated

preferentially around charophyte bioclasts (Figure 23B). A few carbonate shrubs, i.e two shrubs, similar to what is found in the pre-salt reservoirs, were observed in one of the studied thin sections, not enough for a meaningful comparison.

Round and mosaic calcite, and aragonite, were formed in minor amounts during diagenesis. Spherulites were only rarely observed.

Despite the expectation that the sedimentary processes in LP could serve as analogs for carbonate precipitation in the pre-salt reservoirs, the results of the analyses carried out in LP06-2A indicate substantial differences between them. The pre-salt reservoirs, specifically in the Santos Basin, are composed of up to 95% of calcite, dolomite, and quartz, with clay content of 0-10% on average, up to 30% in localized areas (Vasquez et al., 2019). The study core from LP, on the other hand, is composed of mostly clay (average 62% in the lake margin F.A.; average 47% in the lacustrine F.A. and average 12% in the sheet flood F.A.), with very little, if any, carbonate. Carbonate content in LP is not high enough to be analogous to pre-salt reservoirs in either the lake margin (average 10%; maximum 16%) or lacustrine (average 25%; maximum 44%) facies associations, while not even occurring in the sheet flood F.A and, hence, it should not be used as an analog. Moreover, the high altitude of the Laguna de los Pozuelos (approximately 3600 m) is much different from the elevation in which the pre-salt reservoirs were formed (near or at sea level), which could potentially affect the development of specific types of carbonates as well. Finally, the precipitation of pre-salt carbonates (and porosity generation) are closely associated with Mg clays (and their diagenetic dissolution), and no Mg clays were found in the study core.

Conclusions

Laguna de los Pozuelos is a climatically-controlled lake in the Atacama Desert. Over the last 43,000 years this lake has gone through multiple lake cycles, recording the changes as facies associations related to lake expansion and contraction (sheet flood, lake margin, and lacustrine F.A.). The base of the study core was accumulated under a more arid environment where a shallow, saline lake was formed. Progressively wetter environments led to deepening and expansion of the lake, with a peak at around 4.5 m of depth. The top half of the core is characterized by an overall decrease in aridity and salinity, with high frequency expansion and contraction of the lake. Sediments are dominantly siliciclastic (clayey), with minor carbonate precipitation. Water chemistry seems to be characterized by mostly low Mg/Ca ratio, conducive to precipitation of calcite, rather than aragonite.

Carbonates comprise less than 12% of the total sediment in the study core. Carbonate particles are mostly bioclasts, with minor contribution of microbially-mediated precipitation as bioconstruction around bioclasts as a syngenetic process. Diagenetic carbonates are minimal, and include replacive calcite, particle-rimming aragonite and intraparticle pore-filling calcite.

Clay textures suggest mostly in-situ settling of clay, but portions of the core, specifically the lake margin F.A., contain peloidal and intraclastic clay suggestive of slight reworking, possibly by waves along the shoreline. The zebra-like textures in the clay are hypothesized to have formed from desiccation along lake margins and/or freezing-thawing processes associated with high altitudes.

Laguna de los Pozuelos does not have the necessary characteristics to serve as an analog for the pre-salt reservoirs. The water chemistry and sediment type are incompatible with the conditions required to produce the Mg-silicate gels and/or precipitate the expected amount and

texture of carbonates found in those reservoirs. Despite not offering insights into the genesis of the pre-salt reservoirs, the study core provided insights into the environmental and climatic changes that have happened in LP basin in the past 43,000 years.

References

- Alabaster, J.S. and Lloyd, R.S. (2013) *Water Quality Criteria for Freshwater Fish* (No. 3117). Elsevier, Amsterdam.
- Beasley, C.J., Fiduk, J.C., Bize, E., Boyd, A., Frydman, M., Zerilli, A., Dribus, J.R., Moreira, J.L.P., Pinto, A.C.C. 2010. Brazil's presalt play. *Oilfield Review* 22(3): 28-37.
- Becker, R. T., & Kirchgasser, W. T. (2007). *Devonian events and correlations*. London: The Geological Society. doi: 0.1144/SP278
- Bertani, R.T. and Carozzi, A.V. (1985), Lagoa Feia formation (Lower Cretaceous), Campos basin, offshore Brazil: rift valley stage lacustrine carbonate reservoirs - I. *Journal of Petroleum Geology*, 8: 37-58. doi:10.1111/j.1747-5457.1985.tb00190.x
- Best, Jim., & Bridge, John. (1992). The morphology and dynamics of low amplitude bedwaves upon upper stage plane beds and the preservation of planar laminae. *Sedimentology*, 39(5), 737-752. <https://doi.org/10.1111/j.1365-3091.1992.tb02150.x>
- Boever, Eva & T. Brasier, Alexander & Foubert, Anneleen & Kele, Sándor. (2017). What do we really know about early diagenesis of non-marine carbonates?. *Sedimentary Geology*, v. 361, p. 25-51
- Bosak, T., Souza-Egipsy, V. and Newman, D.K. (2004), A laboratory model of abiotic peloid formation. *Geobiology*, 2: 189-198. doi:10.1111/j.1472-4677.2004.00031.x
- Bouchard, F., Pienitz, R., Ortiz, J.D., Francus, P., Laurion, I., 2013. Palaeolimnological conditions inferred from fossil diatom assemblages and derivative spectral properties of sediments in thermos karst ponds of subarctic Quebec, Canada. *Boreas* 42 (3), 575–595.
- Bridge, J.S. and Best, J.L. (1988), Flow, sediment transport and bedform dynamics over the transition from dunes to upper-stage plane beds: implications for the formation of planar laminae. *Sedimentology*, 35: 753-763. doi:10.1111/j.1365-3091.1988.tb01249.x
- Calvert, S. & Pedersen, Thomas. (2007). Elemental proxies for paleoclimatic and palaeoceanographic variability in marine sediments: interpretation and application. *Developments in Marine Geology*. 1. 568-644.
- Camacho, María & Kulemeyer, julio José. (2017). The Quaternary of the Laguna de los Pozuelos Basin, Northern Puna, Argentina. 10.1007/978-3-319-54371-0_10.
- Carminatti, M., Wolff, B. & Gamboa, L. 2008. New exploratory frontiers in Brazil. *Proceedings of the 19th World Petroleum Congress*. Madrid, 2008.

- Cerling, T.E. 1991. Carbon dioxide in the atmosphere: evidence from Cenozoic and Mesozoic paleosols. *American Journal of Science*, 291: 377-400.
- Chitale, D.V., Alabi, G., Gramin, P., Lepley, S. & Piccoli, L., 2015, Reservoir Characterization Challenges Due to the Multiscale Spatial Heterogeneity in the Presalt Carbonate Sag Formation, North Campos Basin, Brazil. *Petrophysics*, v. 56, No. 6. p. 552–576.
- Clark, R.N., Swayze, G.A., Wise, R., Livo, E., Hoefen, T., Kokaly, R., Sutley, S.J., 2007. USGS Digital Spectral Library splib06a: U.S. Geological Survey, Digital Data Series 231.
- Clarkson, Matthew & Poulton, Simon & Wood, Rachel & Guilbaud, Romain. (2014). Assessing the utility of Fe/Al and Fe-speciation to record water column redox conditions in carbonate-rich sediments. *Chemical Geology*. 382. 10.1016/j.chemgeo.2014.05.031.
- Della Porta, G., Barilaro, F. & Ripamonti, M. 2011. Non-marine carbonates – Facies, diagenesis and porosity development. AAPG Search and Discovery article #30173.
- Della Porta, Giovanna. (2015). Carbonate build-ups in lacustrine, hydrothermal and fluvial settings: Comparing depositional geometry, fabric types and geochemical signature. Geological Society, London, Special Publications. 418. 10.1144/SP418.4.
- De Ros L.F., Golberg K., Abel M., Victoreti F., Mastella M., Castro E. 2007. Advanced acquisition and management of petrographic information from reservoir rocks using the Petroledge® System. *In: AAPG Annual Convention and Exhibition, Long Beach, Expanded Abstracts*.
- Dickson, J. A Modified Staining Technique for Carbonates in Thin Section. *Nature* 205, 587 (1965). <https://doi.org/10.1038/205587a0>
- Dupraz, Christophe & Visscher, Pieter & Baumgartner, K. & Reid, R.. (2004). Microbe-mineral interactions: early carbonate precipitation in a hypersaline lake (Eleuthera Island, Bahamas). *Sedimentology*. 51. 10.1111/j.1365-3091.2004.00649.x.
- Eberl, D.D. (1993). Three Zones for Illite Formation During Burial Diagenesis and Metamorphism. *Clays and Clay Minerals*, 41, 26-37.
- Eberl, D.D., 2003. User guide to RockJock—a program for determining quantitative mineralogy from X-ray diffraction data. USGS Open File Report OF 03-78p. 40.
- Eberl, D.D., 2004. Quantitative mineralogy of the Yukon River system: variations with reach and season, and determining sediment provenance. *American Mineralogist* 89, 1784–1794.
- Foix, Nicolás & Paredes, José & Giacosa, Raul. (2013). Fluvial architecture variations linked to changes in accommodation space: Río Chico Formation (Late Paleocene), Golfo San Jorge basin, Argentina. *Sedimentary Geology*. 294. 342-355. 10.1016/j.sedgeo.2013.07.001.

- Gangui, A.H. (1998) A combined structural interpretation based on seismic data and 3D gravity modeling in the northern Puna/Eastern Cordillera, Argentina. PhD Thesis, Freie Universität, Berlin, 176 pp.
- Gantt, E., 1975. Phycobilisomes: light-harvesting pigment complexes. *Bioscience* 25 (12), 781–788.
- Gierlowski-Kordesch, Elizabeth. (2010). Chapter 1 Lacustrine Carbonates. *Developments in Sedimentology*. 61. 10.1016/S0070-4571(09)06101-9.
- Graham, L., Wilcox, L., 2000. *Algae*. Prentice Hall, p. 640.
- Harms, J.C., Southard, J.B., Spearing, D.R., and Walker, R.G., 1975. *Depositional Environments as Interpreted from Primary Sedimentary Structures and Stratification Sequences*. Society of Economic Paleontologists and Mineralogists, Short Course 2, 2nd edn, 1982.
- Herlinger Jr., R., Zambonato, E. E. & De Ros, L. F., 2017. Influence of diagenesis on the quality of Lower Cretaceous pre-salt carbonate reservoirs from northern Campos Basin, offshore Brazil. *Journal of Sedimentary Research* 87: 1285-1313.
- Horne, David & Holmes, Jonathan & Rodriguez-Lazaro, Julio & Viehberg, Finn. (2012). Ostracoda as Proxies for Quaternary Climate Change. *Development in Quaternary Science*. 17. 10.1016/B978-0-444-53636-5.00018-4.
- Jo, H. R., & Chough, S. K. (2001). Architectural analysis of fluvial sequences in the northwestern part of Kyongsang basin (early Cretaceous), SE Korea. *Sedimentary Geology*, 144(3-4), 307-334. doi:10.1016/S0037-0738(01)00123-3
- Jordan, Teresa & Herrera, Christian & Godfrey, Linda & Colucci, Stephen & Gamboa, Carolina & Urrutia, Javier & L., Gabriel & Paul, Jacob. (2018). Isotopic characteristics and paleoclimate implications of the extreme precipitation event of March 2015 in northern Chile. *Andean Geology*. 46. 1. 10.5027/andgeoV46n1-3087.
- Kiessling Wolfgang 2015; RESEARCH FOCUS: Fuzzy seas. *Geology* ; 43 (2): 191–192. <https://doi.org/10.1130/focus022015.1>
- Legates, D.R. and Willmott, C.J. (1990a) Mean seasonal and spatial variability in gauge-corrected, global precipitation. *Int. J. Clim.*, 10, 111–127.
- Legates, D.R. and Willmott, C.J. (1990b) Mean seasonal and spatial variability in global surface air temperature. *Theor. Appl. Climatol.*, 41, 11–21.
- Leng, Melanie & Marshall, Jim. (2004). Palaeoclimate interpretation of stable isotope data from lake sediment archives. *Quaternary Science Reviews*. 23. 811-831. 10.1016/j.quascirev.2003.06.012.

- Macintyre IG (1985) Submarine cements – the peloidal question. In Carbonate Cements (eds Schneidermann N, Harris PM). SEPM, Tulsa, OK, pp. 109–116.
- Maizels, J.. (1993). Quantitative regime modelling of fluvial depositional sequences: Application to Holocene stratigraphy of humid-glacial braid-plains (Icelandic sandurs). Geological Society, London, Special Publications. 73. 53-78. 10.1144/GSL.SP.1993.073.01.05.
- Mascitti, V. (2001) Habitat changes in Laguna de Pozuelos, Jujuy, Argentina: implications for South American Flamingo populations. *Waterbirds*, 24, 16–21.
- Mazzullo, S. & Boardman, Darwin & Grossman, Ethan & Dimmick-Wells, Kimberly. (2007). Oxygen-carbon isotope stratigraphy of upper carboniferous to lower Permian marine deposits in Midcontinent U.S.A. (Kansas and ne Oklahoma): Implications for sea water chemistry and depositional cyclicity. *Carbonates and Evaporites*. 22. 55-72. 10.1007/BF03175846.
- McGlue, M.M., Ellis, G.S., Cohen, A.S. and Swarzenski, P.W. (2012), Playa-lake sedimentation and organic matter accumulation in an Andean piggyback basin: the recent record from the Cuenca de Pozuelos, North-west Argentina. *Sedimentology*, 59: 1237-1256. doi:10.1111/j.1365-3091.2011.01304.x
- McGlue, Michael & Cohen, Andrew & Ellis, Geoffrey & Kowler, Andrew. (2013). Late Quaternary stratigraphy, sedimentology and geochemistry of an underfilled lake basin in the Puna plateau (northwest Argentina). *Basin Research*. 25. 10.1111/bre.12025.
- Mercedes-Martín, Ramon & Rogerson, Mike & Brasier, Alexander & Vonhof, Hubert & Prior, Timothy & Fellows, S.M. & Reijmer, John & Billing, Ian & Pedley, H.M.. (2016). Growing spherulitic calcite grains in saline, hyperalkaline lakes: Experimental evaluation of the effects of Mg-clays and organic acids. *Sedimentary Geology*. 335.10.1016/j.sedgeo.2016.02.008.
- Miall, Andrew D. (1977), A Review of the Braided-river Depositional Environment.
- Miall A. D. (1990), Principles of Sedimentary Basin Analysis, 2nd ed. xv + 668 pp. Berlin, Heidelberg, New York, London, Paris, Tokyo, Hong Kong, Barcelona: Springer-Verlag. Price DM 128.00 (hard covers). ISBN 3 540 97119 X
- Mihindukulasooriya L.N., Ortiz, J. D., Pompeani D., Steinman B., Abbott M., (2015), Late Quaternary paleohydrologic conditions in southeastern British Columbia by visible derivative spectroscopy of Cleland Lake sediment, *Quaternary Research* 83.3 (2015): 531-544.
- Mirande, V. and Tracanna, B.C. (2009) Estructura y controles abioticos del fitoplancton en humedales de altura. *Ecol. Aust.*, 19, 119–128.
- Morse, J.W., Wang, Q. and Tsio, M.Y. (1997) Influences of temperature and Mg: Ca ratio on CaCO₃ precipitates from seawater. *Geology*, 25, 85– 87.

- Muniz, M. C. & Bosence, D. W. J. 2015. Pre-salt microbialites from the Campos Basin (Offshore Brazil); Image Log Facies, Facies Model and Cyclicity in Lacustrine Carbonates. In: Bosence, D. W. J., Gibbons, K., Le Heron, D. P., Pritchard, T. & Vining, B. (eds) *Microbial Carbonates in Space and Time: Implications for Global Exploration and Production*. Geological Society of London Special Publication 418.
- Nakano, C. M. F., Pinto, A. C. C., Marcusso, J. L. & Minami, K. . 2009. Pre-Salt Santos Basin – extended well test and production pilot in the Tupi area – the planning phase. Offshore Technology Conference, Houston, TX, 4–7 May 2009, OTC 19886.
- Ortiz, J.D., 2011. Application of Visible/near Infrared derivative spectroscopy to Arctic paleoceanography, IOP Conference. Series: Earth and Environmental Science 14, pp. 1–13.
- Ortiz, J.D., Polyak, L., Grebmeier, J.M., Darby, D.A., Eberl, D.D., Naidu, S., Nof, D., 2009. Provenance of Holocene sediment on the Chukchi-Alaskan margin based on combined diffuse spectral reflectance and quantitative X-ray diffraction analysis. *Global and Planetary Change* 68, 73–84.
- Page, R. (1996) Mapa Geológico de la Provincia de Jujuy, Republica Argentina, Escala 1:500000. Servicio Geológico Minero de Argentina, Buenos Aires.
- Perri, Edoardo & Tucker, Maurice & Mawson, Mike. (2013). Biotic and Abiotic Processes In the Formation and Diagenesis of Permian Dolomitic Stromatolites (Zechstein Group, NE England). *Journal of Sedimentary Research*. 83. 896-914. 10.2110/jsr.2013.65.
- Petersohn, E., and M. Abelha, 2013, Brasil pre-salt, geological assessment: National Agency of Petroleum Natural Gas and Biofuels (ANP), http://www.brasil-rounds.gov.br/arquivos/Seminarios_P1/Apresentacoes/partilha1_tecnico_ambiental_ingles.pdf.
- Rezende, M. F. & Pope, M. C. 2015. Importance of depositional texture in pore characterization of subsalt microbialite carbonates, offshore Brazil. In: Bosence, D. W. J., Gibbons, K., Le Heron, D. P., Pritchard, T. & Vining, B. (eds) *Microbial Carbonates in Space and Time: Implications for Global Exploration and Production*. Geological Society of London Special Publication 418.
- Robertson, P.K., Lawton, L.A., Cornish, B.J., 1999. The involvement of phycocyanin pigment in the photo decomposition of the cyanobacterial toxin, microcystin-LR. *Journal of Porphyrins and Phthalocyanines* 3, 544–551.
- Roberts, S.M., Spencer, R.J. & Lowenstein, T.K. (1994) Late Pleistocene saline lacustrine sediments, Badwater Basin, Death Valley, California. In: *Lacustrine Reservoirs and Depositional Systems* (Ed. by A.J. Lomando, B.C. Schreiber & P.M. Harris), SEPM Core Workshop, 19, 61–103.

- Rubiolo, D.G. (1997) Esquema de evolucion tectonosedimentaria para las Cuencas Cenozoicas de la Cordillera Oriental (22_ a 23_ lat. S.), Argentina. *Acta Geol. Hisp.*, 32, 77–92.
- Rushdi, A.I., Pytkowicz, R.M., Suess, E. et al. The effects of magnesium-to-calcium ratios in artificial seawater, at different ionic products, upon the induction time, and the mineralogy of calcium carbonate: a laboratory study. *Geol Rundsch* 81, 571–578 (1992).
<https://doi.org/10.1007/BF01828616>
- Saller, Arthur & Rushton, Shawn & Buambua, Lino & Inman, Kerry & McNeil, Ross & Dickson, J.A.D.. (2016). Presalt stratigraphy and depositional systems in the Kwanza Basin, offshore Angola. *AAPG Bulletin*. 100. 1135-1164. 10.1306/02111615216.
- Schagerl, M., Donabaum, K., 2003. Patterns of major photosynthetic pigments in freshwater algae. 1. Cyanoprokaryota, Rhodophyta and Cryptophyta *Annales de limnologie* Cambridge University Press, pp. 35–47.
- Schagerl, M., Pichler, C., Donabaum, K., 2003. Patterns of major photosynthetic pigments in freshwater algae. 2. Dinophyta, Euglenophyta, Chlorophyceae and Charales *Annales de limnologie* Cambridge University Press, pp. 49–62.
- Singer A (1984). The paleoclimatic interpretation of clay minerals in sediments - a review, *Earth Science Reviews*, 21 (4), pp. 251-293.
- Smoot, J.P. & Lowenstein, T.K. (1991) Depositional environments of non-marine evaporites. In: *Evaporites, Petroleum and Mineral Resources* (Ed by J.L. Melvin), *Dev. Sedimentol.*, 50, 189–347.
- Terra, G.J.S. & Spadini, A.R. & França, A.B. & Sombra, Cristiano & Zambonato, Eveline & Juschaks, L.C. & Arienti, L.M. & Erthal, Marcelle & Blauth, M. & Franco, M.P. & Matsuda, N.S. & Carramal da Silva, Nívea & Moretti, Paulo & Davila, Roberto & Souza, Rogério & Tonietto, Sandra & Anjos, S.M.C. & Campinho, Vania & Winter, Wilson. (2009). Carbonate rock classification applied to brazilian sedimentary basins. *Boletim de Geociencias da Petrobras*. 18. 9-29.
- Thompson, Daniel & Stilwell, Jeffrey & Hall, Mike. (2015). Lacustrine carbonate reservoirs from Early Cretaceous rift lakes of Western Gondwana: Pre-Salt coquinas of Brazil and West Africa. *Gondwana Research*. 28. 10.1016/j.gr.2014.12.005.
- Todd, S. P. 1989. Stream-driven, high-density gravelly traction carpets: possible deposits in the Trabeg Conglomerate Formations, SW Ireland and theoretical considerations of their origin. *Sedimentology* 36:513–530.
- Toepel, J., Langner, U., Wilhelm, C., 2005. Combination of flow cytometry and single cell absorption spectroscopy to study the phytoplankton structure and to calculate the chlorophyll-a specific absorption coefficients at the taxon level 1. *Journal of Phycology* 41, 1099–1109.

- Tosca, N. J. & Wright, V. P., 2015, Diagenetic pathways linked to labile Mg-clays in lacustrine carbonate reservoirs: a model for the origin of secondary porosity in the Cretaceous pre-salt Barra Velha Formation, offshore Brazil. From: Armitage, P. J., Butcher, A. R., Churchill, J. M., Csoma, A. E., Hollis, C., Lander, R. H., Omma, J. E. & Worden, R. H. (eds) Reservoir Quality of Clastic and Carbonate Rocks: Analysis, Modelling and Prediction. Geological Society of London Special Publication 435.
- Tribouvillard, Nicolas & Lyons, Timothy & Riboulleau, Armelle. (2006). Trace metals as paleoredox and paleoproductivity proxies: An update. *Chemical Geology*. 232. 12-32. 10.1016/j.chemgeo.2006.02.012.
- Turner P. 1980. Continental Red Beds. *Developments in Sedimentology*. Amsterdam, Elsevier, 562p.
- Tutolo, Benjamin & Tosca, Nicholas. (2018). Experimental examination of the Mg-silicate-carbonate system at ambient temperature: Implications for alkaline chemical sedimentation and lacustrine carbonate formation. *Geochimica et Cosmochimica Acta*. 225. 80-101. 10.1016/j.gca.2018.01.019.
- Vasquez Fernandes Guilherme, Morschbacher José Marcio, Anjos dos Dias Wense Camila, Silva Parisek Moisés Yaro, Madrucci Vanessa, and Justen Ramos Cesar Julio, (2019), "Petroacoustics and composition of presalt rocks from Santos Basin," *The Leading Edge* 38: 342–348. <https://doi.org/10.1190/tle38050342.1>
- Velde, B. & Meunier, Alain. (2008). *The Origin of Clay Minerals in Soils and Weathered Rocks*. 10.1007/978-3-540-75634-7.
- Wright, V.P. 2012. Lacustrine carbonates in rift settings: the interaction of deposition volcanic and microbial processes on carbonate. Geological Society, London, Special Publications v.370, doi: 10.1144/SP370.2
- Wright, V. P. & Barnett, A. J. 2015. An abiotic model for the development of textures in some South Atlantic early Cretaceous lacustrine carbonates. In: Bosence, D. W. J., Gibbons, K. A. et al. (eds) *Microbial Carbonates in Space and Time: Implications for Global Exploration and Production*. Geological Society, London, Special Publications, 418, <http://dx.doi.org/10.1144/SP418.1034>
- Wright, P., & A. (2017, April 3). Classifying reservoir carbonates when the status quo simply does not work: A case study from the Cretaceous of the South Atlantic. Lecture presented at AAPG Annual Convention & Exhibition in Texas, Houston.
- Yurco, L.N., Ortiz, J.D., Polyak, L., Darby, D.A., Crawford, K.A., 2010. Clay mineral cycles identified by diffuse spectral reflectance in Quaternary sediments from the Northwind Ridge: implications for glacial–interglacial sedimentation patterns in the Arctic Ocean. *Polar Research* 29 (2), 176–197.

Zuffa G.G. 1985. Optical analyses of arenites: influence of methodology on compositional results. *In: Zuffa G.G. (ed.) Provenance of Arenites*. NATO-ASI Series C. D. Reidel Pub. Co., 148, Dordrecht, The Netherlands, p. 165-168

Appendix 1 – Petrographic quantification tables

Complete petrographic quantification

ID	LP2A	LP2A	LP2A	LP2A	LP2A	LP2A	LP2A	LP2A	LP2A	LP2A	LP2A	LP2A	LP2A	LP2A	LP2A	LP2A
	2.7 m	3.2 m	3.85 m	4.9 m	5.1 m	5.6 m	6.65 m	8.35 m	10.1 m	10.4 m	10.75 m	10.8 m	11.1 m	11.3 m	11.7 m	11.9 m
Depth (m)	1.4	1.55	1.8	2.3	2.42	2.57	2.7	3.6	4.0	4.3	4.6	4.65	4.75	4.92	5.31	5.54
Well	LP06-2A	LP06-2A	LP06-2A	LP06-2A	LP06-2A	LP06-2A	LP06-2A	LP06-2A	LP06-2A	LP06-2A	LP06-2A	LP06-2A	LP06-2A	LP06-2A	LP06-2A	LP06-2A
Facies code	CIL	CIL	CIM	CIM	CIM	CIM	CIL	CIM	CIM	CIL	CIL	CIL	CIL	CIM	SM	SL
Constituents	%	%	%	%	%	%	%	%	%	%	%	%	%	%	%	%
Argillaceous mud intraclast - As intrabasinal constituent	8.67	4.00	4.00	0	1.67	0	1.67	1.33	2.67	0	0	0	0	14.33	2.33	0
Argillaceous mud intraclast - As intrabasinal constituent - zebra-like texture	0	0	0	0	3.00	0	0	0	0	0	0	0	0	0	0	0
Bioclastic intraclast - As intrabasinal constituent	0	0	0	0	0	0	0	0	0	0	0.67	0	0	0	0	0
Bioconstrucster microbial carbonate - As intrabasinal constituent - shrubby	0	0	0	0	0	0	0	1.00	0	0	0	0	0	0	0	0
Bioconstrucster stromatolite on organic-walled bioclast	0	0	0	0	0	0	0	0	0	0	2.67	0	0	0	0	0
Bioconstrucster stromatolite on ostracode	0	0	0	0	0	0	0	0	0	0	0.33	0	0	0	0	0
Bioconstrucster stromatolite on charophyte	0	0	0	0	0	0	0	0	0	0	4.33	0	0	0	0	0
Bioconstrucster trombolite - covering stromatolite	0	0	0	0	0	0	0	0	0	0	6.33	0	0	0	0	0
Biotite - As monomineralic grain	1.33	1.33	1.00	1.00	2.00	1.00	0.67	1.67	1.00	0.33	0.33	0.33	0	0	0	0
Organic-walled bioclast - As intrabasinal constituent (Arcella?)	0	0	0	0	0	0	0	0	0.33	0.67	1.00	0.67	0.67	0.33	0	0
Carbonaceous organic matter - As intrabasinal constituent	4.33	2.00	2.33	1.67	1.33	1.33	9.67	2.67	1.33	3.33	0.67	0	0.33	0.33	1.00	0
Carbonate bioclast undifferentiated - As intrabasinal constituent - fragments	0.33	0	0	0	0	0	4.33	0	0	0	0.33	0	0	0	0	0
Carbonate oolith - As intrabasinal constituent	0	0	0	0	0	0	0	0	0	0	0	0.33	0	0	0	0
Carbonate peloid - As intrabasinal constituent	3.33	1.33	1.33	2.67	3.33	2.33	3.00	4.00	0.33	1.33	8.33	3.00	4.00	3.00	0	0
Charophyte algae bioclast - As intrabasinal constituent	0	0	0	0	0	0	0	0	0	0	8.33	25.00	14.67	0	0	0
Clay ooid/peloid - As intrabasinal constituent	7.00	5.33	13.33	12.00	2.00	6.67	5.33	12.00	15.67	4.67	2.00	1.33	1.33	6.67	1.00	0
Clay ooid/peloid - As intrabasinal constituent - oriented fibers	0	0	0	0	9.33	1.00	0	0	0	0	0	0	0	0	0	0
Detrital K-feldspar - As monomineralic grain	0.33	0	0	0	0	0	0	0.00	0	0	0	0	0	0	0	0
Detrital feldspar - As monomineralic grain	0	0	0	0	0	0	0	0	0	0	0	0	0	0	0	0.33
Detrital feldspar - In plutonic rock fragment	0	0	0	0	0	0	0	0	0	0	0	0	0	0	0	1.33
Detrital microcline - As monomineralic grain	0	0	0	0	0	0	0	0	0	0	0	0	0	0	0.33	0
Detrital plagioclase - As monomineralic grain	1.00	0.67	0.33	0.33	0.33	0	0.33	0.67	0.33	0	0	0	0	0	0	0.33
Detrital quartz - As monomineralic grain	4.33	2.67	2.67	2.00	1.00	0	0.67	2.00	2.67	0.67	0.67	0.33	1.00	0.33	1.67	1.33
Detrital quartz - As volcanic rock fragment	0	0	0	0	0	1.33	0	0	0	0	0	0	0	0	0	0
Detrital quartz - In metamorphic rock fragment - phyllite	0	0	0	0	0	0	0	0	0	0	0	0	0	0	0	0.33
Detrital quartz - In plutonic rock fragment	0	0	0	0	0	0	0	0	0	0	0	0	0	0	0	3.33
Diatom - As intrabasinal constituent	0	1.67	0	3.33	0.33	1.67	3.67	1.33	2.00	4.67	1.00	0	0.67	0.67	0	0
Granitic/gneissic plutonic rock fragment - As plutonic rock fragment	2.67	1.33	1.33	1.00	1.33	1.00	0.67	1.33	2.00	0.67	0	0	0	0	2.00	12.67

Heavy mineral undifferentiated - As monomineralic grain	0	0.33	0	0.33	0.00	0.33	0	0.67	0	0	0.33	0	0	0.33	0	0
Heavy mineral undifferentiated - In plutonic rock fragment	0	0	0	0	0	0	0	0	0	0	0	0	0	0	0	0.33
Metamorphic rock fragment - As metamorphic rock fragment	0	0	0	0	0	0	0	0	0	0	0	0	0	0	0.33	0
Ostracode bioclast - As intrabasinal constituent	2.67	1.33	1.33	2.67	2.33	2.00	0.33	2.00	0.33	6.33	3.33	0.33	6.33	0.33	0	0
Phosphate bioclast undifferentiated - As intrabasinal constituent	0.33	0	0	0	0.33	0	0	0	0.33	0	0	0	0	0	0	0
Phyllite rock fragment - As metamorphic rock fragment	0	0	0	0	0	0	0	0	0	0	0	0	0	0	0	23.00
Schist rock fragment - As metamorphic rock fragment	0	0	0	0	0	0	0	0	0	0	0	0	0	0	0	2.00
Siliciclastic mud matrix syndeositional - As intrabasinal constituent	48.00	45.00	48.33	53.67	28.67	52.33	45.00	34.33	46.67	24.33	29.00	23.33	42.00	46.67	20.00	2.00
Siliciclastic mud matrix syndeositional - As intrabasinal constituent - Higher crystallinity	0	14.33	19.33	13.00	21.00	13.00	8.33	9.33	16.00	6.00	6.67	1.67	0	6.00	0	0
Siliciclastic mud matrix syndeositional - As intrabasinal constituent - Zebra-like textures	0	0	0	0	11.00	6.33	3.33	8.00	0	0	0.00	0	0	0	0	0
Siliciclastic mud matrix syndeositional - As intrabasinal constituent - laminated	0	0	0	0	0.00	0.00	0.00	0	0	28.33	0	5.00	0	0	0	0
Siltstone rock fragment - As sedimentary rock fragment	0	0	0	0	0	0	0	0	0	0	0	0	0	0	0	3.67
Volcanic rock fragment - As volcanic rock fragment	0	0	0	0	0	0.67	0.67	0	0.33	0	0	0	0	0	0	0
Zircon - As monomineralic grain	0.67	0	0	0.33	0	0	0	0	0	0	0	0	0	0	0	0
Aragonite - Acicular - Intergranular discontinuous pore-lining - Covering <Primary-Constituent> - Charophyte algae bioclast - As intrabasinal constituent	0	0	0	0	0	0	0	0	0	0	1.00	2.00	3.67	0	0	0
Aragonite - Coating - Intergranular continuous pore-lining - Covering <Primary-Constituent> - Carbonate bioclast undifferentiated - As intrabasinal constituent	0	0.33	0	0	0	0	0	2.00	0	0	0	0	0	0	0	0
Calcite - Round crystal - Filling vugular pore - Within <pore> - Vug pore - Framework and interstitial	4.00	1.00	0	0	0	0	0.33	1.00	0	0	0	0	0	0	0	0
Calcite - Round crystal - Intergranular displacive - Displacing <Primary-Constituent> - Siliciclastic mud matrix syndeositional - As intrabasinal constituent	0	0	0	0	0	0	0	0	0	0	0	0.33	0	0	0	0
Calcite - Round crystal - Intergranular replacive - Replacing <Primary-Constituent> - Siliciclastic mud matrix syndeositional - As intrabasinal constituent	2.33	4.33	0.33	0.67	2.67	1.33	0.67	4.33	0.33	0.67	1.67	1.67	0.33	1.33	0	0
Calcite - Round crystal - Intragranular replacive - Replacing <Primary-Constituent> - Argillaceous mud intraclast - As intrabasinal constituent	0	0	0	0	1.00	0	0	0	0	0	0	0	0	0	0	0
Calcite - Anhedral crystal - Intragranular replacive - Replacing <Primary-Constituent> - Charophyte algae bioclast - As intrabasinal constituent	0	0	0	0	0	0	0	0	0	0	1.00	0	0	0	0	0
Calcite - Fine mosaic - Intergranular replacive - Replacing <Primary-Constituent> - Siliciclastic mud matrix syndeositional - As intrabasinal constituent	0	0	0	0	0	0	0	0	0	0	0	0	0.67	0	0	0
Calcite - Fine mosaic - Intragranular replacive - Replacing <Primary-Constituent> - Charophyte algae bioclast - As intrabasinal constituent	0	0	0	0	0	0	0	0	0	0	0	9.33	4.00	0	0	0
Calcite - Microcrystalline - Filling shelter pore - Within <Primary-Constituent> - Charophyte algae bioclast - As intrabasinal constituent	0	0	0	0	0	0	0	0	0	0	0	2.33	0	0	0	0

Calcite - Microcrystalline - Filling shelter pore - Within <Primary-Constituent> - Undifferentiated carbonate bioclast - As intrabasinal constituent	0	0	0	0	0	0	0	0	0	0	0	1.33	0	0.33	0	0	0
Calcite - Microcrystalline - Filling vugular pore - Within <pore> - Vug pore - Framework and interstitial	0	0	0	0	0	0	0.67	0	0	0	0	0	0	0	0	0	0
Calcite - Microcrystalline - Intergranular replacive - Replacing <Primary-Constituent> - Siliciclastic mud matrix syndepositional - As intrabasinal constituent	2.67	1.33	1.00	1.00	1.00	0.33	2.33	1.33	0	1.00	3.00	1.67	3.00	5.67	0	0	
Calcite - Microcrystalline - Intergranular replacive - Replacing <Primary-Constituent> - Siliciclastic mud matrix syndepositional (clotted) - As intrabasinal constituent	0	0	0	0	0	0	0	0	0	0	0	0	0	0	5.00	0	0
Calcite - Microcrystalline - Intragranular replacive - Replacing <Primary-Constituent> - Carbonaceous organic matter - As intrabasinal constituent	0	0	0	0.33	0	0	1.00	0	0	0	0	0	0	0	0	0	0
Calcite - Mosaic - Intergranular replacive - Replacing <Primary-Constituent> - Siliciclastic mud matrix syndepositional - As intrabasinal constituent	0	0	0	0	0	0	0	0	0	0	0.33	0	0	0	0	0	0
Calcite - Mosaic - Intragranular replacive - Replacing <Primary-Constituent> - Charophyte algae bioclast - As intrabasinal constituent	0	0	0	0	0	0	0	0	0	0	0	1.33	0	0	0	0	0
Calcite - Prismatic - Intergranular pore-lining - Covering <Primary-Constituent> - Charophyte algae bioclast - As intrabasinal constituent	0	0	0	0	0	0	0	0	0	0	0	0	0.33	0	0	0	0
Diagenetic iron oxide/hydroxide - Microcrystalline - Intergranular continuous pore-lining - Covering <Primary-Constituent> - Granitic/gneissic plutonic rock fragment	0	0	0	0	0	0	0	0	0	0	0	0	0	0	0	0	14.00
Diagenetic iron oxide/hydroxide - Microcrystalline - Intergranular replacive - Replacing <Primary-Constituent> - Siliciclastic mud matrix syndepositional (clotted) - As intrabasinal constituent	0	0	0	0	0	0	0	0	0	0	0	0	0	0	0	64.33	12.00
Fe-dolomite/ankerite - Discrete crystal - Intergranular replacive - Replacing <Diagenetic-Constituent> - Calcite - Intergranular replacive	0	0	0	0	0	0	0	0.33	0	0	0	0	0	0	0	0	0
Fe-dolomite/ankerite - Discrete crystal - Intergranular replacive - Replacing <Primary-Constituent> - Siliciclastic mud matrix syndepositional - As intrabasinal constituent	0	0	0	0	0	0	0	0.33	0	0	0	0	0	0	0	0	0
Gypsum - Lenticular - Intergranular displacive - Displacing <Primary-Constituent> - Siliciclastic mud matrix syndepositional - As intrabasinal constituent	0	0	0	0	0	0	0	0.33	0.67	4.33	0.67	2.33	1.00	0.67	0	0	
Gypsum - Lenticular - Intergranular replacive - Replacing <Primary-Constituent> - Siliciclastic mud matrix syndepositional - As intrabasinal constituent	0	0	0	0	0	0	0.67	0.33	1.33	6.00	4.00	3.33	1.67	2.67	0	0	
Gypsum - Lenticular - Intragranular displacive - - Displacing <Primary-Constituent> - Carbonate bioclast undifferentiated - As intrabasinal constituent	0	0	0	0	0	0	0	0	0	0	0.67	0	0	0	0	0	
Gypsum - Lenticular - Intragranular replacive - Replacing <Primary-Constituent> - Carbonate bioclast undifferentiated - As intrabasinal constituent	0	0	0	0	0	0	0	0	0	1.67	0	0	0	0	0	0	
Gypsum - Lenticular - Intragranular replacive - Replacing <Primary-Constituent> - Charophyte algae bioclast - As intrabasinal constituent	0	0	0	0	0	0	0	0	0	0	0	0.67	0.33	0	0	0	

Gypsum - Prismatic - Intergranular displacive - Displacing <Primary-Constituent> - Siliciclastic mud matrix syndeositional - As intrabasinal constituent	0	0	0	0	0	0	0	0	0	0.33	0	0	0	0	0.67	0.33	0
Gypsum - Prismatic - Intergranular replacive - Replacing <Primary-Constituent> - Siliciclastic mud matrix syndeositional - As intrabasinal constituent	0	0	0	0	0	0	0	0	0	0	0	0	0	0	0.00	2.33	0
Gypsum - Rosette - Intergranular displacive - Displacing <Primary-Constituent> - Siliciclastic mud matrix syndeositional - As intrabasinal constituent	0	0	0	0	0	0	0	0	0	0	0	0	0	0	0	0.33	0
Gypsum - Rosette - Intergranular replacive - Replacing <Primary-Constituent> - Siliciclastic mud matrix syndeositional - As intrabasinal constituent	0	0	0	0	0	0	0	0	0	0	0	0	0	0	0	0.33	0
Jarosite - Discrete crystal - Intergranular replacive - Replacing <Primary-Constituent> - Siliciclastic mud matrix syndeositional - As intrabasinal constituent	0	0	0	0	0	0	0	0.33	0	0	0	0	0	0	0	0	0
Jarosite - Microcrystalline - Intragranular replacive - Replacing <Diagenetic-Constituent> - Pyrite - Intragranular replacive	0	0	0	0	0	0	0	0	0	0	0.67	0	0	0	0	0	0
Pyrite - Framboid - Filling shelter pore - Within <Primary-Constituent> - Ostracode bioclast - As intrabasinal constituent	0.33	0	0	0	0	0	0	0	0	0	0	0.33	0	0	0	0	0
Pyrite - Framboid - Intergranular replacive - Replacing <Primary-Constituent> - Siliciclastic mud matrix syndeositional - As intrabasinal constituent	2.00	5.00	1.33	2.33	1.67	3.67	2.67	1.67	2.67	3.33	3.33	3.00	3.33	0.67	2.00	0	0
Pyrite - Framboid - Intragranular replacive - Replacing <Primary-Constituent> - Carbonaceous organic matter - As intrabasinal constituent	1.00	0.00	1.00	0.33	0	2.33	1.67	0	0	1.00	0.67	0	1.67	0.33	0	0	0
Pyrite - Framboid - Intragranular replacive - Replacing <Primary-Constituent> - Ostracode bioclast - As intrabasinal constituent	0	0.00	0	0	0	0	0	0	0	0	0.33	0	0.33	0	0	0	0
Siderite - Discrete crystal - Intergranular replacive - Replacing <Primary-Constituent> - Siliciclastic mud matrix syndeositional - As intrabasinal constituent	0	1.33	0	0	0	0	0	0.33	2.33	0	0	0	0	0	0.67	0	0
Fracture pore - Framework and interstitial	0	0	0	1.33	0	0	0	0	0	0	0	0	0	0	0	0	0
Growth framework pore - Framework and interstitial - Within <Primary-Constituent> - Bioconstrucster stromatolite - As intrabasinal constituent	0	0	0	0	0	0	0.33	0	0	0	0	0	0	0	0	0	0
Intergranular pore - Interstitial	0	0	0	0	0	0	0	0	0	0	0	5.33	2.67	3.33	1.67	6.67	0
Intragranular pore - Framework	0	0	0	0	0	0	0	0	0	0	0	5.67	4.00	0	0	16.67	0
Shelter pore - Framework - Within <Primary-Constituent> - Calcisphere bioclast - As intrabasinal constituent	0	0	0	0	0	0	0	0	0	0.33	0	0	0.33	0	0	0	0
Shelter pore - Framework - Within <Primary-Constituent> - Charophyte algae bioclast - As intrabasinal constituent	0	0	0	0	0	0	0	0	0	0	3.00	0.33	0.00	0	0	0	0
Shelter pore - Framework - Within <Primary-Constituent> - Ostracode bioclast - As intrabasinal constituent	0.67	0	0	0.00	0	0.33	0	0.33	0	0	0.33	0	1.67	0	0	0	0
Shrinkage pore - Framework and interstitial	0	0	0	0	4.67	0.67	0	1.67	0	0	0	0	0	0	0	0	0
Vug pore - Framework and interstitial	2.00	3.33	1.00	0	0	0.33	2.00	3.33	0.33	0.33	0.33	0	0	0	0	0	0

Total																	
Volume	%	%	%	%	%	%	%	%	%	%	%	%	%	%	%	%	%
Framework	45.00	26.33	29.67	27.67	34.00	22.33	37.00	37.67	29.67	26.00	50.33	55.33	44.33	26.67	8.67	65.33	
Intergranular	55.00	73.67	70.33	72.33	66.00	77.67	63.00	62.33	70.33	74.00	49.67	44.67	55.67	73.33	91.33	34.67	
Cement	0.00	0.33	0.00	0.33	0.00	0.00	0.00	2.33	1.00	4.33	1.67	5.00	4.67	1.33	0.67	14.00	
Matrix	48.00	59.33	67.67	66.67	60.67	71.67	56.67	51.67	62.67	58.67	35.67	30.00	42.00	52.67	20.00	2.00	
Porosity	2.67	5.33	1.00	1.33	4.67	1.33	2.33	5.33	0.33	0.67	3.67	11.33	8.67	3.33	1.67	23.33	
Total diagenetic constituents	12.33	13.33	3.67	4.67	6.33	7.67	10.00	12.33	7.67	18.00	20.00	27.33	20.33	17.67	69.67	26.00	
Rigid grains	12.33	8.00	5.67	10.00	5.67	7.00	10.67	8.00	8.33	13.00	15.00	26.67	23.33	2.00	4.00	20.00	
Ductile grains	21.33	12.67	20.67	14.67	19.33	10.00	17.33	17.67	20.67	8.33	3.00	1.67	1.67	21.33	4.67	28.67	
Extrabasinals	%	%	%	%	%	%	%	%	%	%	%	%	%	%	%	%	%
Total extrabasinal constituents	58.33	65.67	73.00	71.67	65.33	74.67	59.67	58.00	69.00	60.33	37.00	30.67	43.00	53.33	24.33	51.00	
Extrabasinal grains	10.33	6.33	5.33	5.00	4.67	3.00	3.00	6.33	6.33	1.67	1.33	0.67	1.00	0.67	4.33	49.00	
Detrital quartz	4.33	2.67	2.67	2.00	1.00	0.00	0.67	2.00	2.67	0.67	0.67	0.33	1.00	0.33	1.67	1.33	
Detrital feldspar	1.33	0.67	0.33	0.33	0.33	0.00	0.33	0.67	0.33	0.00	0.00	0.00	0.00	0.00	0.33	0.67	
Plutonic rock fragments	2.67	1.33	1.33	1.00	1.33	1.00	0.67	1.33	2.00	0.67	0.00	0.00	0.00	0.00	2.00	17.67	
Volcanic rock fragments	0.00	0.00	0.00	0.00	0.00	0.67	0.67	0.00	0.33	0.00	0.00	0.00	0.00	0.00	0.00	0.00	
Sedimentary rock fragments	0.00	0.00	0.00	0.00	0.00	0.00	0.00	0.00	0.00	0.00	0.00	0.00	0.00	0.00	0.00	3.67	
Carbonate rock fragments	0.00	0.00	0.00	0.00	0.00	0.00	0.00	0.00	0.00	0.00	0.00	0.00	0.00	0.00	0.00	0.00	
Metamorphic rock fragments	0.00	0.00	0.00	0.00	0.00	0.00	0.00	0.00	0.00	0.00	0.00	0.00	0.00	0.00	0.33	25.33	
Detrital matrix	48.00	59.33	67.67	66.67	60.67	71.67	56.67	51.67	62.67	58.67	35.67	30.00	42.00	52.67	20.00	2.00	
Intrabasinals	%	%	%	%	%	%	%	%	%	%	%	%	%	%	%	%	%
Intrabasinal primary constituents	22.67	13.67	20.00	20.67	23.33	13.67	18.33	20.67	21.67	19.33	27.67	43.33	32.33	25.33	3.33	0.00	
Present primary carbonate constituents	6.33	2.67	2.67	5.33	5.67	4.33	7.67	7.00	1.00	8.33	35.67	29.33	25.67	3.67	0.00	0.00	
Original primary carbonate constituents	6.67	2.67	2.67	5.33	5.67	4.33	7.67	7.00	1.00	10.00	38.33	42.00	30.33	3.67	0.00	0.00	
Intrabasinal grains	22.67	13.67	20.00	20.67	22.33	13.67	18.33	20.67	21.67	19.33	27.67	43.33	32.33	25.33	3.33	0.00	
Present Carbonate allochems	6.33	2.67	2.67	5.33	5.67	4.33	7.67	6.00	1.00	8.33	22.00	29.33	25.67	3.67	0.00	0.00	
Original carbonate allochems	6.67	2.67	2.67	5.33	5.67	4.33	7.67	6.00	1.00	10.00	24.67	42.00	30.33	3.67	0.00	0.00	
Primary proportion of original carbonate allochems	100.0	100.0	100.0	100.0	100.0	100.0	100.0	100.0	100.0	100.0	100.0	100.0	100.0	100.0	100.0	100.0	
Present carbonate bioclasts	0	0	0	0	0	0	0	85.71	0	0	64.35	0	0	0	0.00	0.00	
Original carbonate bioclasts	3.00	1.33	1.33	2.67	2.33	2.00	4.67	2.00	0.67	7.00	13.00	26.00	21.67	0.67	0.00	0.00	
Carbonate intraclasts	3.00	1.33	1.33	2.67	2.33	2.00	4.67	2.00	0.67	7.00	13.00	26.00	21.67	0.67	0.00	0.00	
Carbonate ooids	0.00	0.00	0.00	0.00	0.00	0.00	0.00	0.00	0.00	0.00	0.00	0.67	0.00	0.00	0.00	0.00	
Carbonate ooids	0.00	0.00	0.00	0.00	0.00	0.00	0.00	0.00	0.00	0.00	0.00	0.33	0.00	0.00	0.00	0.00	
Carbonate peloids/pellets	0.00	0.00	0.00	0.00	0.00	0.00	0.00	0.00	0.00	0.00	0.00	0.00	0.00	0.00	0.00	0.00	
Carbonate peloids/pellets	3.33	1.33	1.33	2.67	3.33	2.33	3.00	4.00	0.33	1.33	8.33	3.00	4.00	3.00	0.00	0.00	
Original bioconstructors	0.00	0.00	0.00	0.00	0.00	0.00	0.00	0.00	0.00	0.00	0.00	0.00	0.00	0.00	0.00	0.00	
Present carbonate bioconstructors	0.00	0.00	0.00	0.00	0.00	0.00	0.00	1.00	0.00	0.00	13.67	0.00	0.00	0.00	0.00	0.00	

Original carbonate bioconstructers	0.00	0.00	0.00	0.00	0.00	0.00	0.00	0.00	1.00	0.00	0.00	13.67	0.00	0.00	0.00	0.00
Primary proportion of original carbonate bioconstructers	0.00	0.00	0.00	0.00	0.00	0.00	0.00	0.00	14.28	0.00	0.00	35.65	0.00	0.00	0.00	0.00
Present carbonate matrix	0.00	0.00	0.00	0.00	0.00	0.00	0.00	0.00	0.00	0.00	0.00	0.00	0.00	0.00	0.00	0.00
Original carbonate matrix	0.00	0.00	0.00	0.00	0.00	0.00	0.00	0.00	0.00	0.00	0.00	0.00	0.00	0.00	0.00	0.00
Primary proportion of original carbonate matrix	0.00	0.00	0.00	0.00	0.00	0.00	0.00	0.00	0.00	0.00	0.00	0.00	0.00	0.00	0.00	0.00
Carbonate cement	4.00	1.33	0.00	0.00	0.00	0.00	1.00	3.33	0.00	0.00	2.33	5.00	4.00	0.00	0.00	0.00
Present intrabasinal non-carbonate grains	16.00	11.00	17.33	15.33	16.67	9.33	10.67	14.67	20.67	9.33	3.00	1.33	2.00	21.67	3.33	0.00
Original intrabasinal non-carbonate grains	16.00	11.00	17.33	15.33	17.67	9.33	10.67	14.67	20.67	9.33	3.00	1.33	2.00	21.67	3.33	0.00
Dolomite/Calcite ratio	0.00	0.00	0.00	0.00	0.00	0.00	0.00	0.10	0.00	0.00	0.00	0.00	0.00	0.00	0.00	0.00
Gravel	0.00	0.00	0.00	0.00	0.00	0.00	0.00	0.00	0.00	0.00	1.00	0.00	0.00	0.00	0.00	10.00
Sand	2.00	1.00	1.00	2.00	1.00	1.00	2.00	2.00	1.00	2.00	5.00	30.00	20.00	1.00	5.00	89.00
Mud	98.00	99.00	99.00	98.00	99.00	99.00	98.00	98.00	99.00	98.00	94.00	70.00	80.00	99.00	95.00	1.00

Rock Classification

												Slightly conglomeric mudrock	Sandy mudrock	Sandy mudrock	Mudrock	Mudrock	Conglomeratic sandstone
Folk Textural	Mudrock	Mudrock	Mudrock	Mudrock	Mudrock	Mudrock	Mudrock	Mudrock	Mudrock	Mudrock	Mudrock	Mudrock	Mudrock	Mudrock	Mudrock	Mudrock	Mudrock
Gravel	0.00	0.00	0.00	0.00	0.00	0.00	0.00	0.00	0.00	0.00	0.00	1.00	0.00	0.00	0.00	0.00	10.00
Mud	98.00	99.00	99.00	98.00	99.00	99.00	98.00	98.00	99.00	98.00	94.00	70.00	80.00	99.00	95.00	1.00	
Sand	2.00	1.00	1.00	2.00	1.00	1.00	2.00	2.00	1.00	2.00	5.00	30.00	20.00	1.00	5.00	89.00	

Microscopic - Modal grain size

Main/single size mode:	Clay	Clay	Clay	Clay	Clay	Clay	Clay	Clay	Clay	Clay	Clay	Clay	Clay	Clay	Clay	Clay	Coarse sand
Main/single size mode(mm):	0.00	0.00		0.00					0.00	0.00	0.00						0.90
#2 size mode:	Very fine sand	Very fine sand	Fine sand	Very fine sand	Very fine sand	Very fine sand	Very coarse sand	Fine sand	Fine sand	Medium sand	Medium sand	Very fine sand	Medium sand				
#2 size mode(mm):	0.08	0.09	0.17	0.10	0.10	0.10	1.10	0.20	0.16	0.30	0.46	0.12	0.40				
#3 size mode:				Fine sand				Coarse sand		Fine sand							
#3 size mode(mm):				0.20				1.00			0.13						

Microscopic - Sorting:

Very poorly

Summary of quantitative petrographic data

ID	LP2A 2.7 n	LP2A 3.2 n	LP2A 6.65	LP2A 10.4	LP2A 10.7	LP2A 10.8	LP2A 11.1 m			LP2A 3.85	LP2A 4.9 n	LP2A 5.1 n	LP2A 5.6 n	LP2A 8.35	LP2A 10.1	LP2A 11.3 m			LP2A 11.7	LP2A 11.9 m		
Depth (m)	2.70	3.20	6.65	10.40	10.75	10.80	11.10			3.85	4.90	5.10	5.60	8.35	10.10	11.30			11.70	11.90		
Adjusted depth (m)	1.40	1.55	2.70	4.30	4.60	4.68	4.75			1.80	2.30	2.42	2.57	3.60	4.00	4.92			5.31	5.54		
Well	LPO6-2A	LPO6-2A	LPO6-2A	LPO6-2A	LPO6-2A	LPO6-2A	LPO6-2A			LPO6-2A	LPO6-2A	LPO6-2A	LPO6-2A	LPO6-2A	LPO6-2A	LPO6-2A			LPO6-2A	LPO6-2A		
Facies code	CIL	CIL	CIL	CIL	CIL	CIL	CIL	Average	Maximum	CIM	CIM	CIM	CIM	CIM	CIM	CIM	Average	Maximum	SM	SL	Average	Maximum
Constituents	%	%	%	%	%	%	%			%	%	%	%	%	%	%			%	%		
In situ clay	48.00	59.33	56.66	58.66	35.67	30.00	42.00	47.19	59.33	67.66	66.67	60.67	71.66	51.66	62.67	52.67	61.95	71.66	20.00	2.00	11.00	20.00
Reworked clay	15.67	9.33	7.00	4.67	2.00	1.33	1.33	5.90	15.67	17.33	12.00	16.00	7.67	13.33	18.34	21.00	15.10	21.00	3.33	0.00	1.66	3.33
Bioconstruction	0.00	0.00	0.00	0.00	13.66	0.00	0.00	1.95	13.66	0.00	0.00	0.00	0.00	1.00	0.00	0.00	0.14	1.00	0.00	0.00	0.00	0.00
Carbonate peloid - As intrabasinal constituent	3.33	1.33	3.00	1.33	8.33	3.00	4.00	3.47	8.33	1.33	2.67	3.33	2.33	4.00	0.33	3.00	2.43	4.00	0	0		
Carbonate bioclasts (total)	9.33	6.66	5.66	7.00	14.33	27.33	21.33	13.09	27.33	1.66	3.34	6.00	3.33	7.33	0.66	1.66	3.43	7.33	0.00	0.00	0.00	0.00
Non-carbonate bioclasts	0.33	1.67	3.67	5.34	2.00	0.67	1.34	2.15	5.34	0.00	3.33	0.66	1.67	1.33	2.66	1.00	1.52	3.33	0.00	0.00	0.00	0.00
Total bioclasts	3.33	3.00	8.33	11.67	14.66	26.00	22.34	12.76	26.00	1.33	6.00	2.99	3.67	3.33	2.99	1.33	3.09	6.00	0.00	0.00	0.00	0.00
Carbonaceous organic matter - As intrabasinal constituent	4.33	2.00	9.67	3.33	0.67	0	0.33	2.90	9.67	2.33	1.67	1.33	1.33	2.67	1.33	0.33	1.57	2.67	1.00	0	0.50	1.00
Rock fragments	2.67	1.33	1.34	0.67	0.00	0.00	0.00	0.86	2.67	1.33	1.00	1.33	1.67	1.33	2.33	0.00	1.28	2.33	2.33	41.34	21.84	41.34
Accessories	2.00	1.66	0.67	0.33	0.66	0.33	0.00	0.81	2.00	1.00	1.66	2.00	1.33	2.34	1.00	0.33	1.38	2.34	0.00	0.33	0.17	0.33
Total aragonite	0.00	0.33	0.00	0.00	1.00	2.00	3.67	1.00	3.67	0.00	0.00	0.00	0.00	2.00	0.00	0.00	0.29	2.00	0.00	0.00	0.00	0.00
Other calcite	0.00	0.00	0.00	0.00	2.66	9.66	4.67	2.43	9.66	0.00	0.00	0.00	0.00	0.00	0.00	0.00	0.00	0.00	0.00	0.00	0.00	0.00
Microcrystalline calcite	2.67	1.33	4.00	1.00	4.33	4.00	3.33	2.95	4.33	1.00	1.33	1.00	0.33	1.33	0.00	10.67	2.24	10.67	0.00	0.00	0.00	0.00
Total calcite	9.00	6.66	5.00	1.67	8.66	15.66	8.33	5.38	13.66	1.33	2.00	4.67	1.66	6.66	0.33	12.00	4.09	12.00	0.00	0.00	0.00	0.00
Total Fe oxide	0.00	0.00	0.00	0.00	0.00	0.00	0.00	0.00	0.00	0.00	0.00	0.00	0.00	0.00	0.00	0.00	0.00	0.00	64.33	26.00	45.17	64.33
Lenticular gypsum	0.00	0.00	0.67	12.00	5.34	6.33	3.00	3.91	12.00	0.00	0.00	0.00	0.00	1.32	2.00	3.34	0.95	3.34	0.00	0.00	0.00	0.00
Other gypsum	0.00	0.00	0.00	0.00	0.00	0.00	0.00	0.00	0.00	0.00	0.00	0.00	0.00	0.00	0.33	0.67	0.14	0.67	3.32	0.00	1.66	3.32
Total gypsum	0.00	0.00	0.67	12.00	5.34	6.33	3.00	3.91	12.00	0.00	0.00	0.00	0.00	1.32	2.33	4.01	1.09	4.01	3.32	0.00	1.66	3.32
Total pyrite	3.33	5.00	4.34	4.33	5.00	3.33	5.33	4.38	5.33	2.33	2.66	1.67	6.00	2.00	2.67	1.00	2.62	6.00	2.00	0.00	1.00	2.00

Appendix 2 - Photomicrographs from thin sections in LP06-2A

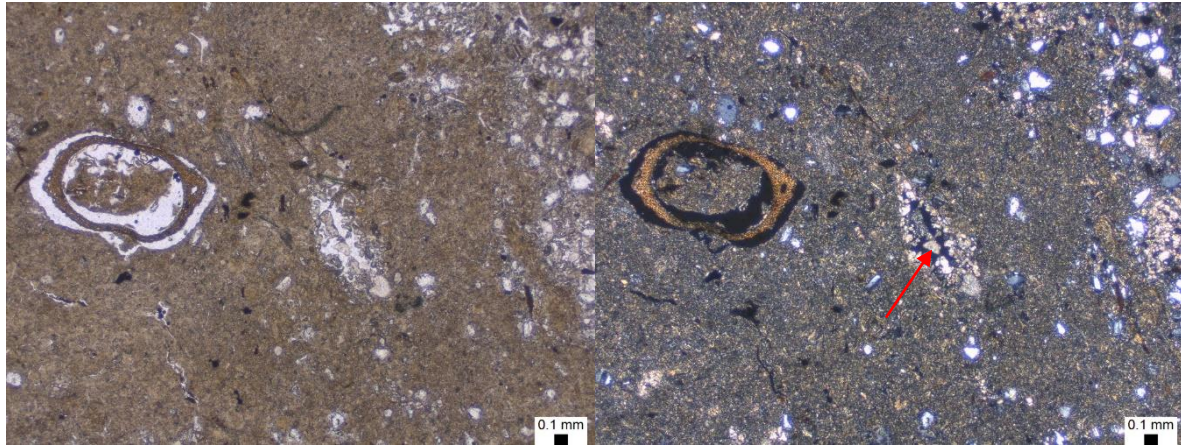


Figure 1: LP2A 2.7 m general photo of the mud with ostracod (large bioclast) and round carbonate in pore space (red arrow). (PPL & XPL 2.5X)

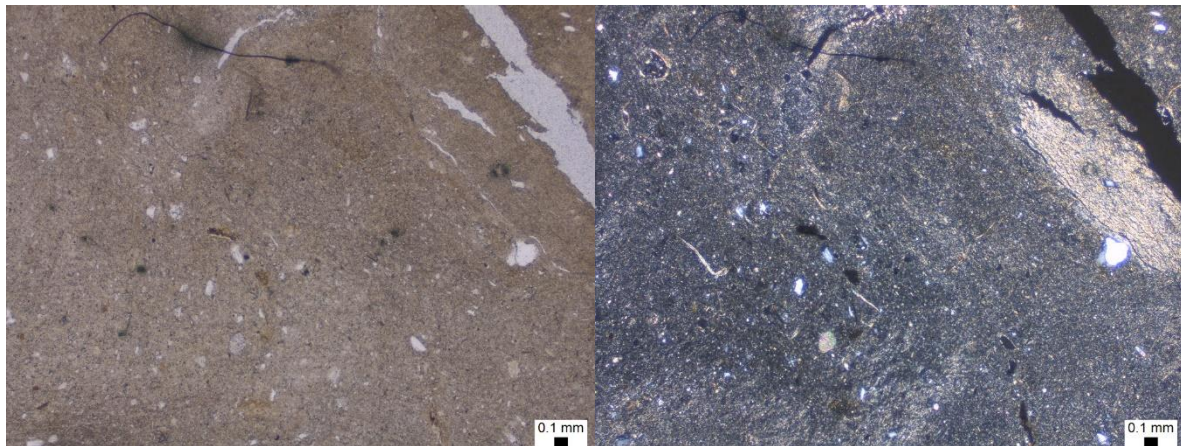


Figure 2: LP2A 3.2 m general photo of the mud with scattered grains and bioclasts (PPL & XPL 5X)

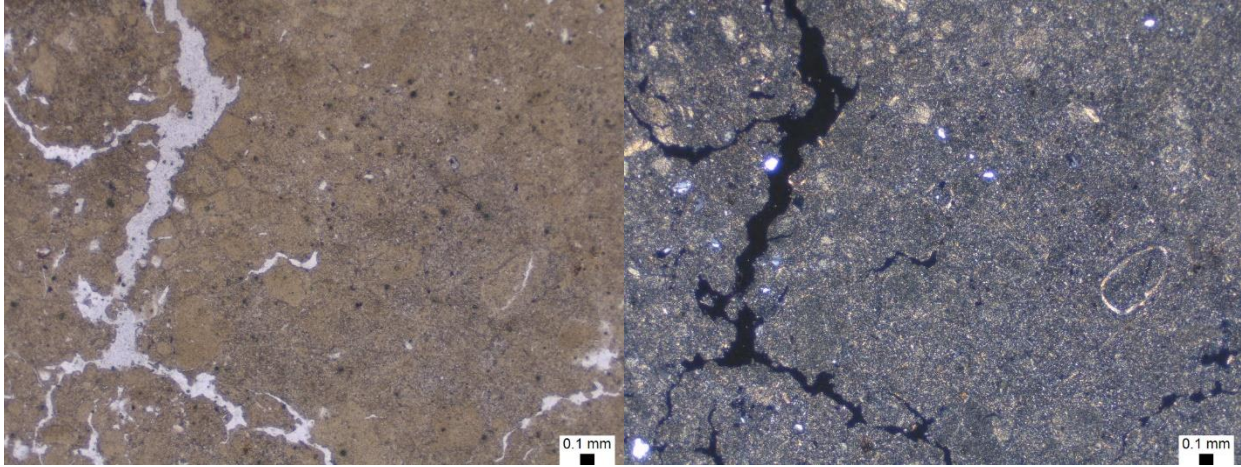


Figure 3: LP2A 3.85 m general photo of the mud (PPL & XPL 2.5X)

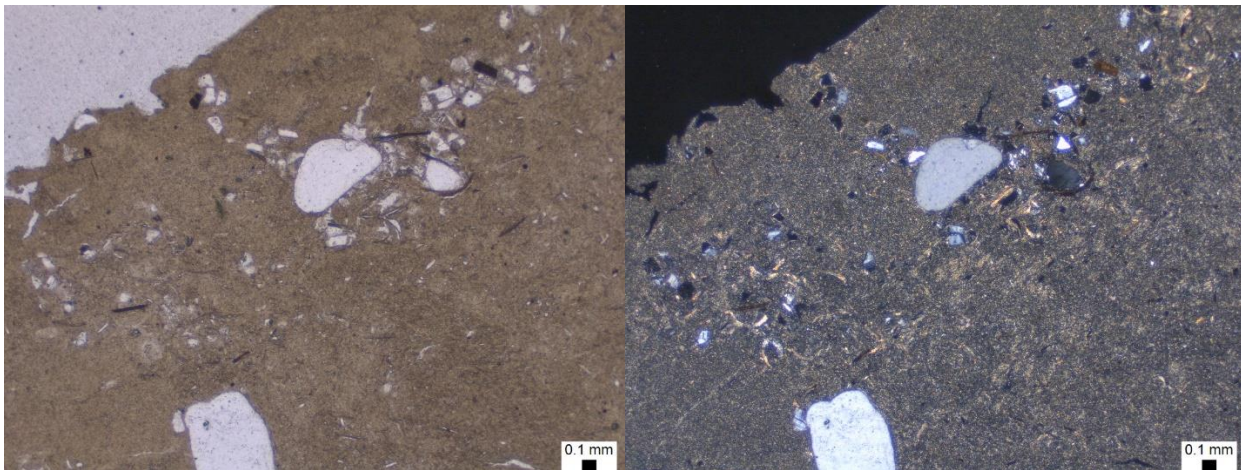


Figure 4: LP2A 4.9 m general photo of the mud, showing a sand laminae (PPL & XPL 2.5X)

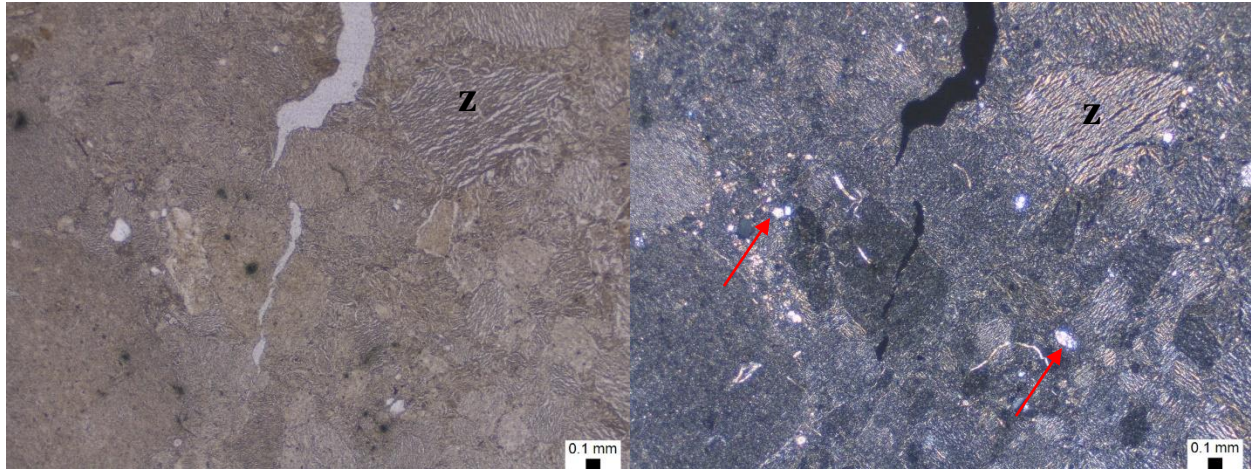


Figure 5: LP2A 5.1 m general photo of the mud with round carbonates (red arrows) and intraclast with zebra-like texture (z) (PPL & XPL 2.5X)

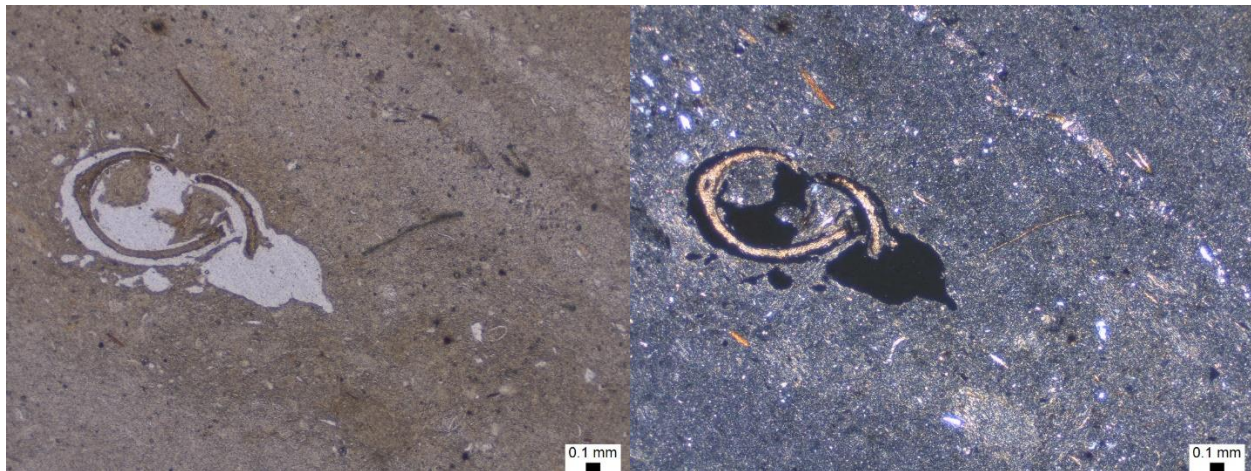


Figure 6: LP2A 5.8 m general photo of the mud with ostracod bioclast (PPL & XPL 2.5X)

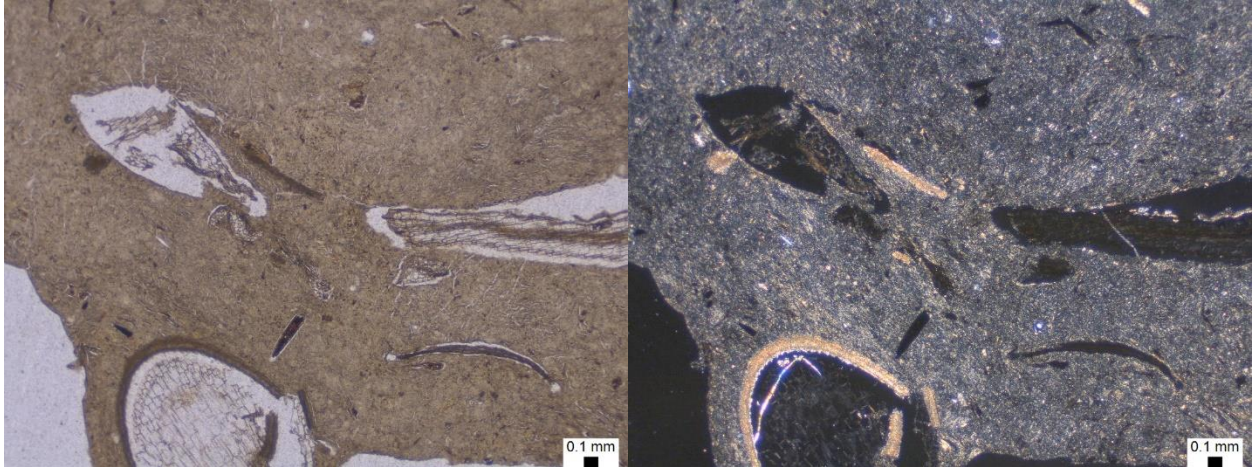


Figure 7: LP2A 6.65 m general photo of the mud with ostracod and phosphate bioclasts (fish bones?) (PPL & XPL 2.5X)

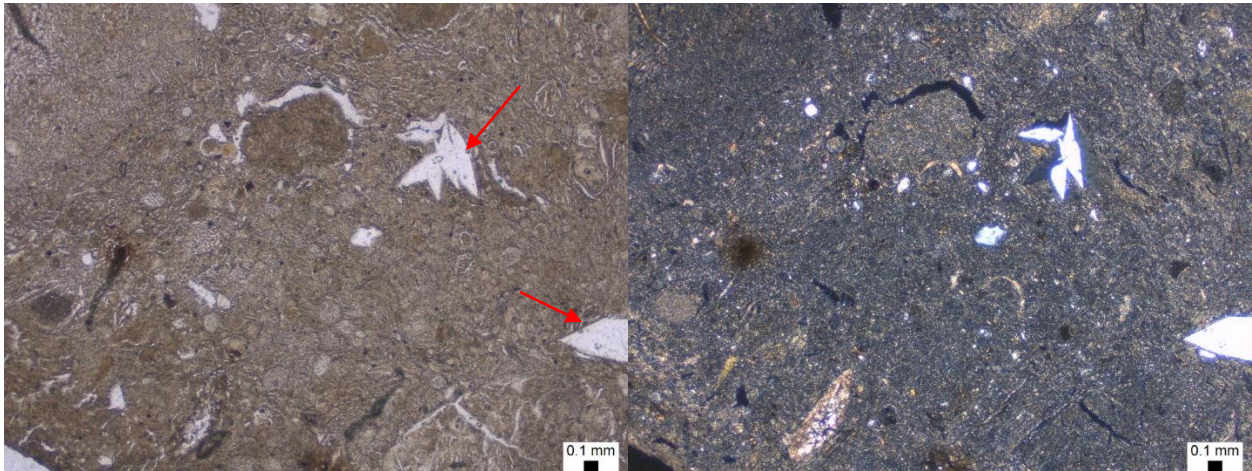


Figure 8: LP2A 8.35 m general photo of the mud with displacive gypsum crystals (red arrows) (PPL & XPL 2.5X)

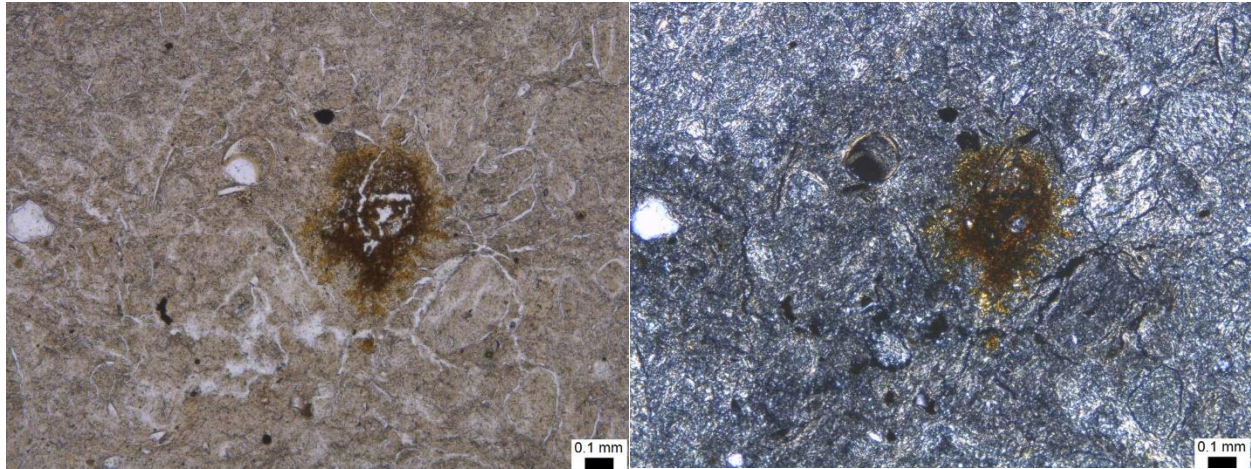


Figure 9: LP2A 10.1 m general photo of the mud locally replaced by siderite (PPL & XPL 5X)

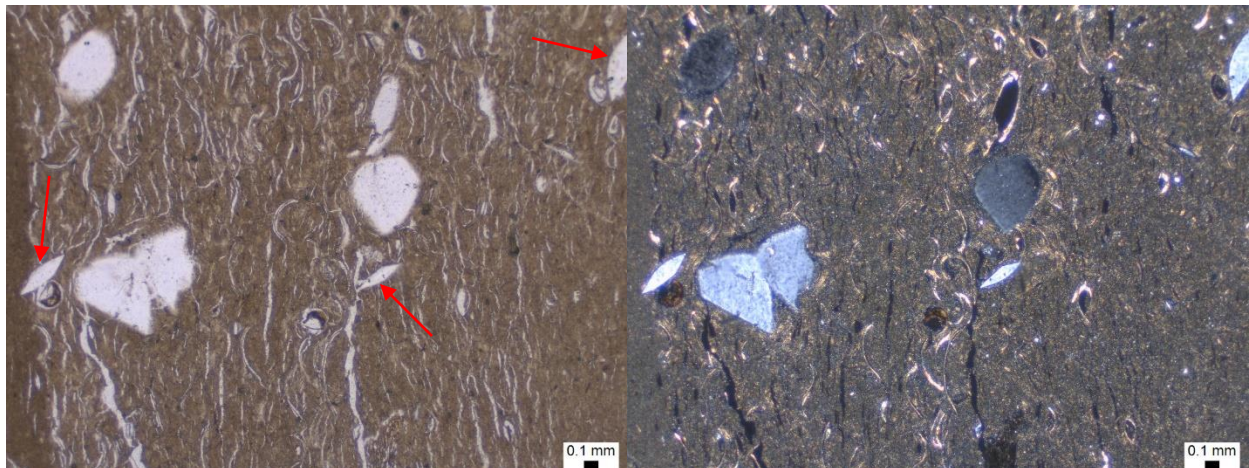


Figure 10: LP2A 10.4 m general photo of the bioclastic mud with scattered sand grains and displacive gypsum crystals (red arrows) (PPL & XPL 2.5X)

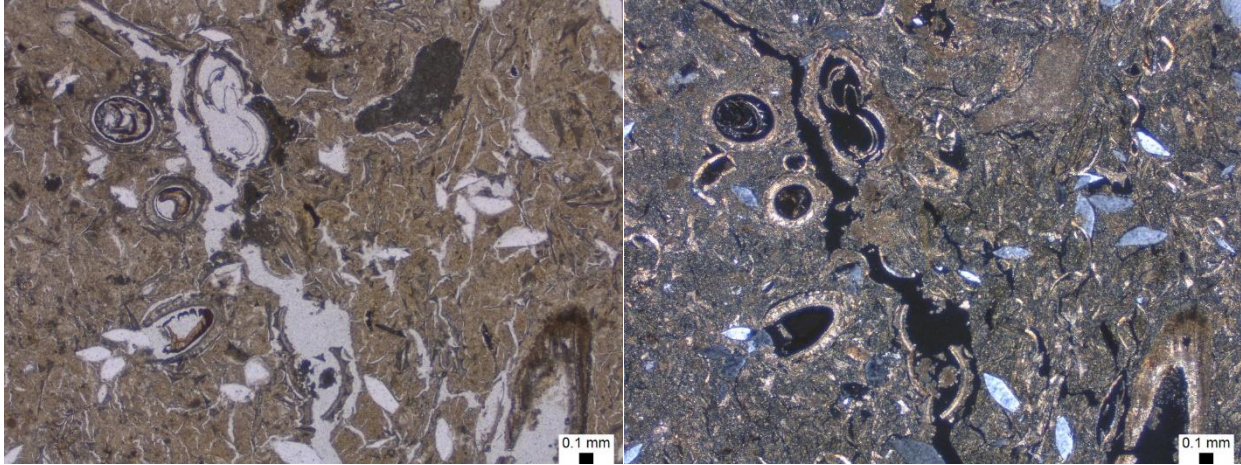


Figure 11: LP2A 10.75 m general photo of the mud with charophytes and displacive gypsum crystals (gray) (PPL & XPL 2.5X)

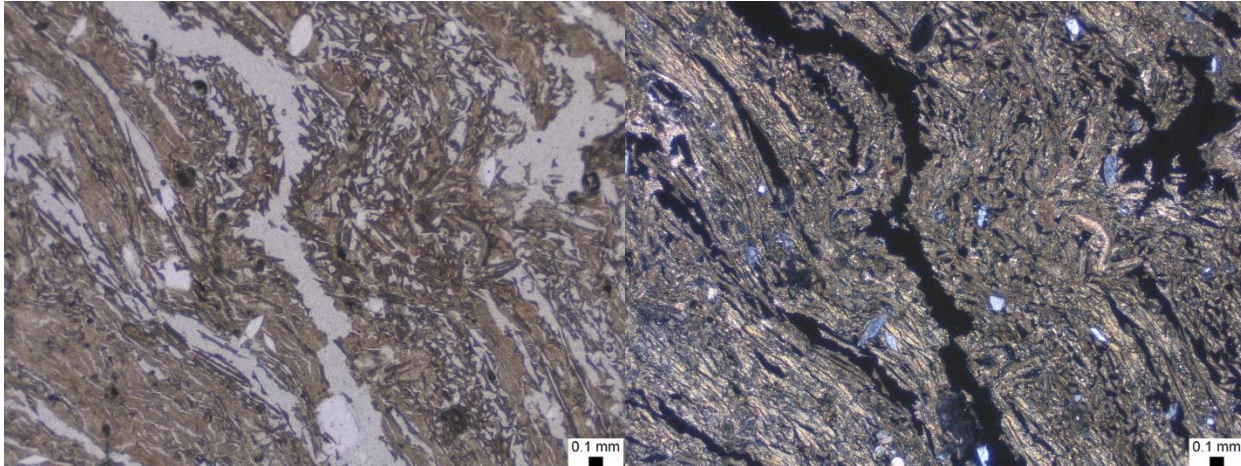


Figure 12: LP2A 10.8 m general photo of laminated mud and laminated charyophyte bioclast pieces (PPL & XPL 2.5X)

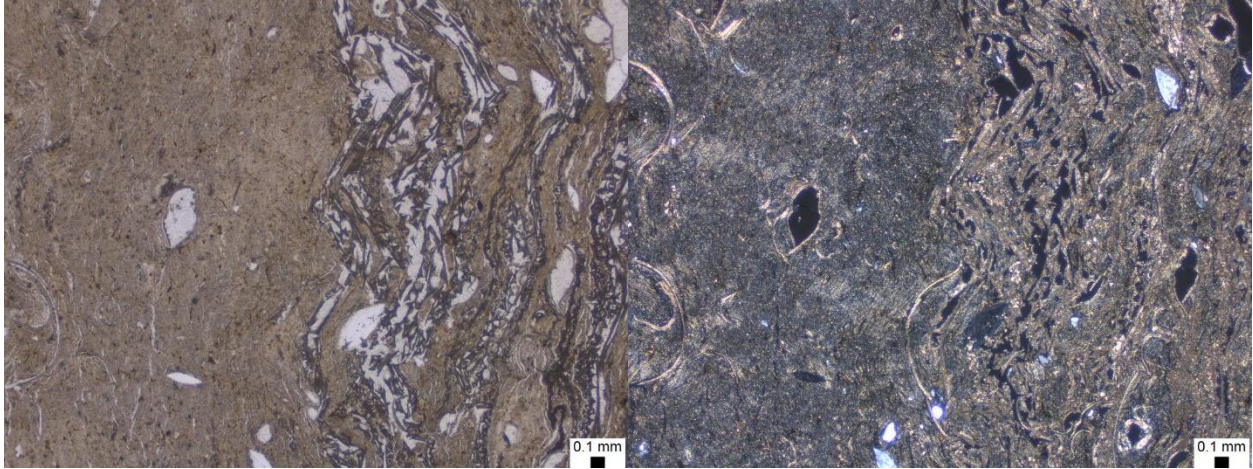


Figure 13: LP2A 11.1 m general photo showing the alternation of mud and bioclastic laminae (PPL & XPL 2.5X)

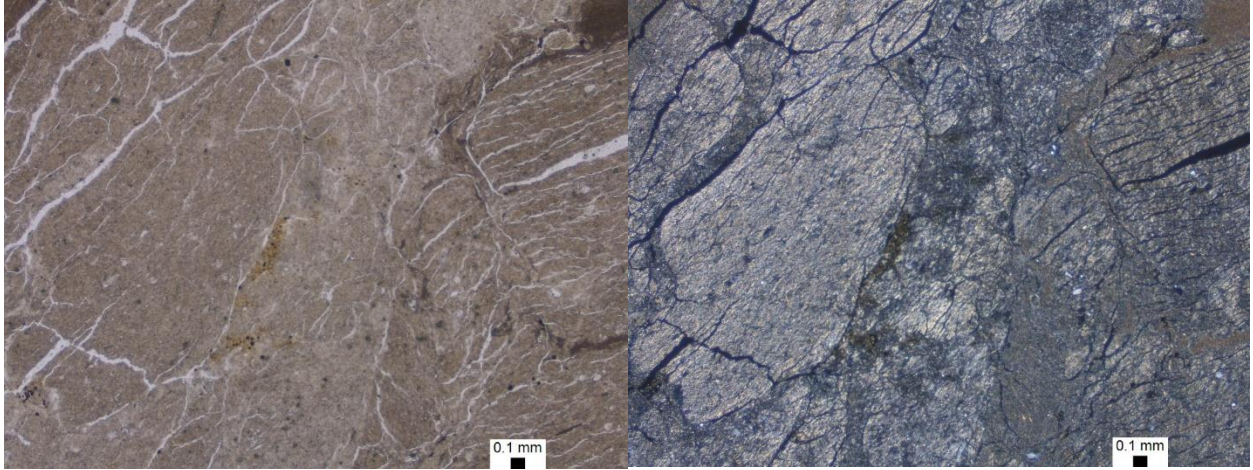


Figure 14: LP2A 11.3 m general photo of the intraclastic mud (PPL & XPL 2.5X)

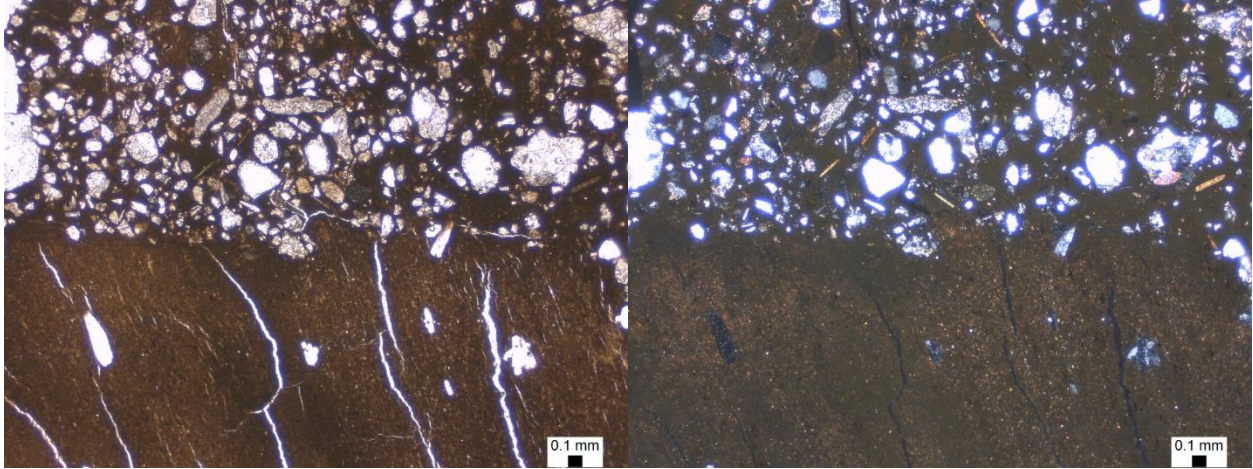


Figure 15: LP2A 11.7 m general photo of Fe oxides replacing mud and sandy laminae (PPL & XPL 2.5X)

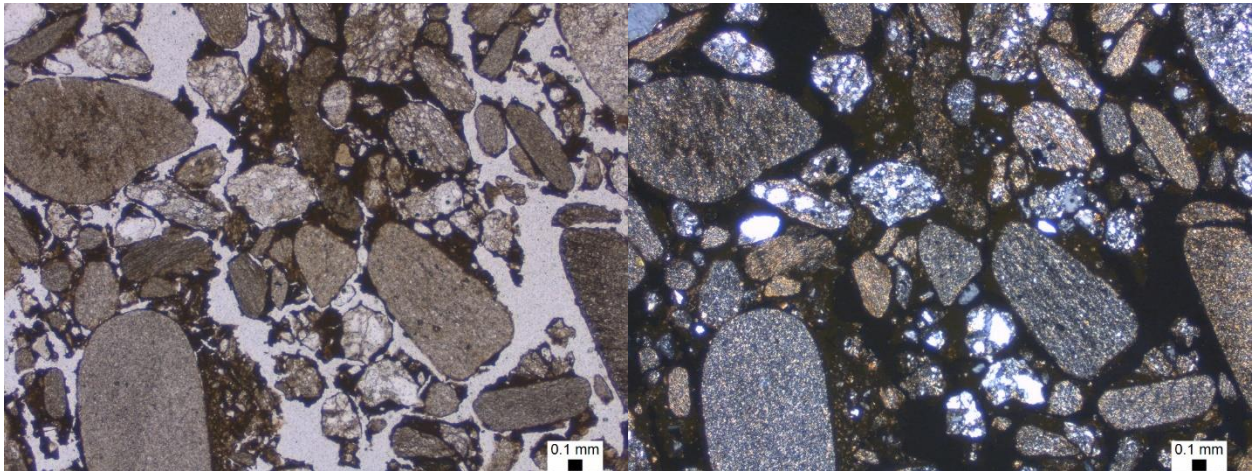


Figure 16: LP2A 11.9 m general photo of the lithic sand (PPL & XPL 2.5X)

Appendix 3 – XRD Diffractograms

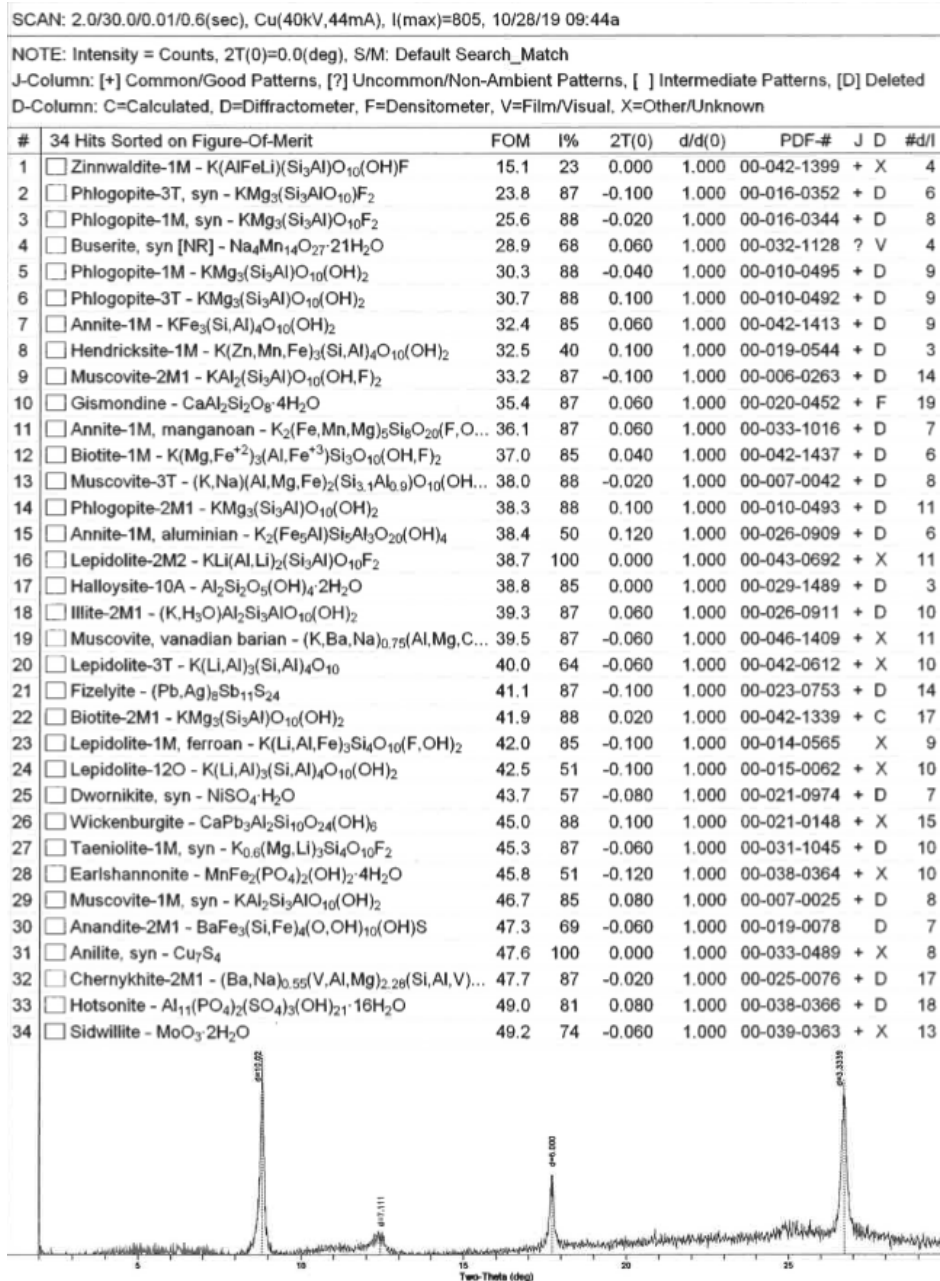


Figure 1: LP-2A 1.4 m KCL

SCAN: 2.0/30.0/0.01/0.6(sec), Cu(40kV,44mA), I(max)=749, 10/28/19 10:14a

NOTE: Intensity = Counts, 2T(0)=0.0(deg), S/M: Default Search_Match

J-Column: [+] Common/Good Patterns, [?] Uncommon/Non-Ambient Patterns, [] Intermediate Patterns, [D] Deleted

D-Column: C=Calculated, D=Diffractometer, F=Densitometer, V=Film/Visual, X=Other/Unknown

#	6 Hits Sorted on Figure-Of-Merit	FOM	I%	2T(0)	d/d(0)	PDF-#	J	D	#d/I
1	<input type="checkbox"/> Zinnwaldite-1M - $K(AlFeLi)(Si_3Al)O_{10}(OH)F$	15.2	50	-0.040	1.000	00-042-1399	+	X	4
2	<input type="checkbox"/> Phlogopite-3T, syn - $KMg_3(Si_3AlO_{10})F_2$	39.0	82	-0.080	1.000	00-016-0352	+	D	6
3	<input type="checkbox"/> Buserite, syn [NR] - $Na_4Mn_{14}O_{27} \cdot 21H_2O$	41.3	43	0.020	1.000	00-032-1128	?	V	4
4	<input type="checkbox"/> Matlockite, syn - $PbClF$	42.6	12	0.020	1.000	00-026-0311	+	D	3
5	<input type="checkbox"/> Muscovite, vanadian barian - $(K,Ba,Na)_{0.75}(Al,Mg,C...)$	48.0	17	0.080	1.000	00-046-1409	+	X	11
6	<input type="checkbox"/> Phlogopite-1M, syn - $KMg_3(Si_3Al)O_{10}F_2$	48.9	33	0.040	1.000	00-016-0344	+	D	8

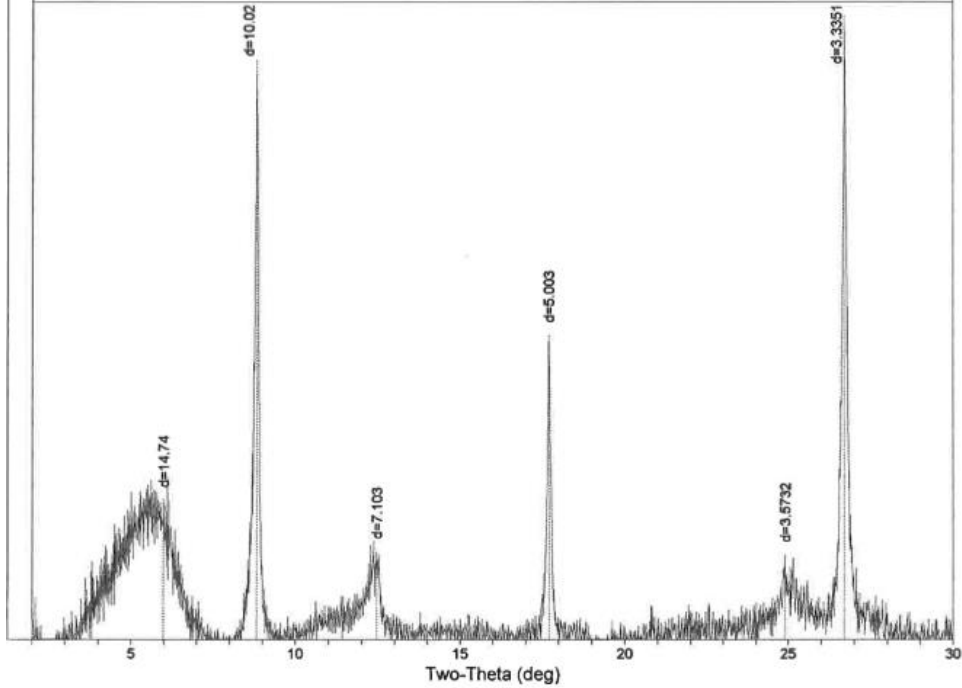


Figure 2: LP-2A 1.4 m MgCL

Figure 3: LP-2A 1.4 m Glycerol

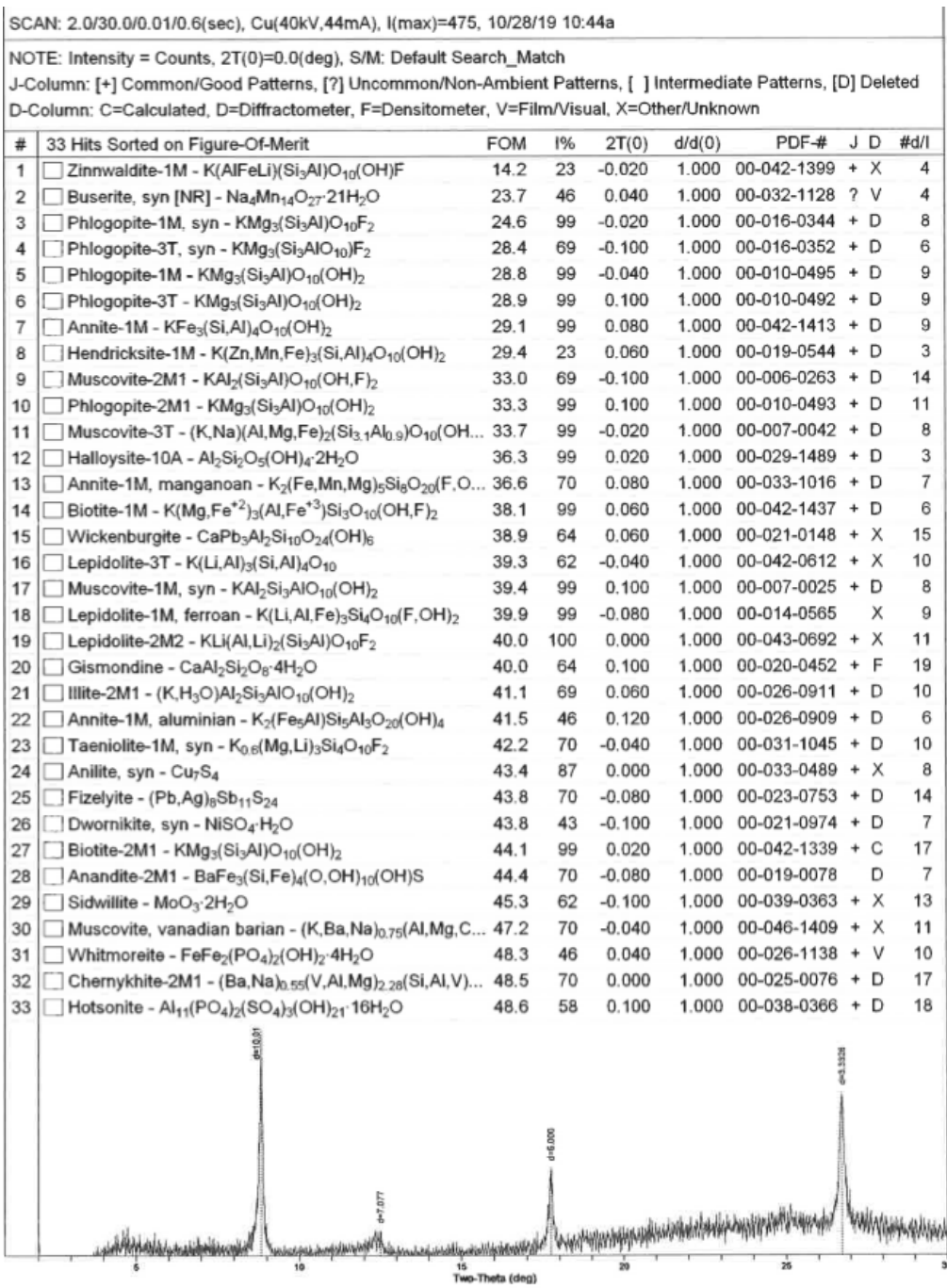


Figure 4: LP-2A 1.55 m KCL

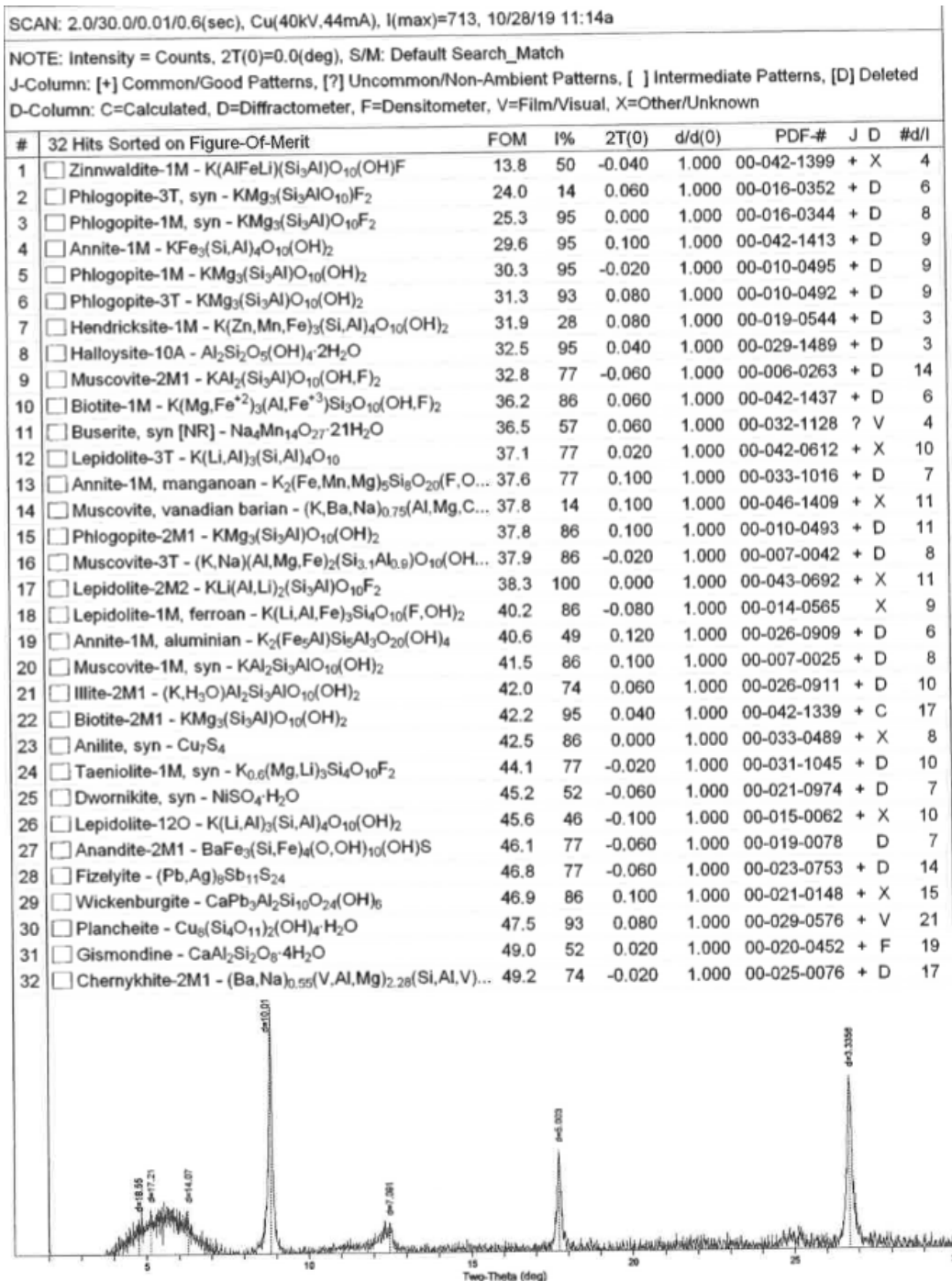


Figure 5: LP-2A 1.55 m MgCL

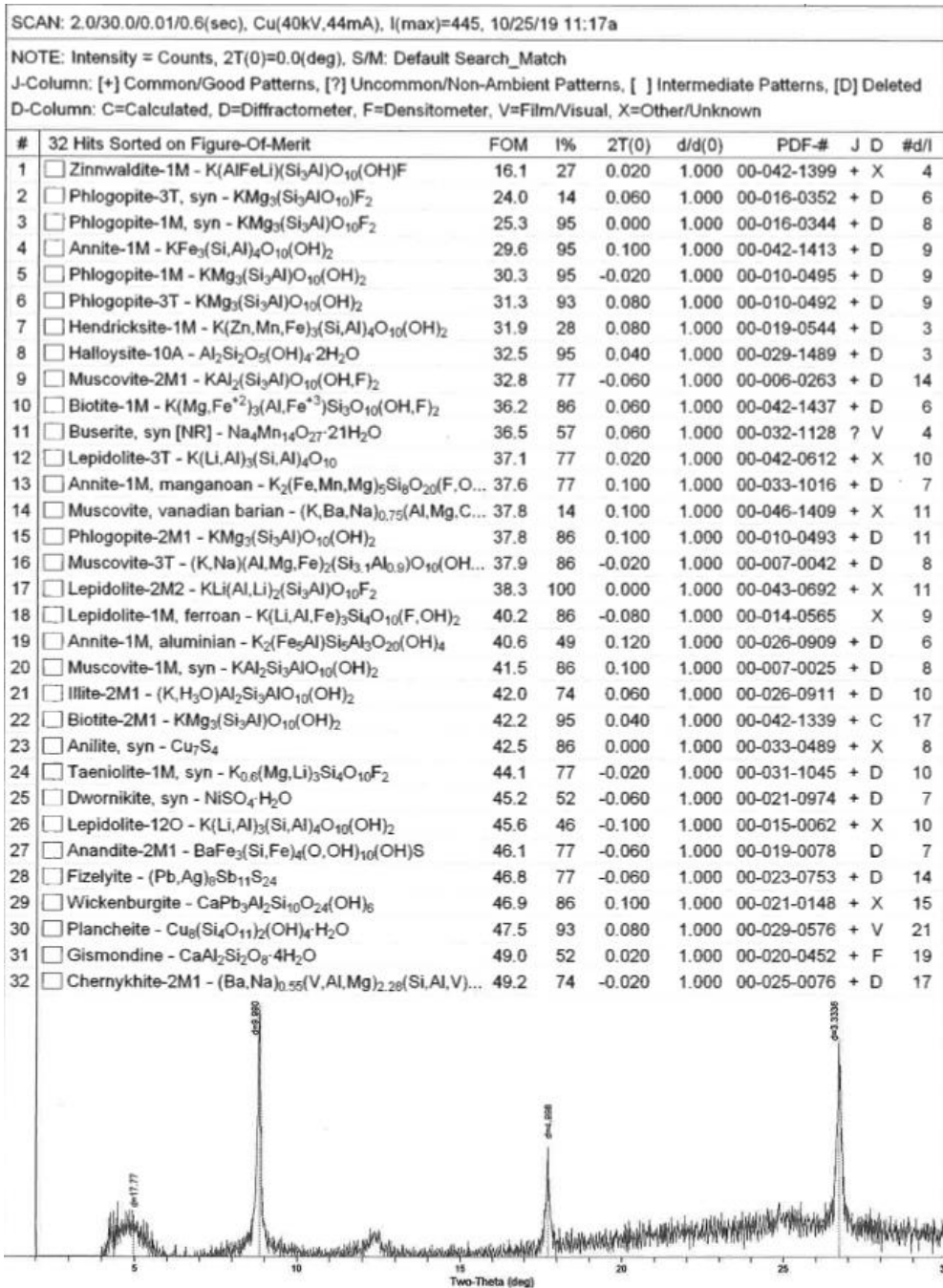


Figure 6: LP-2A 1.55 m Glycerol

SCAN: 2.0/30.0/0.01/0.6(sec), Cu(40kV,44mA), I(max)=184, 10/24/19 01:52p

NOTE: Intensity = Counts, 2T(0)=0.0(deg), S/M: Default Search_Match

J-Column: [+] Common/Good Patterns, [?] Uncommon/Non-Ambient Patterns, [] Intermediate Patterns, [D] Deleted

D-Column: C=Calculated, D=Diffractometer, F=Densitometer, V=Film/Visual, X=Other/Unknown

#	8 Hits Sorted on Figure-Of-Merit	FOM	I%	2T(0)	d/d(0)	PDF-#	J	D	#d/I
1	<input type="checkbox"/> Zinnwaldite-1M - K(AlFeLi)(Si ₃ Al)O ₁₀ (OH)F	18.3	34	-0.020	1.000	00-042-1399	+	X	4
2	<input type="checkbox"/> Phlogopite-3T, syn - KMg ₃ (Si ₃ AlO ₁₀)F ₂	22.8	17	0.040	1.000	00-016-0352	+	D	6
3	<input type="checkbox"/> Buserite, syn [NR] - Na ₄ Mn ₁₄ O ₂₇ ·21H ₂ O	29.1	92	0.080	1.000	00-032-1128	?	V	4
4	<input type="checkbox"/> Halloysite-10A - Al ₂ Si ₂ O ₅ (OH) ₄ ·2H ₂ O	30.5	92	0.000	1.000	00-029-1489	+	D	3
5	<input type="checkbox"/> Biotite-1M - K(Mg,Fe ⁺²) ₃ (Al,Fe ⁺³)Si ₃ O ₁₀ (OH,F) ₂	41.3	92	0.040	1.000	00-042-1437	+	D	6
6	<input type="checkbox"/> Muscovite, vanadian barian - (K,Ba,Na) _{0.75} (Al,Mg,C...	42.6	17	0.080	1.000	00-046-1409	+	X	11
7	<input type="checkbox"/> Phlogopite-1M - KMg ₃ (Si ₃ Al)O ₁₀ (OH) ₂	46.3	74	-0.080	1.000	00-010-0495	+	D	9
8	<input type="checkbox"/> Muscovite-3T - (K,Na)(Al,Mg,Fe) ₂ (Si _{3.1} Al _{0.9})O ₁₀ (OH...	49.3	74	-0.060	1.000	00-007-0042	+	D	8

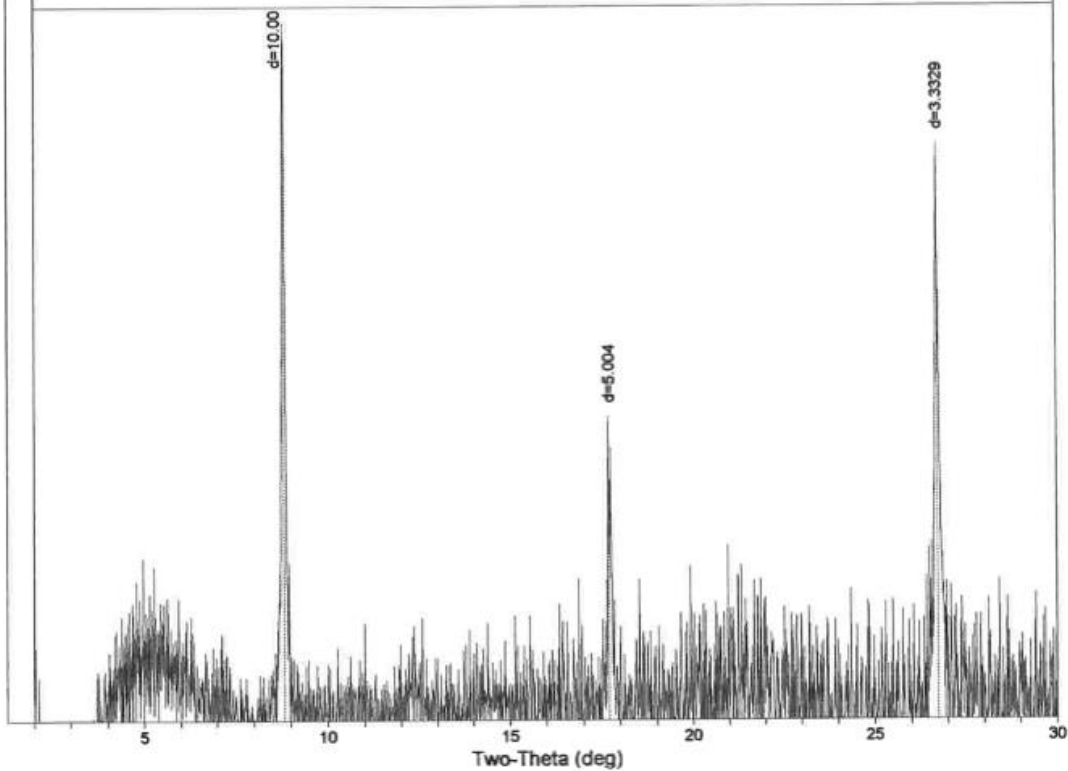


Figure 7: LP-2A 2.42 m KCL

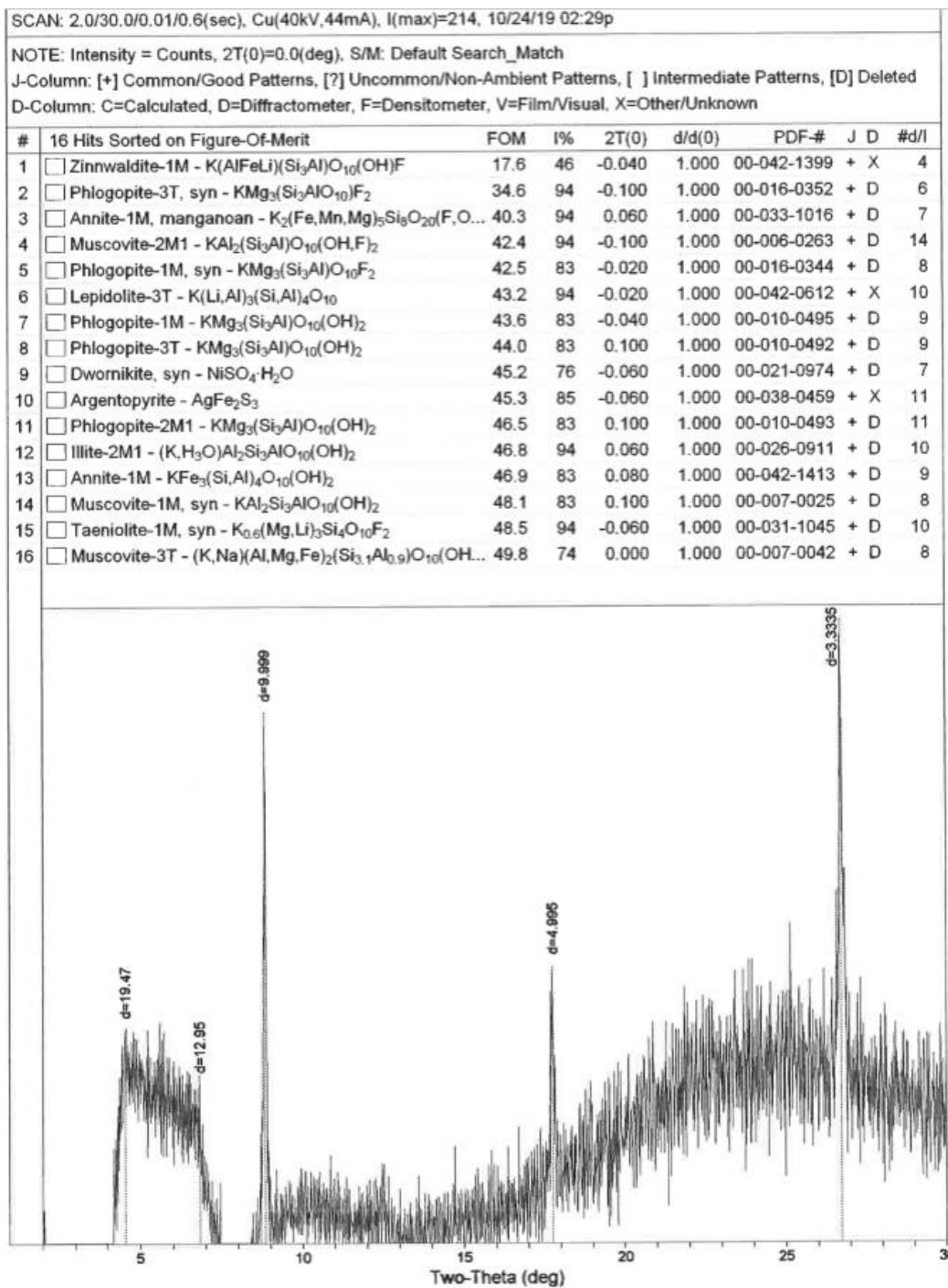


Figure 8: LP-2A 2.42 m MgCL

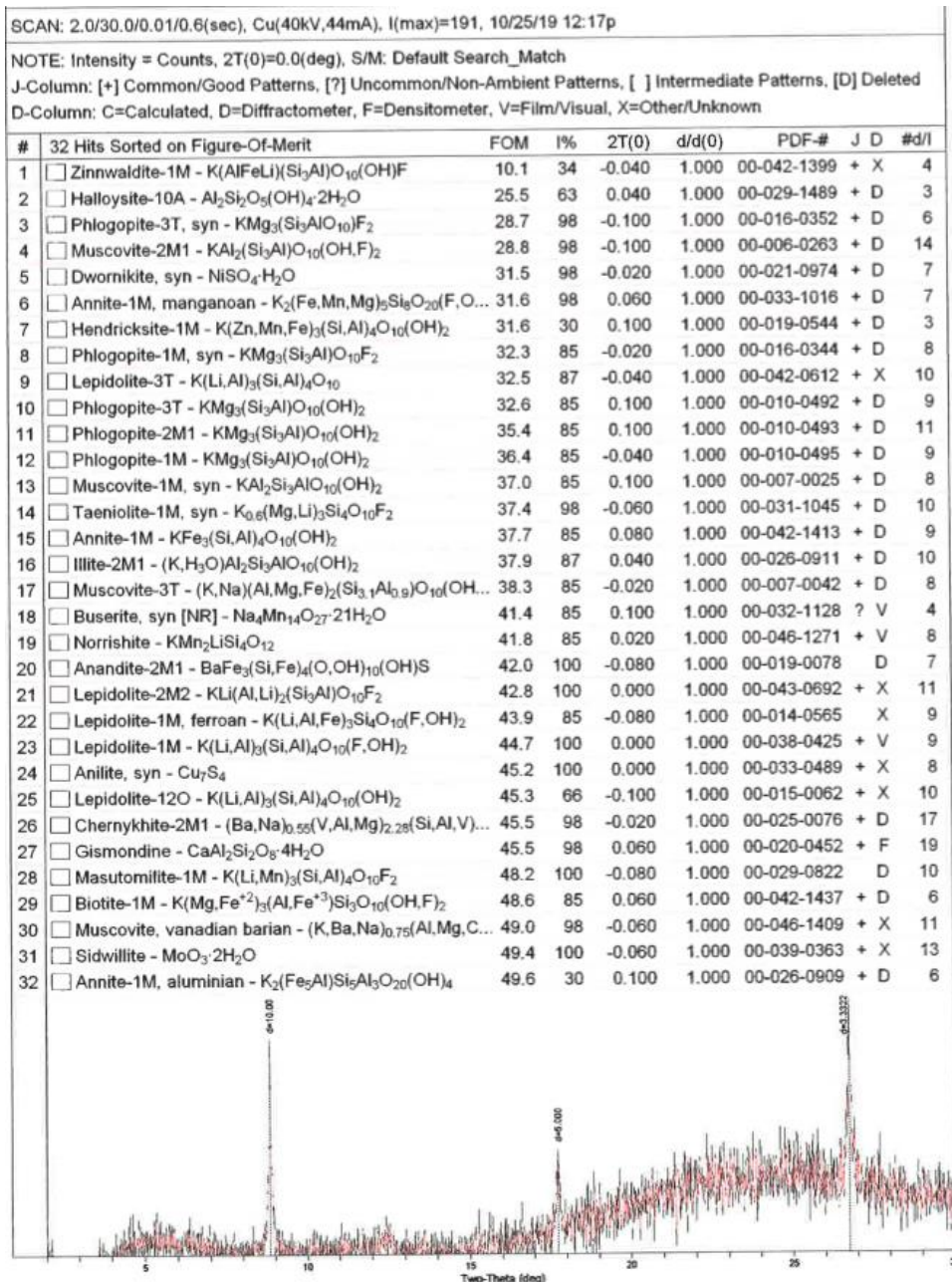


Figure 9: LP-2A 2.42 m Glycerol

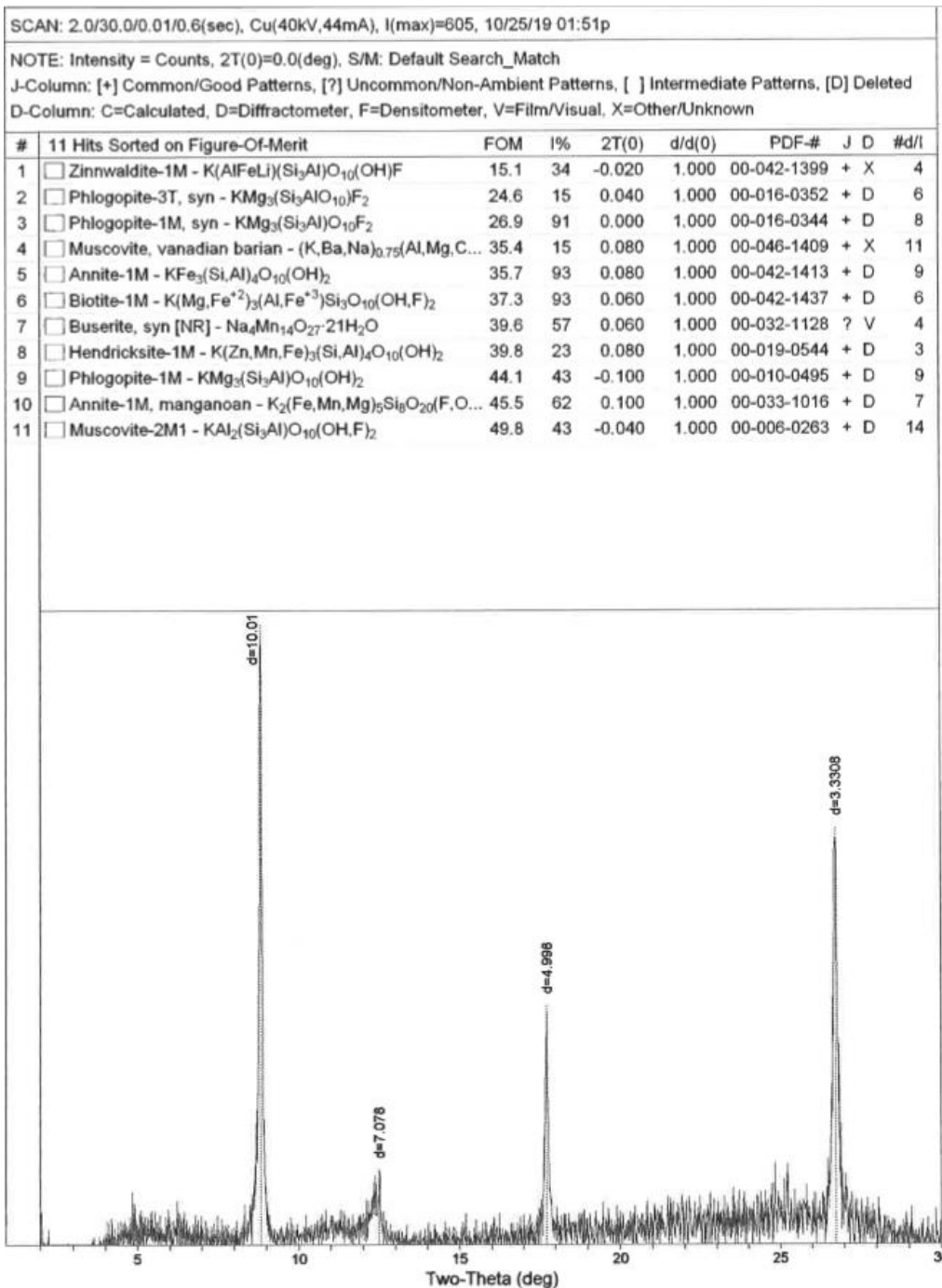


Figure 10: LP-2A 3.6 m KCL

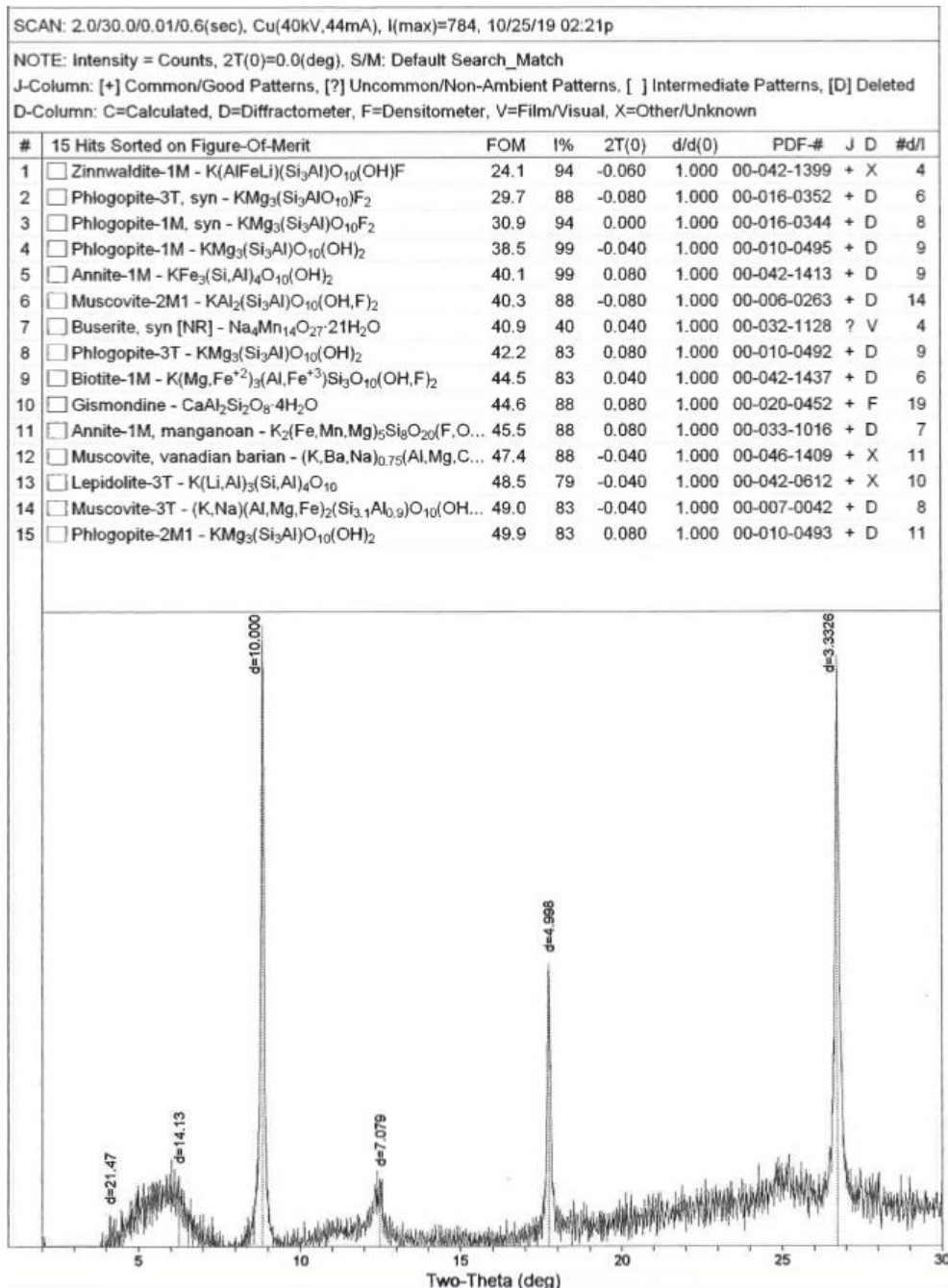


Figure 11: LP-2A 3.6 m MgCL

SCAN: 2.0/30.0/0.01/0.6(sec), Cu(40kV,44mA), I(max)=492, 10/24/19 10:24a

NOTE: Intensity = Counts, 2T(0)=0.0(deg), S/M: Default Search_Match
 J-Column: [+] Common/Good Patterns, [?] Uncommon/Non-Ambient Patterns, [] Intermediate Patterns, [D] Deleted
 D-Column: C=Calculated, D=Diffractionmeter, F=Densitometer, V=Film/Visual, X=Other/Unknown

#	7 Hits Sorted on Figure-Of-Merit	FOM	I%	2T(0)	d/d(0)	PDF-#	J	D	#d/I
1	<input type="checkbox"/> Zinnwaldite-1M - K(AlFeLi)(Si ₃ Al)O ₁₀ (OH)F	15.2	41	-0.020	1.000	00-042-1399	+	X	4
2	<input type="checkbox"/> Phlogopite-3T, syn - KMg ₃ (Si ₃ AlO ₁₀)F ₂	27.0	7	0.060	1.000	00-016-0352	+	D	6
3	<input type="checkbox"/> Buserite, syn [NR] - Na ₄ Mn ₁₄ O ₂₇ ·21H ₂ O	33.9	56	0.060	1.000	00-032-1128	?	V	4
4	<input type="checkbox"/> Biotite-1M - K(Mg,Fe ⁺²) ₃ (Al,Fe ⁺³)Si ₃ O ₁₀ (OH,F) ₂	35.4	18	-0.040	1.000	00-042-1437	+	D	6
5	<input type="checkbox"/> Halloysite-10A - Al ₂ Si ₂ O ₅ (OH) ₄ ·2H ₂ O	40.0	41	0.080	1.000	00-029-1489	+	D	3
6	<input type="checkbox"/> Phlogopite-1M, syn - KMg ₃ (Si ₃ Al)O ₁₀ F ₂	41.6	41	0.040	1.000	00-016-0344	+	D	8
7	<input type="checkbox"/> Muscovite, vanadian barian - (K,Ba,Na) _{0.75} (Al,Mg,C...	45.5	72	-0.060	1.000	00-046-1409	+	X	11

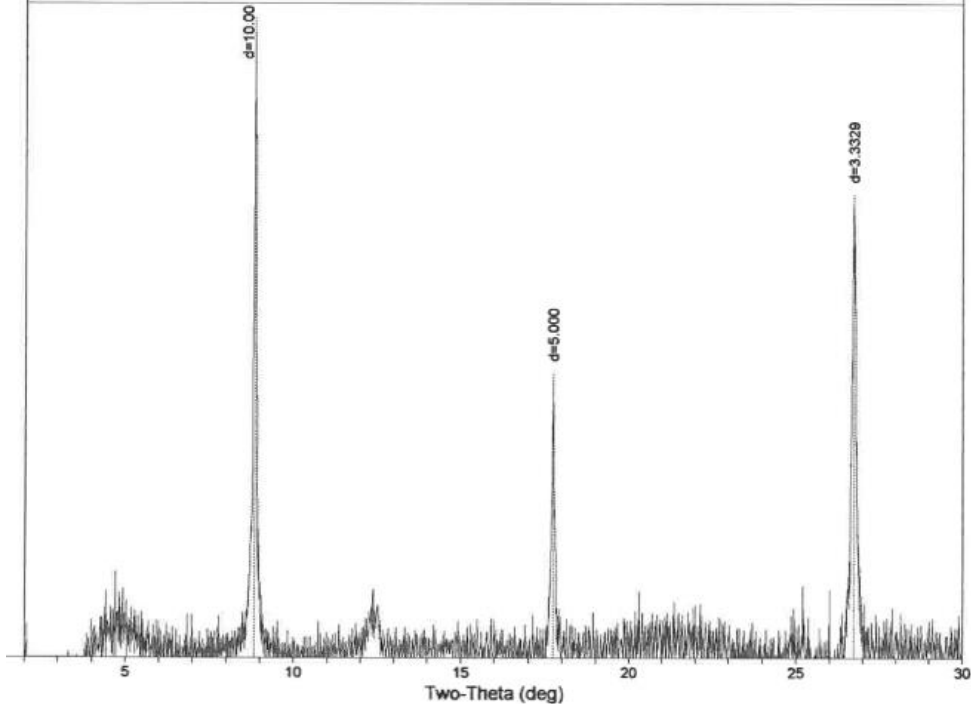


Figure 12: LP-2A 3.6 m Glycerol

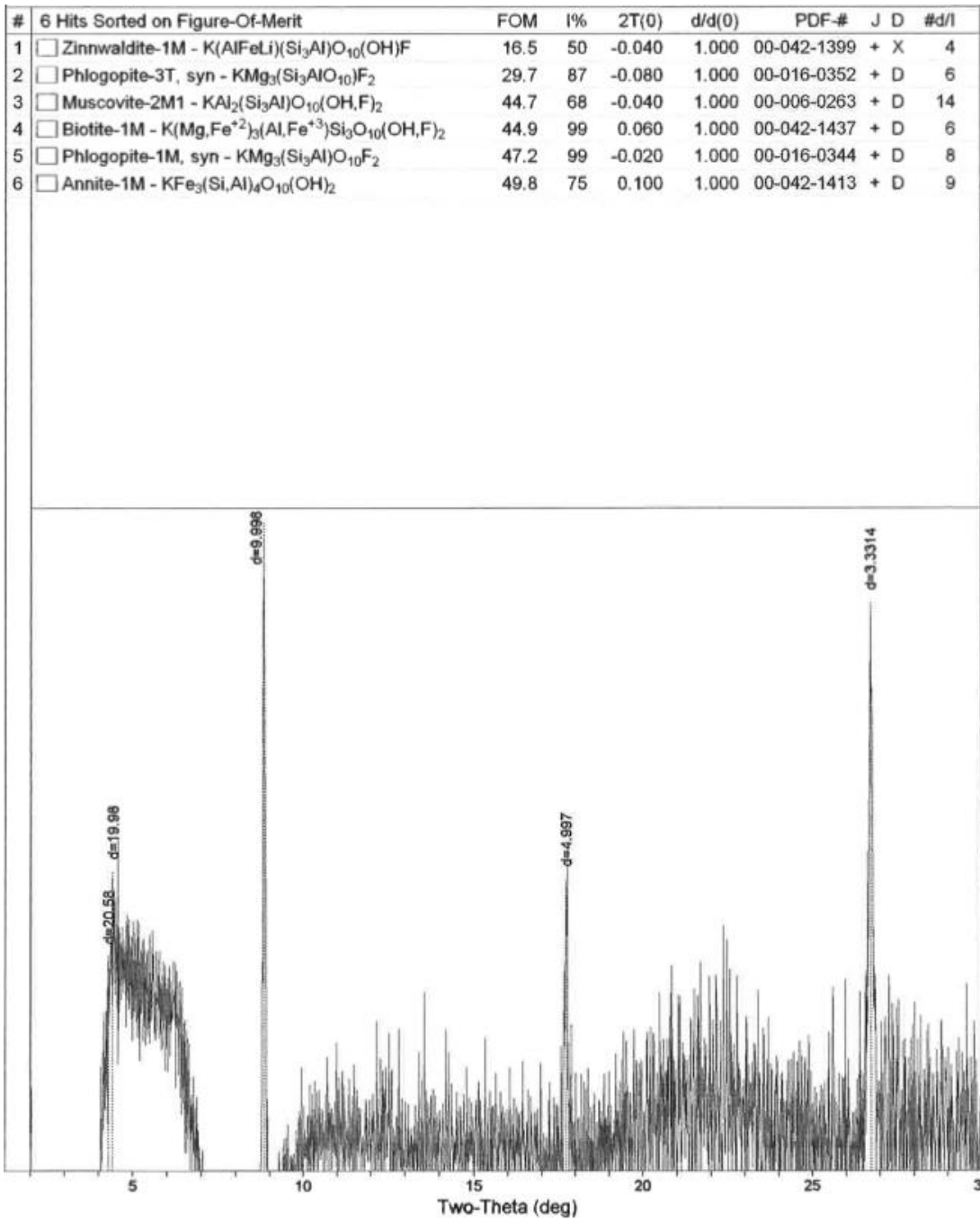


Figure 13: LP-2A 4.3 m KCL

SCAN: 2.0/30.0/0.01/0.6(sec), Cu(40kV,44mA), I(max)=313, 10/24/19 01:22p

NOTE: Intensity = Counts, 2T(0)=0.0(deg), S/M: Default Search_Match

J-Column: [+] Common/Good Patterns, [?] Uncommon/Non-Ambient Patterns, [] Intermediate Patterns, [D] Deleted

D-Column: C=Calculated, D=Diffractometer, F=Densitometer, V=Film/Visual, X=Other/Unknown

#	9 Hits Sorted on Figure-Of-Merit	FOM	I%	2T(0)	d/d(0)	PDF-#	J	D	#d/l
1	<input type="checkbox"/> Zinnwaldite-1M - K(AlFeLi)(Si ₃ Al)O ₁₀ (OH)F	8.3	46	-0.040	1.000	00-042-1399	+	X	4
2	<input type="checkbox"/> Phlogopite-3T, syn - KMg ₃ (Si ₃ AlO ₁₀)F ₂	20.2	11	0.040	1.000	00-016-0352	+	D	6
3	<input type="checkbox"/> Muscovite, vanadian barian - (K,Ba,Na) _{0.75} (Al,Mg,C...	25.3	11	0.060	1.000	00-046-1409	+	X	11
4	<input type="checkbox"/> Phlogopite-1M, syn - KMg ₃ (Si ₃ Al)O ₁₀ F ₂	25.9	7	0.060	1.000	00-016-0344	+	D	8
5	<input type="checkbox"/> Biotite-1M - K(Mg,Fe ⁺²) ₃ (Al,Fe ⁺³)Si ₃ O ₁₀ (OH,F) ₂	35.2	18	0.000	1.000	00-042-1437	+	D	6
6	<input type="checkbox"/> Biotite-2M1 - KMg ₃ (Si ₃ Al)O ₁₀ (OH) ₂	35.7	7	-0.100	1.000	00-042-1339	+	C	17
7	<input type="checkbox"/> Halloysite-10A - Al ₂ Si ₂ O ₅ (OH) ₄ ·2H ₂ O	40.9	46	0.060	1.000	00-029-1489	+	D	3
8	<input type="checkbox"/> Buserite, syn [NR] - Na ₄ Mn ₁₄ O ₂₇ ·21H ₂ O	47.5	43	0.060	1.000	00-032-1128	?	V	4
9	<input type="checkbox"/> Muscovite-3T - (K,Na)(Al,Mg,Fe) ₂ (Si _{3.1} Al _{0.9})O ₁₀ (OH...	48.5	73	-0.040	1.000	00-007-0042	+	D	8

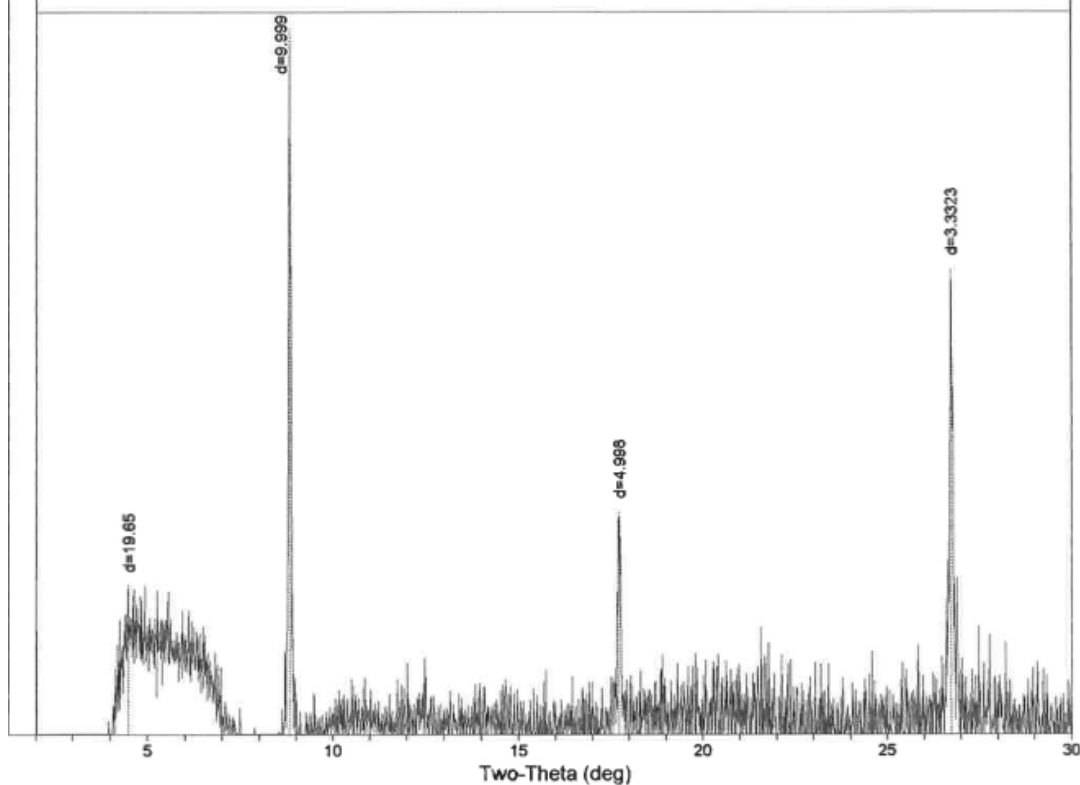


Figure 14: LP-2A 4.3m MgCL

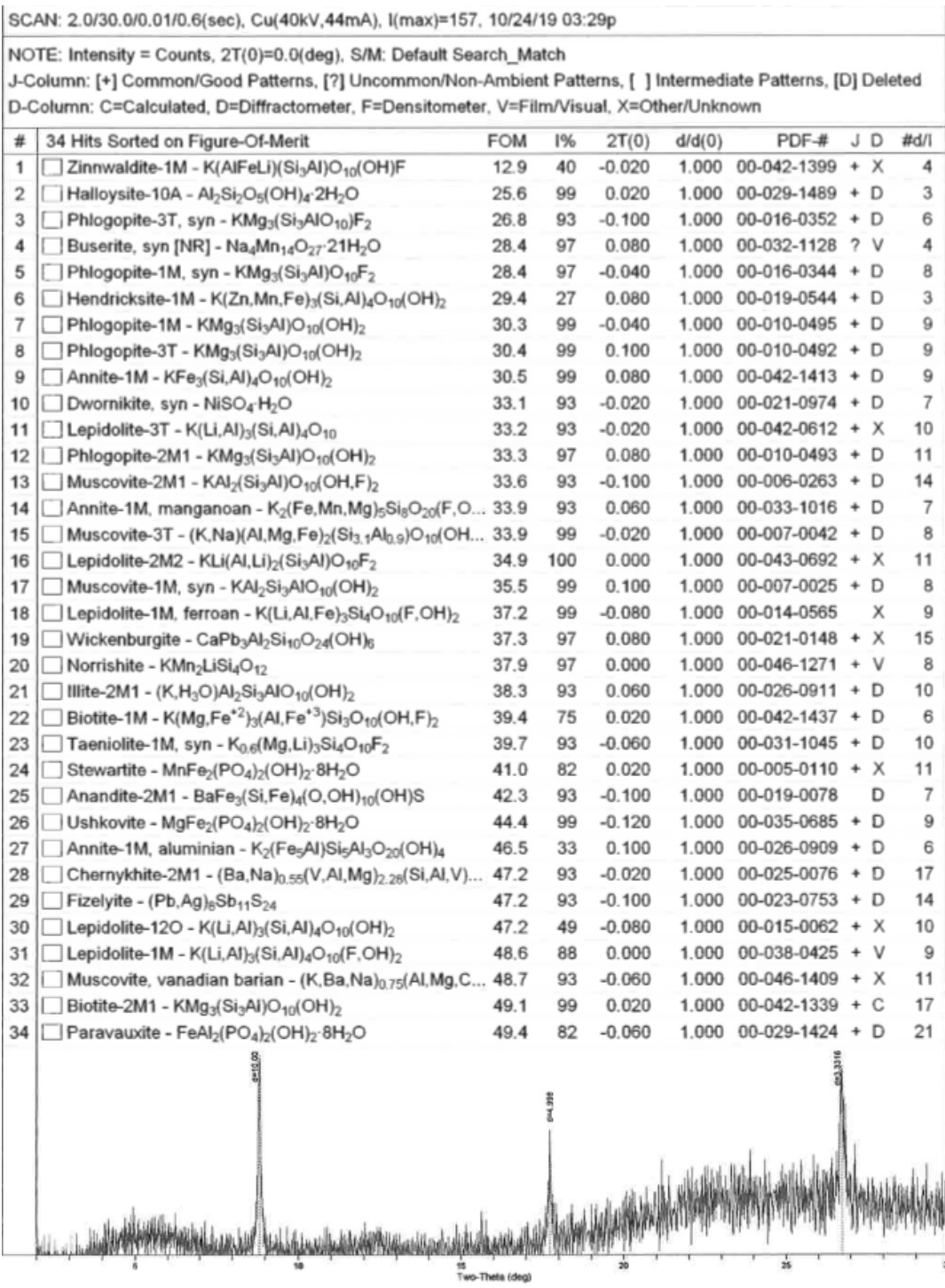


Figure 15: LP-2A 4.6 m MgCL

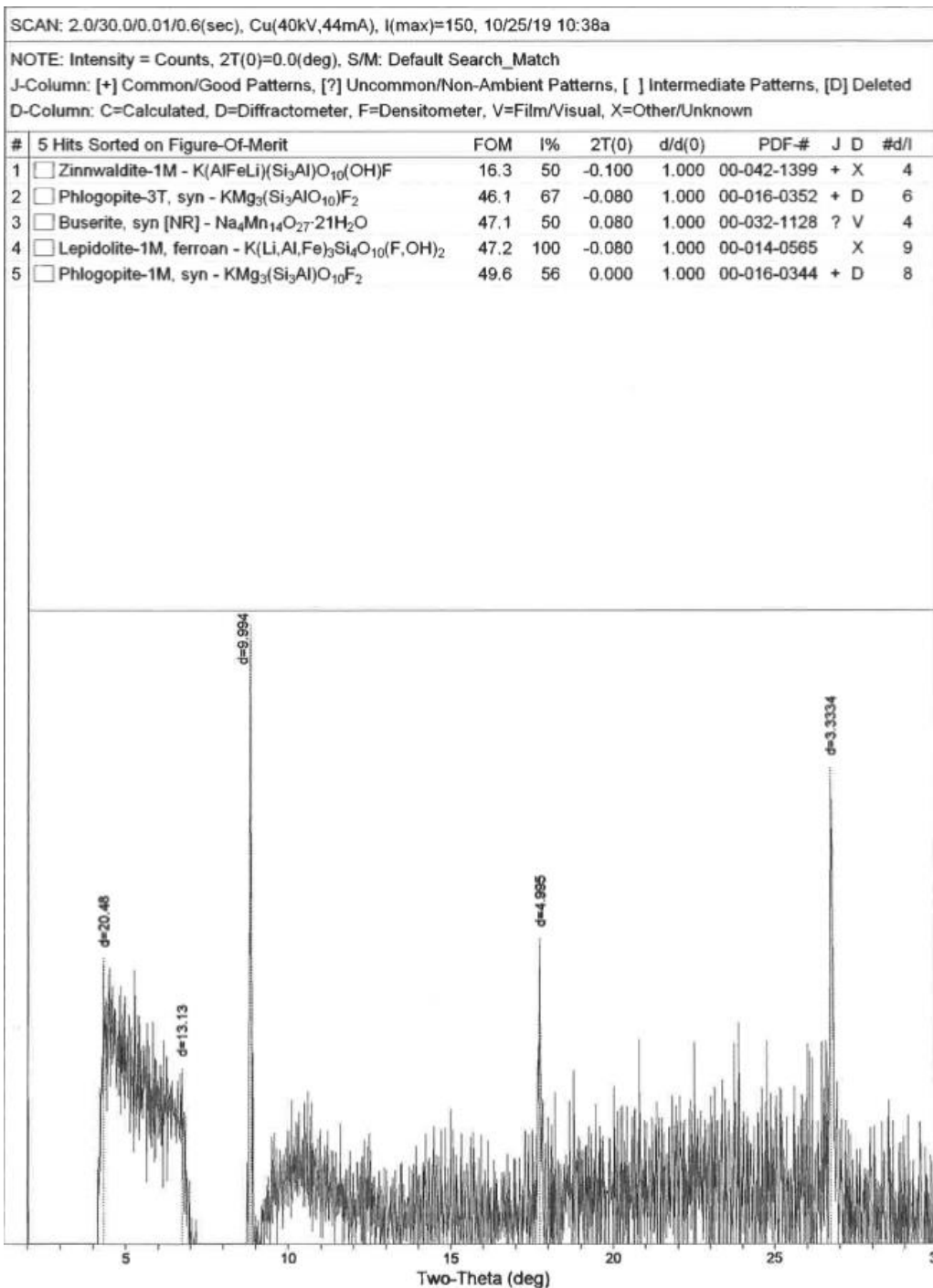


Figure 16: LP-2A 4.6 m Glycerol

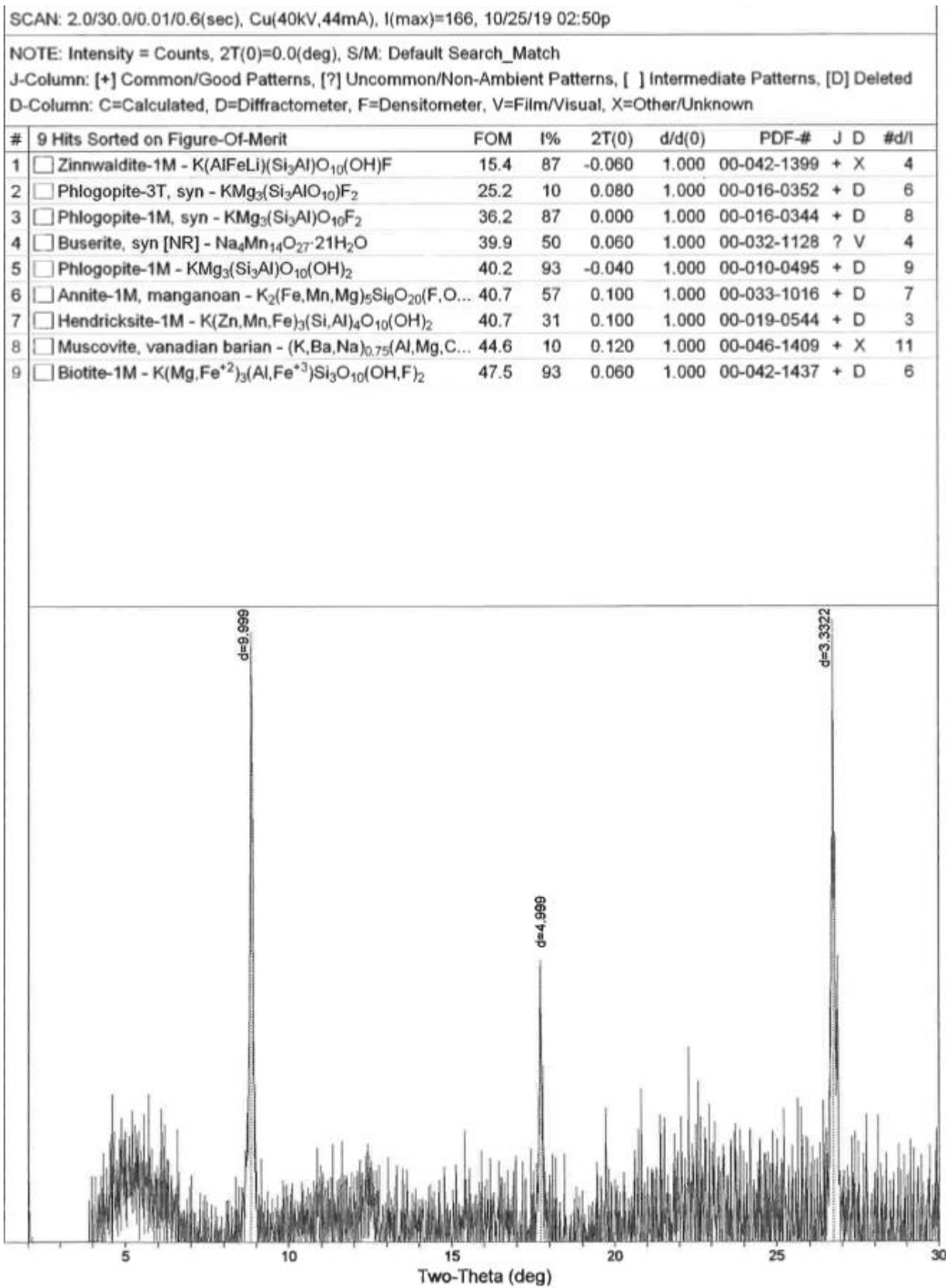


Figure 17: LP-2A 4.92 m KCL

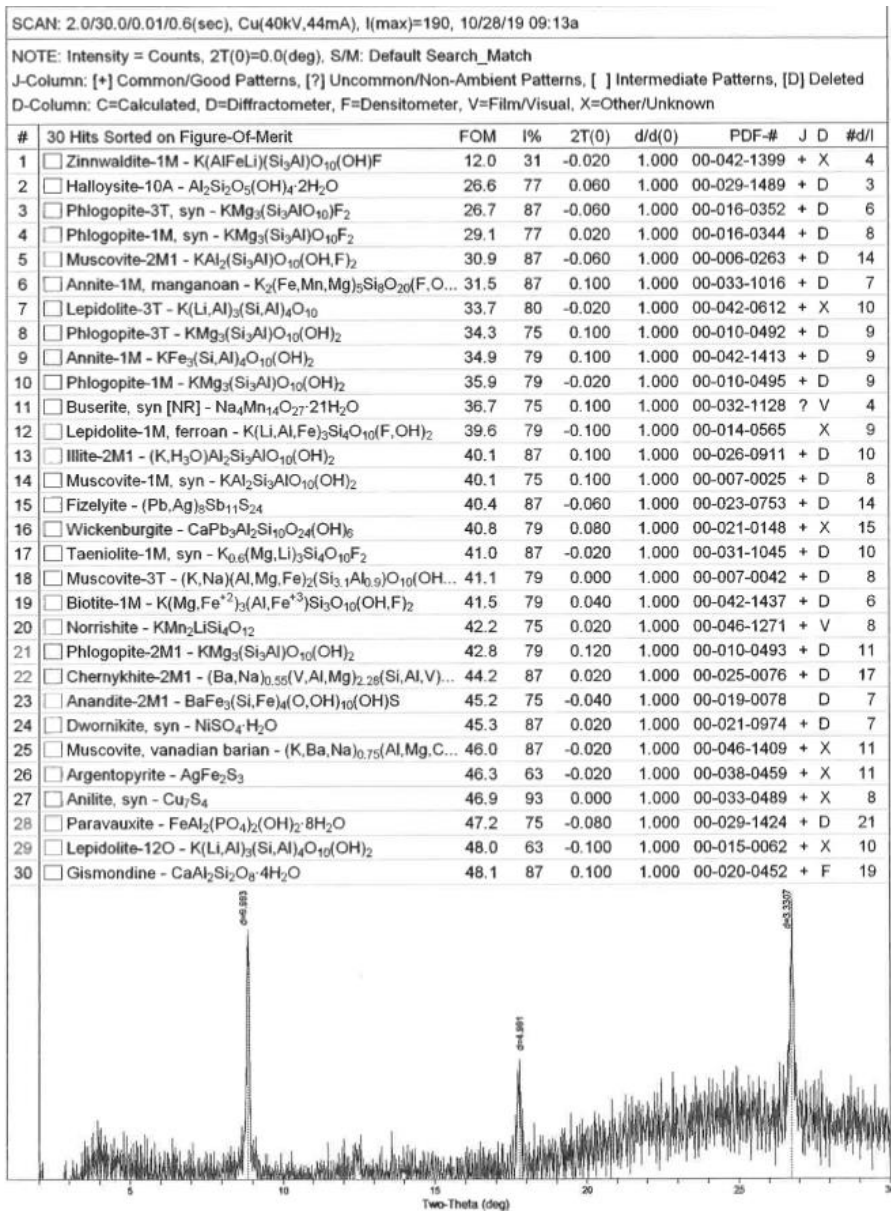


Figure 18: LP-2A 4.92 m MgCL

SCAN: 2.0/30.0/0.01/0.6(sec), Cu(40kV,44mA), I(max)=130, 10/25/19 01:21p

NOTE: Intensity = Counts, 2T(0)=0.0(deg), S/M: Default Search_Match
 J-Column: [+] Common/Good Patterns, [?] Uncommon/Non-Ambient Patterns, [] Intermediate Patterns, [D] Deleted
 D-Column: C=Calculated, D=Diffractionmeter, F=Densitometer, V=Film/Visual, X=Other/Unknown

#	12 Hits Sorted on Figure-Of-Merit	FOM	I%	2T(0)	d/d(0)	PDF-#	J	D	#d/I
1	<input type="checkbox"/> Zinnwaldite-1M - K(AlFeLi)(Si ₃ Al)O ₁₀ (OH)F	12.4	44	-0.060	1.000	00-042-1399	+	X	4
2	<input type="checkbox"/> Phlogopite-3T, syn - KMg ₃ (Si ₃ AlO ₁₀)F ₂	22.8	12	0.020	1.000	00-016-0352	+	D	6
3	<input type="checkbox"/> Muscovite, vanadian barian - (K,Ba,Na) _{0.75} (Al,Mg,C...	31.2	12	0.060	1.000	00-046-1409	+	X	11
4	<input type="checkbox"/> Phlogopite-3T - KMg ₃ (Si ₃ Al)O ₁₀ (OH) ₂	36.0	75	0.080	1.000	00-010-0492	+	D	9
5	<input type="checkbox"/> Biotite-1M - K(Mg,Fe ⁺²) ₃ (Al,Fe ⁺³)Si ₃ O ₁₀ (OH,F) ₂	37.2	17	-0.020	1.000	00-042-1437	+	D	6
6	<input type="checkbox"/> Phlogopite-1M, syn - KMg ₃ (Si ₃ Al)O ₁₀ F ₂	40.5	74	-0.020	1.000	00-016-0344	+	D	8
7	<input type="checkbox"/> Buserite, syn [NR] - Na ₄ Mn ₁₄ O ₂₇ ·21H ₂ O	40.9	60	0.060	1.000	00-032-1128	?	V	4
8	<input type="checkbox"/> Phlogopite-1M - KMg ₃ (Si ₃ Al)O ₁₀ (OH) ₂	42.6	60	-0.080	1.000	00-010-0495	+	D	9
9	<input type="checkbox"/> Halloysite-10A - Al ₂ Si ₂ O ₅ (OH) ₄ ·2H ₂ O	44.2	34	-0.040	1.000	00-029-1489	+	D	3
10	<input type="checkbox"/> Lepidolite-1M, ferroan - K(Li,Al,Fe) ₃ Si ₄ O ₁₀ (F,OH) ₂	46.8	75	-0.100	1.000	00-014-0565		X	9
11	<input type="checkbox"/> Annite-1M - KFe ₃ (Si,Al) ₄ O ₁₀ (OH) ₂	47.4	60	0.040	1.000	00-042-1413	+	D	9
12	<input type="checkbox"/> Muscovite-1M, syn - KAl ₂ Si ₃ AlO ₁₀ (OH) ₂	49.3	60	0.060	1.000	00-007-0025	+	D	8

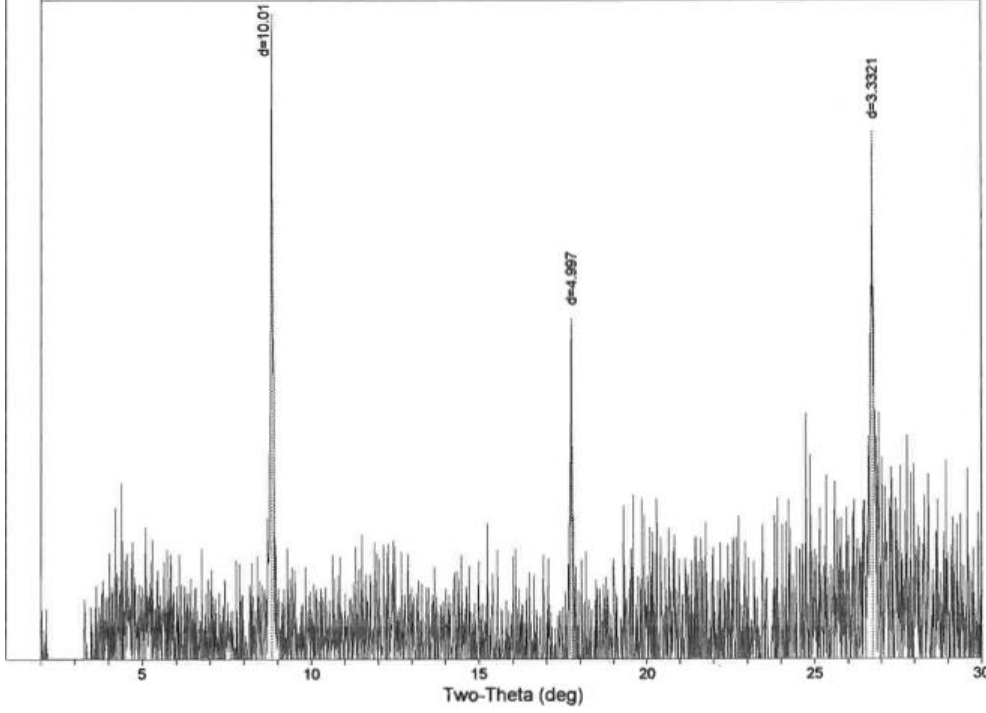


Figure 19: LP-2A 5.31 m MgCL

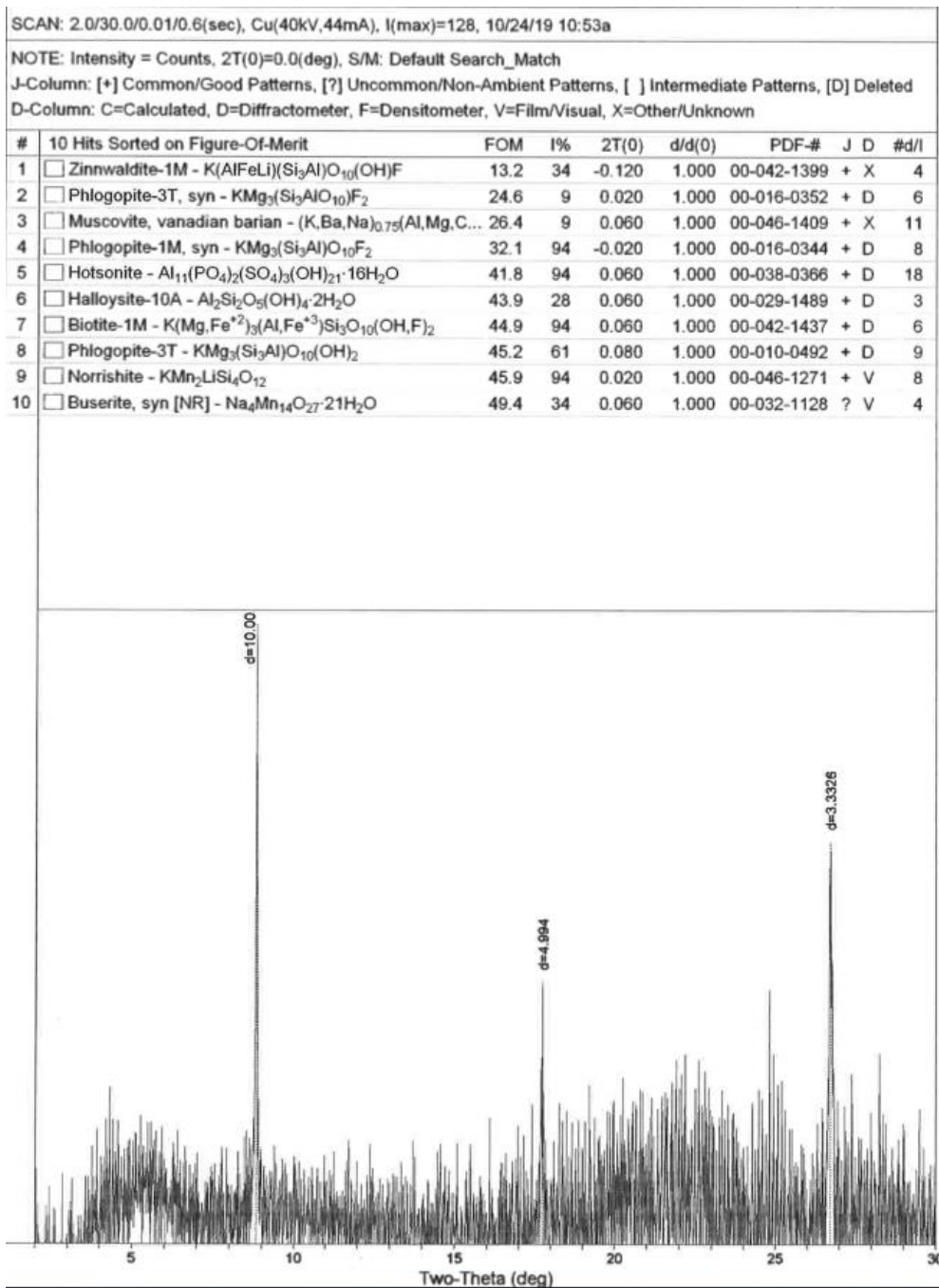


Figure 20: LP-2A 5.31 m Glycerol

Appendix 4 – XRF data

Sample	Depth (m)	Mg	Mg Err	Al	Al Err	Si	Si Err
LP2A 2.7	1.4	2.3477	0.2701	4.6218	0.0342	21.4573	0.0243
LP2A 3.2	1.55	0.927	0.1298	9.7195	0.0412	28.9507	0.0267
LP2A 3.85	1.8	2.0836	0.2526	5.4125	0.0381	22.0577	0.0251
LP2A 4.9	2.3	2.1953	0.2636	4.9655	0.0361	21.4824	0.0242
LP2A 5.1	2.42	1.4644	0.1841	7.9333	0.036	25.639	0.023
LP2A 5.6	2.57	1.7913	0.2447	6.2309	0.0384	23.1892	0.0248
LP2A 6.65	2.7	2.0077	0.2727	5.22	0.0372	21.4794	0.0242
LP2A 8.35	3.6	1.7501	0.2157	7.1181	0.0433	24.8806	0.028
LP2A 10.1	4	2.013	0.2597	5.4456	0.0448	22.1371	0.0288
LP2A 10.4	4.3	2.5555	0.3016	4.0112	0.0337	19.2426	0.0218
LP2A 10.75	4.6	2.2355	0.2969	6.1916	0.0349	21.3455	0.0202
LP2A 10.8	4.65	2.6209	0.3111	5.2942	0.0361	20.1158	0.0211
LP2A 11	4.75	2.525	0.311	4.211	0.0339	18.9681	0.0209
LP2A 11.3	4.92	2.4796	0.3029	4.1346	0.0347	19.0603	0.0217
LP2A 11.7	5.31	2.0515	0.2738	5.0061	0.0384	21.2108	0.0249
LP2A 11.9	5.54	2.3293	0.3195	2.7906	0.0311	17.8137	0.0215
Depth (m)	P	P Err	S	S Err	K	K Err	Ca
1.4	0.0155	0.0017	0.5599	0.0063	1.3668	0.0058	1.9613
1.55	0.0156	0.0018	0.1003	0.004	1.87	0.0069	1.104
1.8	0.017	0.0016	0.1477	0.0045	1.8181	0.0067	1.0548
2.3	0.0107	0.0015	0.0285	0.0038	1.5178	0.0062	0.9123
2.42	0.0084	0.0016	0.1409	0.0043	1.5972	0.0063	0.8918
2.57	< LOD	0.0016	2.0912	0.0106	1.8215	0.0069	0.2115
2.7	0.0146	0.0018	1.0549	0.0081	1.7037	0.0066	2.0633
3.6	0.0169	0.0018	0.5342	0.0061	2.1421	0.0074	1.487
4	0.0127	0.0016	0.5193	0.0062	2.6124	0.0082	0.2922
4.3	0.0152	0.0017	0.642	0.0068	1.4703	0.0061	2.0729
4.6	0.0942	0.0029	0.6004	0.0067	1.1366	0.0053	9.7699
4.65	0.0605	0.0025	0.748	0.0072	1.4073	0.0058	7.597
4.75	0.0338	0.002	0.4273	0.006	1.4444	0.0059	4.7609
4.92	0.047	0.0021	1.0514	0.0083	1.5073	0.0062	2.4955
5.31	< LOD	0.0016	2.1888	0.0111	1.7157	0.0067	0.2388
5.54	< LOD	0.0014	3.3569	0.0137	1.3074	0.0059	0.0457

Depth (m)	Ca Err	Ti	Ti Err	V	V Err	Cr	Cr Err
1.4	0.0062	0.2045	0.0019	0.0097	0.0003	0.0103	0.0007
1.55	0.0046	0.2152	0.0018	0.006	0.0002	0.0068	0.0005
1.8	0.0047	0.204	0.0019	0.0089	0.0003	0.0098	0.0007
2.3	0.0044	0.167	0.0018	0.0078	0.0003	0.0088	0.0007
2.42	0.0042	0.1823	0.0017	0.0083	0.0002	0.0121	0.0005
2.57	0.0028	0.2214	0.0019	0.0106	0.0003	0.0128	0.0006
2.7	0.0064	0.2133	0.0019	0.011	0.0003	0.0107	0.0007
3.6	0.0054	0.272	0.0021	0.0113	0.0002	0.0126	0.0006
4	0.003	0.3153	0.0021	0.0155	0.0003	0.0192	0.0007
4.3	0.0065	0.1782	0.0019	0.0103	0.0003	0.0118	0.0008
4.6	0.0145	0.1293	0.002	0.0054	0.0003	0.0041	0.0008
4.65	0.0125	0.1676	0.002	0.0085	0.0003	0.006	0.0008
4.75	0.0097	0.1649	0.0019	0.0092	0.0003	0.0088	0.0008
4.92	0.0071	0.194	0.0019	0.0112	0.0003	0.0122	0.0008
5.31	0.0029	0.249	0.002	0.013	0.0003	0.0159	0.0007
5.54	0.0023	0.1918	0.0018	0.0118	0.0003	0.0174	0.0008
Depth (m)	Mn	Mn Err	Fe	Fe Err	Co	Co Err	Ni
1.4	0.0198	0.0007	1.9878	0.0087	< LOD	0.0007	0.0023
1.55	0.0194	0.0008	2.6464	0.0097	< LOD	0.0007	0.0017
1.8	0.028	0.0008	2.4415	0.0095	0.0012	0.0007	0.0022
2.3	0.0147	0.0008	2.0785	0.0087	< LOD	0.0007	0.0022
2.42	0.0165	0.0007	2.2603	0.0089	< LOD	0.0008	0.0022
2.57	0.0249	0.0007	3.4734	0.0114	0.0015	0.0009	0.0022
2.7	0.0254	0.0008	2.8723	0.0106	0.0012	0.0008	0.003
3.6	0.0401	0.0008	2.8822	0.0104	< LOD	0.0007	0.003
4	0.0248	0.0007	3.3586	0.0111	< LOD	0.0009	0.0031
4.3	0.0403	0.0009	2.3169	0.0095	< LOD	0.0007	0.0024
4.6	0.0944	0.0012	2.1128	0.0101	< LOD	0.0006	0.0018
4.65	0.0396	0.001	2.3297	0.0104	< LOD	0.0007	0.0022
4.75	0.0591	0.0009	2.1892	0.0096	< LOD	0.0007	0.0023
4.92	0.0592	0.0009	2.8068	0.0106	0.0008	0.0008	0.0028
5.31	0.0387	0.0008	3.5314	0.0116	< LOD	0.0008	0.0037
5.54	0.0139	0.0007	3.4193	0.0116	< LOD	0.0009	0.0027

Depth (m)	Ni Err	Cu	Cu Err	Zn	Zn Err	As	As Err
1.4	0.0004	0.0017	0.0003	0.0063	0.0004	0.0021	0.0002
1.55	0.0004	0.0018	0.0003	0.0068	0.0004	0.0032	0.0002
1.8	0.0004	0.0017	0.0003	0.0084	0.0005	0.0012	0.0002
2.3	0.0004	0.0029	0.0003	0.0068	0.0005	0.0014	0.0002
2.42	0.0004	0.0019	0.0003	0.0062	0.0004	0.0031	0.0002
2.57	0.0004	0.002	0.0003	0.007	0.0004	0.0075	0.0003
2.7	0.0005	0.003	0.0004	0.0089	0.0005	0.0084	0.0003
3.6	0.0005	0.0023	0.0003	0.0081	0.0004	0.0029	0.0002
4	0.0005	0.0026	0.0003	0.0111	0.0005	0.0024	0.0002
4.3	0.0004	0.0022	0.0004	0.0083	0.0005	0.0036	0.0002
4.6	0.0004	0.0017	0.0003	0.0045	0.0004	0.0041	0.0002
4.65	0.0004	0.0022	0.0003	0.0069	0.0005	0.0027	0.0002
4.75	0.0004	0.0019	0.0003	0.0065	0.0004	0.0013	0.0002
4.92	0.0004	0.0024	0.0004	0.009	0.0005	0.0022	0.0002
5.31	0.0005	0.0038	0.0004	0.0113	0.0006	0.0213	0.0004
5.54	0.0004	0.0023	0.0003	0.0058	0.0004	0.0041	0.0002
Depth (m)	Se	Se Err	Rb	Rb Err	Sr	Sr Err	Zr
1.4	< LOD	0.0002	0.009	0.0004	0.0187	0.0004	0.0075
1.55	< LOD	0.0002	0.0106	0.0003	0.0123	0.0003	0.0064
1.8	< LOD	0.0002	0.0134	0.0004	0.0103	0.0003	0.0051
2.3	< LOD	0.0002	0.0101	0.0004	0.0086	0.0003	0.0038
2.42	< LOD	0.0002	0.01	0.0003	0.0114	0.0003	0.0055
2.57	< LOD	0.0002	0.0111	0.0004	0.0071	0.0003	0.0046
2.7	< LOD	0.0002	0.0121	0.0004	0.0176	0.0003	0.0042
3.6	< LOD	0.0002	0.0127	0.0004	0.0143	0.0003	0.0054
4	< LOD	0.0002	0.0155	0.0004	0.0081	0.0003	0.0057
4.3	< LOD	0.0002	0.0116	0.0004	0.0151	0.0003	0.0041
4.6	< LOD	0.0002	0.0076	0.0004	0.0453	0.0005	0.0026
4.65	< LOD	0.0002	0.0106	0.0004	0.0364	0.0004	0.0035
4.75	< LOD	0.0002	0.0099	0.0004	0.0196	0.0004	0.0034
4.92	< LOD	0.0002	0.0128	0.0004	0.0137	0.0003	0.0046
5.31	< LOD	0.0002	0.0143	0.0005	0.006	0.0003	0.0056
5.54	< LOD	0.0002	0.0122	0.0005	0.0035	0.0003	0.0085

Depth (m)	Zr Err	Ag	Ag Err	Cd	Cd Err	Sn	Sn Err
1.4	0.0003	< LOD	0.0008	< LOD	0.0011	< LOD	0.0007
1.55	0.0003	< LOD	0.0007	< LOD	0.001	< LOD	0.0007
1.8	0.0003	< LOD	0.0008	< LOD	0.0009	< LOD	0.0007
2.3	0.0003	< LOD	0.0008	< LOD	0.0009	< LOD	0.0006
2.42	0.0003	< LOD	0.0008	< LOD	0.001	< LOD	0.0007
2.57	0.0003	< LOD	0.0008	< LOD	0.001	< LOD	0.0007
2.7	0.0003	< LOD	0.0008	< LOD	0.001	< LOD	0.0007
3.6	0.0003	< LOD	0.0007	< LOD	0.001	< LOD	0.0007
4	0.0003	< LOD	0.0008	< LOD	0.001	0.001	0.0007
4.3	0.0003	< LOD	0.0008	< LOD	0.001	< LOD	0.0007
4.6	0.0003	< LOD	0.0007	< LOD	0.001	< LOD	0.0007
4.65	0.0003	< LOD	0.0008	< LOD	0.001	< LOD	0.0007
4.75	0.0003	< LOD	0.0008	< LOD	0.001	< LOD	0.0007
4.92	0.0003	< LOD	0.0008	< LOD	0.001	< LOD	0.0007
5.31	0.0003	< LOD	0.0008	< LOD	0.0009	< LOD	0.0006
5.54	0.0003	< LOD	0.0009	< LOD	0.0011	< LOD	0.0007
Depth (m)	Sb	Sb Err	Ba	Ba Err	Hg	Hg Err	Tl
1.4	< LOD	0.0024	0.0137	0.0071	< LOD	0.0005	< LOD
1.55	< LOD	0.0023	0.0274	0.0073	< LOD	0.0005	< LOD
1.8	< LOD	0.0026	0.0241	0.0078	< LOD	0.0005	< LOD
2.3	< LOD	0.0025	0.0182	0.0072	< LOD	0.0006	< LOD
2.42	< LOD	0.0022	0.009	0.0068	< LOD	0.0004	< LOD
2.57	< LOD	0.0024	0.0139	0.0077	< LOD	0.0005	< LOD
2.7	< LOD	0.0025	0.0215	0.0078	< LOD	0.0005	< LOD
3.6	< LOD	0.0025	0.023	0.0076	< LOD	0.0005	< LOD
4	< LOD	0.0026	0.0321	0.0077	< LOD	0.0005	< LOD
4.3	< LOD	0.0025	< LOD	0.0075	< LOD	0.0005	< LOD
4.6	< LOD	0.0024	0.0117	0.0074	< LOD	0.0005	< LOD
4.65	< LOD	0.0025	0.0102	0.0077	< LOD	0.0005	< LOD
4.75	< LOD	0.0024	0.0167	0.007	< LOD	0.0005	< LOD
4.92	< LOD	0.0026	0.0142	0.008	< LOD	0.0005	< LOD
5.31	< LOD	0.0027	0.0251	0.0089	< LOD	0.0005	< LOD
5.54	< LOD	0.0026	0.0188	0.009	< LOD	0.0005	< LOD

Depth (m)	Tl Err	Pb	Pb Err	Mg/Ca	Fe/Mn	Sr/Ca (*10 ⁻³)	Fe/Mg
1.4	0.0004	0.0017	0.0008	1.197012	100.3939		0.846701
1.55	0.0004	0.0016	0.0007	0.839674	136.4124	9.534492	2.8548
1.8	0.0004	0.0013	0.0007	1.975351	87.19643	11.1413	1.17177
2.3	0.0004	0.001	0.0008	2.406336	141.3946	9.764884	0.946795
2.42	0.0004	0.0016	0.0008	1.642072	136.9879	9.426724	1.543499
2.57	0.0004	0.001	0.0008	8.469504	139.494	12.78314	1.939039
2.7	0.0004	0.001	0.0008	0.973053	113.0827	33.56974	1.430642
3.6	0.0004	0.0013	0.0007	1.176933	71.87531	8.530025	1.646877
4	0.0004	0.0016	0.0007	6.889117	135.4274	9.616678	1.668455
4.3	0.0004	0.0011	0.0008	1.232814	57.49132	27.72074	0.906633
4.6	0.0004	< LOD	0.0008	0.228815	22.38136	7.284481	0.945113
4.65	0.0004	< LOD	0.0008	0.344991	58.83081	4.63669	0.888893
4.75	0.0004	0.0013	0.0008	0.530362	37.0423	4.791365	0.86701
4.92	0.0004	0.0008	0.0008	0.993629	47.41216	4.116869	1.131957
5.31	0.0004	0.0008	0.0007	8.590871	91.25065	5.489882	1.721375
5.54	0.0004	0.0012	0.0008	50.96937	245.9928	25.12563	1.467952
						76.58643	